ETH zürich

Laboratory for Solid State Physics
Annual Report 2014

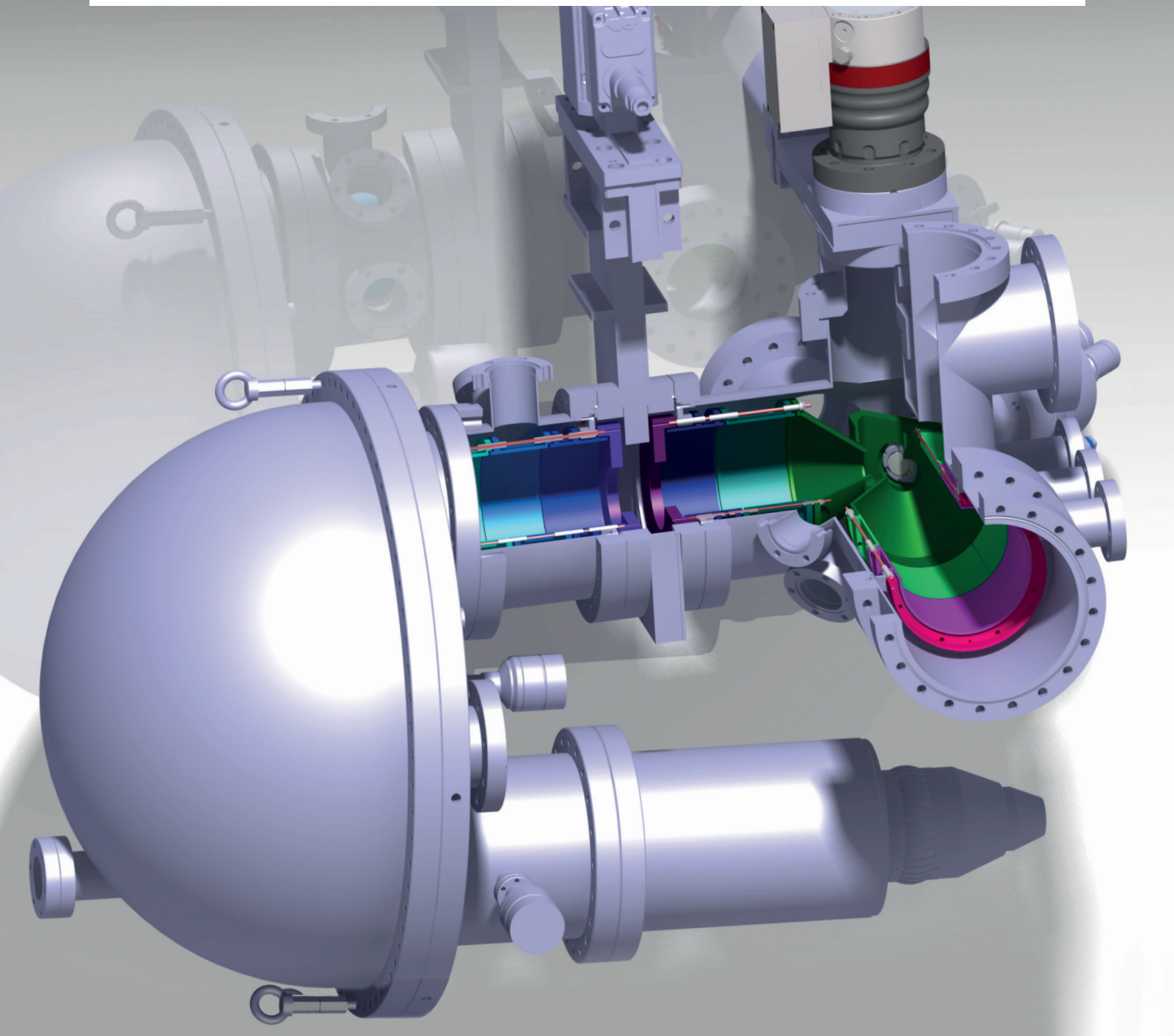

Department of Physics

ANNUAL REPORT
2014

Solid State Physics Laboratory (LFKP)
ETH Zurich

Cover page:

Drawing of a novel spin detector based on low energy scattering of spin polarized electrons on a Iridium crystal (SPLEED) attached to a hemispherical energy analyzer. The detector has been designed by the group of Prof. Vaterlaus and manufactured at the physics workshop at ETH.

This annual report was edited by: Tino Zimmerling

PREFACE

The Laboratory for Solid State Physics at ETH Zurich is pleased to present its Annual Report for 2014. Our report displays the diverse foci in research, which led to numerous publications in high-ranking journals and presentations at international conferences. The members of the Laboratory are also committed to all aspects of teaching. They strive at conveying the fascination of physics in general and in particular of state-of-the-art solid state physics at all levels. Bachelor and Master level courses were offered for physics students as well as for students of other departments. The portfolio of research directions carried out at LFKP covers a rather wide range including the application and development of novel instruments, the synthesis of highest-quality materials and the fabrication of nanoscale quantum devices as summarized below.

The experimental research at the laboratory of solid state physics and our teaching activities benefit from the excellent infrastructure provided by ETH Zurich and in particular by the physics department. We thank the involved people for their dedication and solid support especially in all technical and administrative matters. We very gratefully acknowledge the continuous and substantial support by the Schulleitung of ETH Zurich, but also by the Swiss National Science Foundation, the Commission for Technology and Innovation (KTI), the European Research Council, industrial partners and all other sources.

For preparing this Annual Report, we would like to thank Mrs. Christina Egli and Mr. Tino Zimmerling for editing the report and Mrs. Amanda Eisenhut for the graphical design.

As it became tradition already, in order to avoid producing old-fashioned CDs we again simply print a postcard with a QR-Code on it so that last year's report can be easily downloaded.

Zurich, June 2015

Der Vorsteher

Prof. Dr. W. Wegscheider

Contents

Chapter 1

Physics of New Materials

(http://www.pnm.ethz.ch/)

Head
Prof. Dr. B. Batlogg

Academic Staff

Balthasar Blülle	Stanislaw Galeski	Dr. Alfonso Gonzalez
Jonathan Hanselmann	Dr. Fabio Isa	Arik Jung
Jakob Kanter	Thomas Kreiliger	Dr. Thomas Mathis
Dr. Philip Moll	Tobias Morf	Dr. Ivan Prieto
Dr. Yasmine Sassa	PD Dr. Hans von Känel	Kristin Willa
Tino Zimmerling		

Master Students

Maja Bachmann	Arik Jung	Carol Stelzer

Administrative Staff
Gabriela Strahm

Technical Staff
Kurt Mattenberger

High Pressure Synthesis

Academic Staff
Dr. Nikolai Zhigadlo

Academic Guests
Dr. Roman Puzniak, Polish Academy of Sciences, Warsaw (Poland)
Dr. Krzysztof Rogacki, Polish Academy of Sciences, Wroclaw (Poland)

1.1 Conventional superconductivity in single crystals $MgCNi_3$

N. D. Zhigadlo, in collaboration with R. T. Gordon, R. Prozorov (Ames Laboratory), S. Weyeneth (University Zurich), and S. Katrych (EPFL)

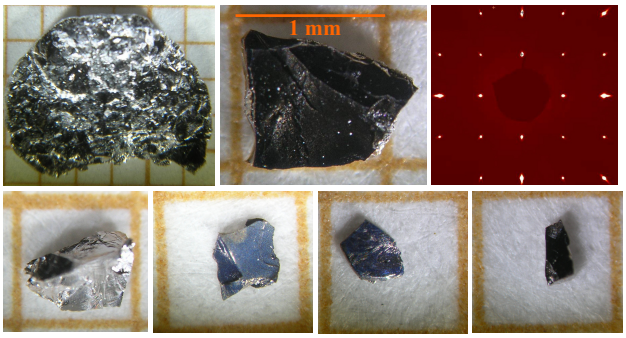

Figure 1.1: (left panel) Optical microscope images of $MgCNi_3$ single crystals. After crushing the lump, a large number of crystals up to 1 mm^2 were found. Upper right frame shows the $kh0$ reciprocal space section determined by XRD of single-crystal $MgC_{0.92}Ni_{2.88}$.

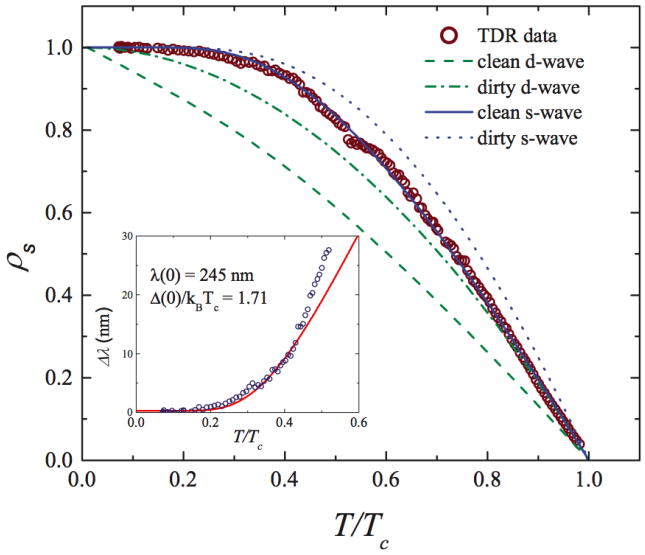

Figure 1.2: (right panel) The superfluid density $\rho_s(T)$ calculated from the London penetration depth. Expectations for the single-gap BCS superconductors are shown for clean-limit s (solid blue), clean-limit d (dashed green), dirty-limit s (dot blue), and dirty-limit d (dashed-dot green) waves. The inset shows the low-temperature variation of the London penetration depth and a weak-coupling BCS isotropic s-wave fit with a fixed $\rho(0) = 245nm$ and the gap $\Delta(0)$ as a free parameter.

Single crystals of $MgCNi_3$, with areas sized up to 1 mm^2, were grown by the self-flux method using a cubic anvil high-pressure technique (see Fig. 1.1). In low applied fields, the dc magnetization exhibited a narrow transition into the superconducting state, demonstrating the good quality of the crystals. The lower critical field H_{c1}, determined from a zero-temperature extrapolation, is around 18 mT. The upper critical field H_{c2} was found to be isotropic with a slope at T_c of -2.6 T/K and $H_{c2}(0) \approx 12.3$ T at zero temperature. This value corresponds to the coherence length of 5.2 nm and together with the London penetration depth $\lambda(0) = 245$ nm gives a Ginsburg-Landau parameter of $\kappa \approx 47$. The superfluid density, $\rho_s = [\lambda(0)/\lambda(T)]^2$, was found to follow the clean isotropic s-wave behavior predicted by the weak-coupling BCS theory in the whole temperature range (see Fig. 1.2). The low-temperature behavior of the London penetration depth fits the BCS analytic form as well and produces a value close to the weak coupling one of $\Delta(0)/(k_BT_c)$ = 1.71 [1].

[1] R. Gordon, N. Zhigadlo, S. Weyenet, S. Katrych, and R. Prozorov, Phys. Rev. B **87**, 094520 (2013)

1.2 Crystal growth of Mo_3Al_2C superconductor with noncentrosymmetric crystal structure

N. D. Zhigadlo, P. J. W. Moll, and B. Batlogg, in collaboration with D. Logvinovich (Laboratory of Crystallography, ETH Zurich)

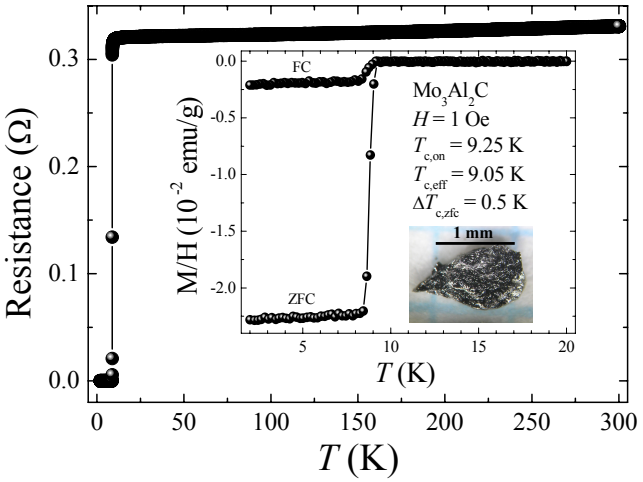

Figure 1.3: Temperature dependence of resistance and in the inset the magnetic susceptibility for Mo_3Al_2C single crystal. In magnetic measurements the data taken on heating after cooling in the absence of a field (zero-field cooling, ZFC), and on cooling (field cooling, FC) in an applied field of 1 Oe.

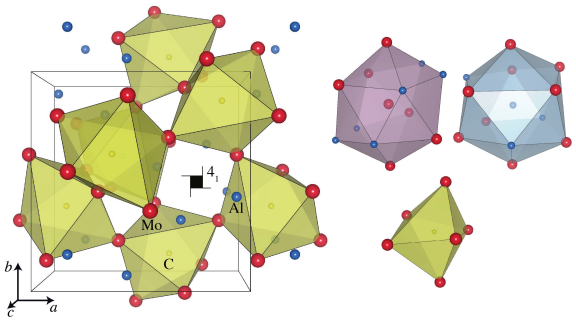

Figure 1.4: Crystal structure of Mo_3Al_2C (space group: $P4_132$) as viewed along c-axis and coordination polyhedra of the constituent atoms.

Single crystals of the noncentrosymmetric superconductor Mo_3Al_2C have been grown by high-pressure and high-temperature technique. The crystals show a superconducting transition at $\sim$ 9.3 K (Fig. 1.3). Single crystals x-ray refinement confirmed high structural perfection of the grown crystals. Structure type of Mo_3Al_2C corresponds to that of β-Mn: both Mo and Al atoms are in a distorted icosahedral and C atoms are in distorted octahedral coordinations built from metal atoms (Fig. 1.4). It is remarkable that Flack parameter values refined for all measured crystals using the model with the space group $P4_132$ were reproducibly close to either 0 or 1, which is a strong indication that the studied crystals correspond to two enantiomorphic space groups, $P4_132$ and $P4_332$.

1.3 High pressure synthesis and superconducting properties of $SrPt_3P$

N. D. Zhigadlo and B. Batlogg, in collaboration with R. Khasanov, P. Biswas, H. Luetkens, and A. Amato (PSI)

Polycrystalline samples of $SrPt_3P$ were synthesized using the cubic anvil high-pressure and high-temperature technique. In a typical run, the sample was first pressurized to 2 GPa and the temperature was ramped up in 2 h to the maximum value of 1050 °C, maintained for 20 – 40 h, and then decreased to room temperature in 1 h. All prepared samples demonstrate large diamagnetic response with the superconducting transition temperature of 8.5 K (see inset in Fig. 1.5). The temperature dependence of the upper critical field (B_{c2}) for two different samples are given in Fig. 1.5. There is a pronounced upward curvature of $B_{c2}(T)$ curve at $T \sim 6 - 6.5$K. Linear fits of $B_{c2}(T)$ in the vicinity of T_c and for T $\leq$ 6 K yield $dB_{c2}/dT = -0.45$ and -0.77 T/K, respectively. Such upward curvature of $B_{c2}(T)$ is often considered the consequence of two-band superconductivity. Indeed, the results of muon-spin rotation (μSR) studies of the magnetic penetration depth (λ) as a function of temperature and magnetic field suggest that $SrPt_3P$ is a multi-band superconductor with the equal gaps but different coherence lengths associated with the various bands.

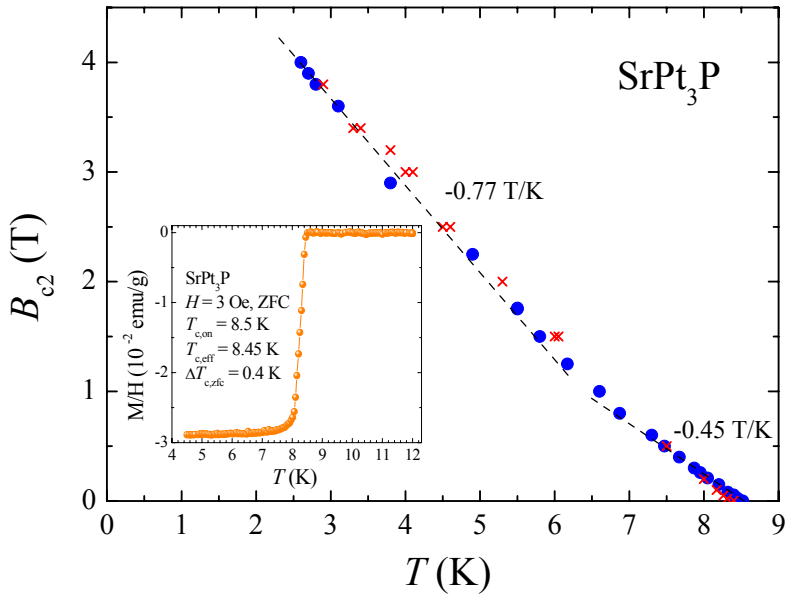

Figure 1.5: Temperature dependence of the upper critical field B_{c2} of $SrPt_3P$. The crosses and the circles correspond to two samples. The solid lines are linear fits of $B_{c2}(T)$ in the vicinity of T_c and for T $\leq$ 6 K. The inset shows the temperature dependence of the magnetic susceptibility.

1.4 High frequency modulation calorimetry for high magnetic fields and high cooling rates

S. Galeski and B. Batlogg

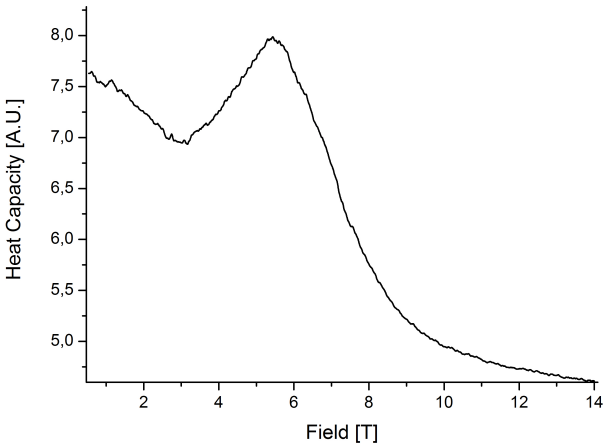

Figure 1.6: Specific heat anomaly of $TbMnO_3$ ferroelectric phase transition measured at 2 K with 23 kHz temperature oscilation.

The possibility of extending the range of conditions available for experiments has always been a driving force for development in physics. Recent developments of MEMS technology allows physicists to access realms previously inaccessible.

In particular membrane based nanocalorimetes allow one one to achieve sample heat capacity of nanogram samples with frequencies above 10kHz. This high frequency originates from the very small thermal mass of the sample and calorimeter cell allowing not only for high sampling rates but also for heating and cooling rates in the range of several thousand Kelvin per minute.

These features make membrane based calorimetry a very versatile tool that can be used for quenching in disorder in system such as spin glasses, fast mapping out of magnetic phase diagrams or even specific heat measurements in short (300 ms) magnetic field pulses.

1.5 Bulk and Interface Charge Transport in Rubrene Single Crystals

B. Blülle, R. Häusermann, P. Kerpen, and B. Batlogg

Charge transport in organic semiconductors is strongly influenced by the presence of trap states (trap DOS) in the band gap, often limiting the performance of semiconductor devices. Todays highly pure crystalline semiconductors can have extremely low density traps — comparable to best inorganic materials — building a promising base for studies of the intrinsic electronic properties of organic semiconductors.

We have performed temperature dependent charge transport measurements of rubrene single crystals using different device structures, allowing us to compare the hole mobility and the trap DOS from *bulk* measurements (space charge limited current measurements, SCLC) to transport properties in field-effect transistors (FET), where charge transport takes place along the *interface* to a gate dielectric. For this purpose we apply new methods to extract the spectral density of deep traps from the temperature dependence of the subthreshold swing [1]. The mobility in c-direction of the crystal is obtained from the charge carrier transit time seen in temperature dependent high frequency conductance measurements.

Our results show the trap DOS in organic FET devices to be in close agreement with the bulk trap density from SCLC measurements. Remarkably, this shows that no additional trap states are formed at the surface when a full FET structure is built, provided a proper dielectric material is employed.

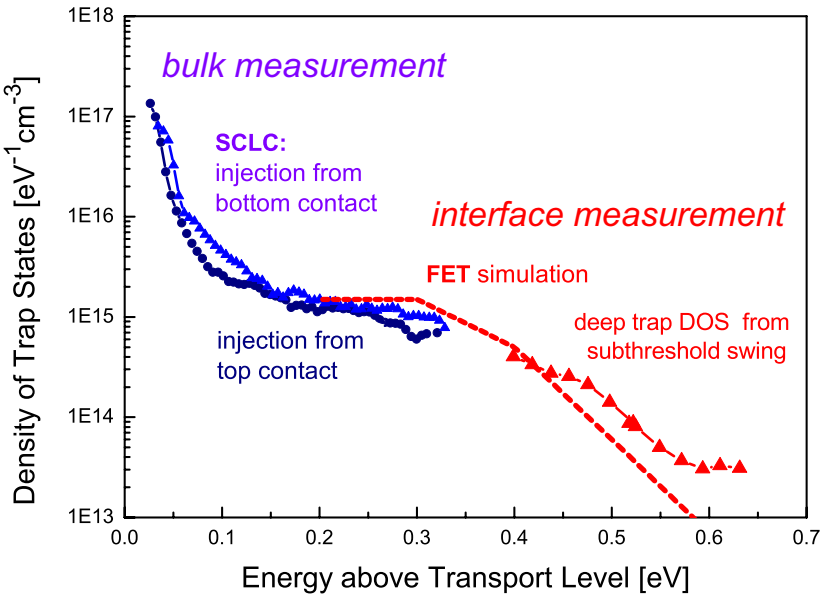

Figure 1.7: Comparison of typical trap density of states (trap DOS) in rubrene single crystals obtained from bulk transport measurements (space-charge limited current, SCLC) and from interface-dominated currents in a field-effect transistor geometry using Cytop as gate dielectric. The trap DOS obtained from FET transfer curves is in the same range as the lowest measured bulk trap densities, suggesting that no additional interface traps are created when the crystal is brought in contact with the Cytop gate dielectric.

[1] B. Blülle, R. Häusermann, and B. Batlogg, Phys. Rev. Applied **1**, 034006 (2014)

1.6 Measuring the Seebeck coefficient in organic semiconductors

K. Willa and B. Batlogg

Measuring the Seebeck coefficient in semiconductors is a powerful tool to gain information about charge tranport mechanisms. In organic semiconductors the mechanisms driving the charge transport are still under debate. Measuring the field dependent Seebeck coefficient of organic semiconductors allows to approach this problem from a new perspective.

We developed a measurement setup that is adapted to fulfil the demanding requirements of measuring the Seebeck coefficient in organic semiconductors. In particular, the measurements are conducted in an inert atmosphere. The contacts are applied by feather pins, replacing the usual glue-attached wires. Furthermore the temperature gradient is measured by on chip thermometry allowing precise results even for small temperature differences.

Seebeck measurements were conducted with this setup for Rubrene single crystals laminated on Cytop. The evaluation shows an exponential dependence of the Seebeck coefficient on the applied gate voltage reproducing the results of Pernstich et al. [1]. Using this setup, measurements can be performed on a wide range of other organic semiconductors leading to exciting possibilities of exploring the charge transport in these materials.

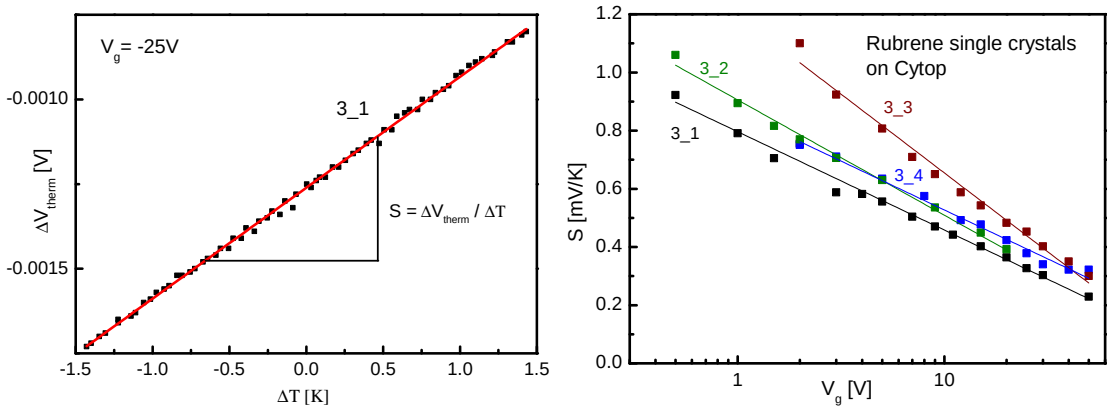

Figure 1.8: On the left hand side: Measurement of the thermal Voltage while varying the temperature gradient applied over a Rubrene single crystal with a fixed gate voltage of -25 V. The slope gives the Seebeck coefficient, which can be seen on the right hand side for several gate voltages and 4 different Rubrene single crystals laminated on Cytop.

[1] K. P. Pernstich, B. Rössner, B. Batlogg, Nature Materials **7**, 321 (2008)

1.7 Controlled charge transfer doping of organic crystals to observe impurity band transport

T. Mathis and B. Batlogg

The interface between the TTF donor molecule crystal and TCNQ acceptor molecule crystal, which are both insulating separately, shows sheet conductivity up to 0.1 mS. The formation dynamics was found to be not physical contact between the crystals but sublimation of molecules from the low sublimation temperature material TTF onto the TCNQ surface [1]. The conductivity increases gradually but at some point shows a jump, which we speculate is due to a percolation effect. At low conductivities a strong temperature dependence was found that was missing at higher conductivities. Therefore we distinguish two regimes: the thermally activated regimes and the weakly temperature dependence regime respectively. By controlled exposure to TTF molecules the TCNQ surface could be doped slowly and temperature dependent measurement performed at different doping levels. The transition between the two regimes was observed and shows a sharp change in behavior within a narrow doping difference. The activation energy extracted

from the resulting Arrhenius plots was found to be around 0.3 eV. This value depends only slightly on different doping levels, but it fell abruptly to zero when the transition into the weakly temperature dependent regime occurred. The impurity band transport observed here could be due to a shift of the Fermi energy into the HOMO band due to an increase in the density of state of the impurity band at 0.3 eV or due to a broadening and shifting of the impurity band level itself into the HOMO band, forming a mixed band state.

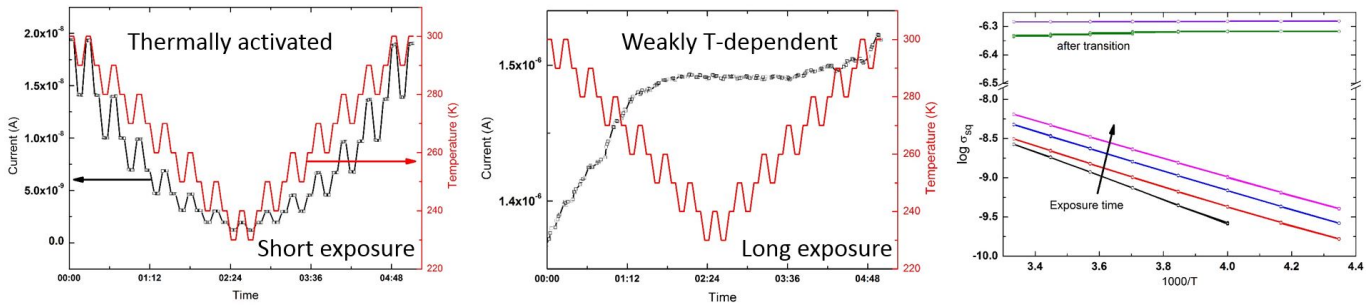

Figure 1.9: The left graph shows the thermally activated transport after short exposure while the center graph shows the same sample after long exposure to TTF molecules. A transition occurred between thermally activated and weakly temperature dependent transport. The right graph shows the conductivity at different temperatures for different exposure times. The transition can be observed by the disappearance of the slope after the transition. The activation energy before the transition in the thermally activated region is approximately 0.3 eV.

[1] T. Mathis, K. Mattenberger, P. Moll and B. Batlogg, Appl. Phys. Lett. **101**, 023302 (2012)

1.8 Monolithic integration of SiGe micro-crystals on deeply patterned Si CMOS substrates for high sensitivity X-ray pixel detector development

F. Isa, A. Jung and H. von Känel in collaboration with Y. Arroyo, R. Erni and P. Gröning (EMPA, Dübendorf, Switzerland), M. Meduňa (Masaryk University, Brno, Czech Republic), G. Isella (L-NESS and Politecnico di Milano, Como, Italy), F. Pezzoli, M. Salvalaglio and F. Montalenti (L-NESS and Università degli studi di Milano-Bicocca, Milano, Italy), and P. Niedermann (CSEM, Neuchâtel, Switzerland)

The growth of low defect density semiconductor material, lattice mismatched to the silicon substrate and differing in thermal expansion coefficients, is still a challenging problem in semiconductor heteroepitaxy. We approach this challenge growing SiGe alloys on deeply patterned silicon substrates by low-energy plasma enhanced chemical vapour deposition, yielding space-filling arrays of closely separated SiGe micro-crystals, as reported in Fig. 1.10 **a)**. Threading dislocations (TDs) escape through the sidewalls such that strain and defect-free crystals are obtained. In addition, crack formation and wafer bowing due to thermally induced stress is avoided.

Thanks to the complete elimination of TDs and full stress relaxation, the SiGe/Si micro-crystals could be successfully used for the integration of high quality Ge/SiGe quantum wells (QWs). Indeed, as reported in Fig. 1.10 **b)**, the QW X-ray diffraction peak FWHM is comparable to that one of the Si substrate. Photoluminescence measurements also confirm that the optical quality of Ge/SiGe QWs on Si pillars by far overwhelms that one of analogous nanostructures deposited on state of the art SiGe/Si(001) planar buffers (see Fig. 1.10 **c)**).This innovative approach is suitable to fabricate high sensitivity X-ray pixel detectors, which requires thick SiGe crystals as absorbing material, monolithically integrated onto Si CMOS substrates with readout electronics.

Besides the epitaxial growth of SiGe/Si crystals, our work includes device fabrication, structural and electrical characterization. We analyze the performance of the absorbing layer by *in-situ* electrical characterization of individual SiGe/Si crystals by means of a micro-probe inside a scanning electron microscope (SEM) chamber (see Fig. 1.10 **d)**).

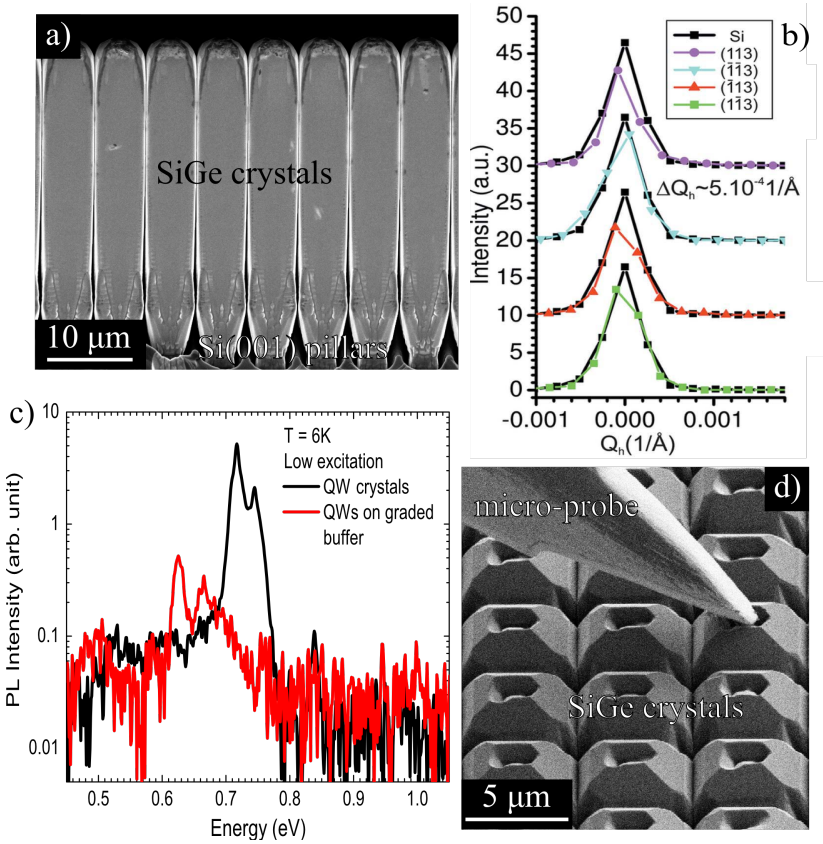

Figure 1.10: **a)** Cross-sectional SEM picture of a regular array of SiGe micro-crystals epitaxially deposited on deeply patterned Si(001) substrate. **b)** Quantum well (004) X-ray diffraction peak FWHM for different facet orientations and Si substrate [M. Meduňa *et al.*, J. Appl. Cryst. **47**, 2030 (2014)]. **c)** Photoluminescence spectra of Ge/SiGe MQWs on Si pillars (black curve) and on state of the art planar SiGe buffer (red curve) [1]. **d)** SEM picture of the micrometer-sized metallic probe used to perform electrical characterization of individual SiGe/Si crystals.

[1] F. Pezzoli *et al.*, Phys. Rev. Applied **1**, 044005 (2014)

1.9 Defect reduction in epitaxial SiC on Si by Deep Substrate Patterning

T. Kreiliger, H. von Känel in collaboration with Leo Miglio (PileGrowth Tech srl, Como, Italy; and L-NESS, Dept. Material Science, University Milano Bicocca, Milano, Italy), Danilo Crippa (LPE spa, Baranzate, Italy), Marco Mauceri, Marco Puglisi (Epitaxial Technology Center srl, Catania, Italy), Fulvio Mancarella (CNR-IMM, Bologna, Italy), Ruggero Anzalone, Nicolo Piluso, and Francesco LaVia (CNR-IMM, Catania, Italy)

Direct hetero-epitaxial growth of cubic silicon carbide (3C-SiC) on silicon (Si) substrates would enable the industry to fabricate power electronic devices on large Si wafers at lower costs. However, the lattice mismatch of $\sim 20\%$ between the 2 materials involved leads to high stacking fault (SF) defect densities and therefore leakage currents through the devices. Furthermore, the $\sim 8\%$ difference of thermal expansion coefficients induces severe wafer bowing or even layer cracking as soon as the SiC layer thickness reaches dozens of micrometers or more, as needed for device applications. In order to tackle both these issues we extended a recently developed concept for the epitaxial growth of germanium on Si (by low-energy plasma enhanced CVD) to the case of SiC on Si (by low-pressure CVD). That is the self-limited lateral expansion of individual epitaxial crystals on deeply patterned Si substrates, which substantially reduces wafer bowing and crystal defect propagation.

A FIB cross-section through such a structure is shown in panel a) of the figure below, consisting of ~ 11 μm thick 3C-SiC grown onto Si(001), 6° off-cut towards [110], substrates which are patterned into 8 μm high and 5 μm wide ridges having 5 μm gap in between. At the beginning of the growth the gap shrinks but then saturates, avoiding the

fusion of neighboring SiC ridges and therefore reducing wafer bowing after cooling down. A more closer look to a cleaved cross-section of a similar structure is shown in panel b), where numerous faint bright lines are visible. These are SF defects originating from the SiC/Si interface and propagating along $\{111\}$ planes. Depending on the aspect ratio between height and width of the SiC ridge, part of the SF end at the sidewall and do not propagate any further upwards. A limiting case of 12 μm high SiC ridges grown on 8 μm wide Si ridges, spaced by 7 μm is shown as a top-view in panel c). The aspect ratio of these SiC structures is just small enough for the last few SF defects lying in $\{111\}$ planes parallel to the ridges to reach the top surface near the edges. First results on fused SiC ridges with high enough aspect ratio before fusion show a significant reduction of the density of SF laying parallel to the ridges, while the SF density in $\{111\}$ planes perpendicular to the ridges is hardly affected. Future work will include not only growth on Si ridges, but also on Si pillar structures which will lead to SiC towers with gaps in both lateral dimensions, lowering the SF density in all 4 possible $\{111\}$ planes.

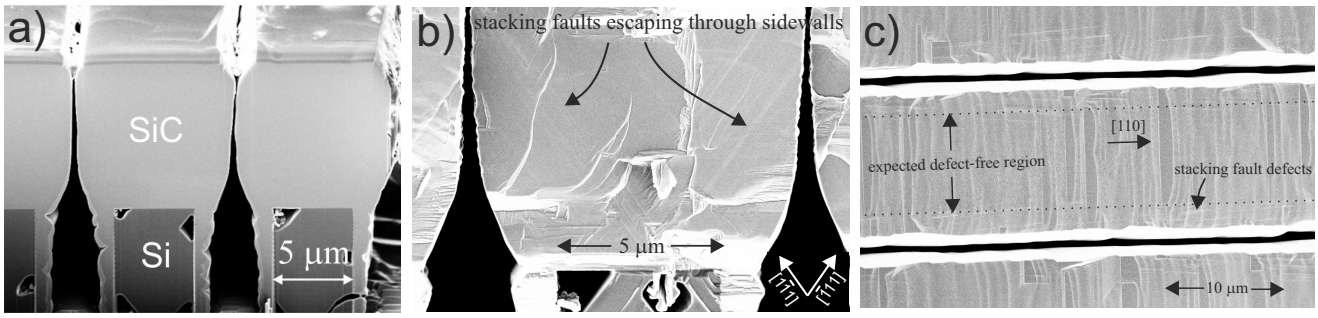

Figure 1.11: SEM images of a) perspective FIB cross-section of SiC grown on Si ridges; b) cleaved cross-section near SiC/Si interface with SF defects visible as faint bright lines; c) top-view of miscut SiC surface, showing SF defects parallel to ridges only in the border region.

1.10 Growth of GaAs on Si nanopatterns

I. Prieto and H. von Kaenel in collaboration with: O. Skibitzki, G. Capellini and T. Schroeder (IHP) R. Kozak, M. D. Rossell, R. Erni, R. Kaufmann, A. Neels, A. Domann, and G. L. Bona (EMPA)

Si and GaAs are dominant materials in microelectronics and optoelectronics, respectively. Their integration in epitaxial heterostructures is expected to provide superior device performance. At the highest level of device integration, a control on the selective area growth is required in order not to alter the performance of the lasers, detectors or modulators on electronic Si-chips.

The early stages of the GaAs nucleation on Si has a three-dimensional character (Fig. 1.12) through a well process and referred to as Volmer-Weber mechanism. The epitaxial growth of GaAs directly on Si is, however, a non-trivial endeavour due to their different structural and thermal characteristics, as well as their polarity mismatch, which leads to misfit dislocations, antiphase domains and other defects.

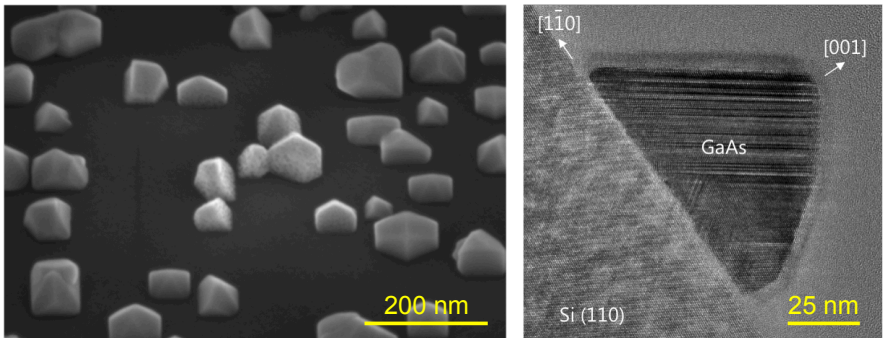

Figure 1.12: Three dimensional nucleation of GaAs on Si. **left** SEM image showing GaAs islands on a Si(001) substrate, **right** TEM image showing a single GaAs particle.

In order to maximize the performance of the GaAs crystals, previous works of our group made use of the aspect ratio

trapping technique by growing GaAs on arrays of μm-sized Si-pillars with an intermediate Ge-layer. The incorporation of a Ge-interlayer in between the Si and the GaAs resulted in a substantial reduction of defects in the structure, thus giving rise to high quality GaAs crystals [1].

One step forward towards the achievement of defect free growth of GaAs/Si consists of the nucleation of GaAs on nm-sized Si features embedded in a SiO_2 matrix. We have used 50 – 80 nm wide Si-nanopillar arrays with SiO_2 passivated sidewalls embedded in a SiO_2 matrix. Selective growth of GaAs on those nm-sized Si-openings was demonstrated (Fig. 1.13), thus providing the possibility to produce epitaxial defect-free GaAs crystals directly on Si(001).

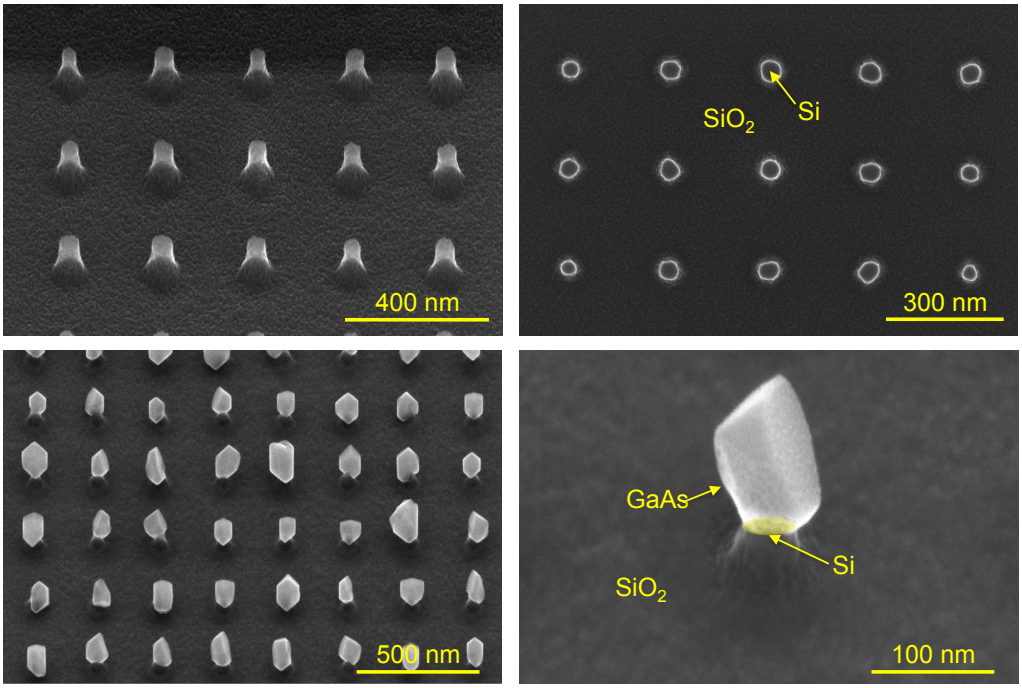

Figure 1.13: Selective area growth of GaAs on Si nm-sized pillars. **top–left** Angled and **top–right** top view of an array of Si–pillars, **bottom–left** Angled view of an array of GaAs crystals selectively grown on the Si–pillars, **bottom-right** Close–up of a single GaAs–Si system. The shadowed region represents the size and the location of he Si–pillars.

[1] A. G. Taboada *et al.*, Appl. Phys. Lett. **104**, 022112 (2014)

Chapter 2

Physics of mesoscopic structures, semiconductor nanostructures

(http://www.nanophys.ethz.ch)

Head
Prof. Dr. K. Ensslin
Prof. Dr. T. Ihn

Academic Staff

J. Arrieta	H. Atci	S. Baer
Dr. J. Basset	D. Bischoff	B. Bräm
M. Eich	P. Butti	T. Choi
S. Hellmüller	S. Hennel	A. Hofmann
M. Karalic	Dr. A. Kozikov	T. Krähenmann
Dr. V. Maisi	S. Müller	F. Nichele
H. Overweg	Dr. A. Pal	N. Pascher
Dr. C. Rössler	P. Simonet	R. Steinacher
A. Stocklauser	Dr. Y. Tian	A. Varlet

Master Students

M. Eich (HS 2014)	S. Hennel (FS 2014)
M. Karalic (HS 2014)	E. Kuznetsova (FS 2014)
P. Sohi (HS 2014)	D. Windey (HS 2014)
C. Winterhalter (FS 2014)	

Technical Staff

C. Barengo	P. Märki

Administrative Staff

C. Vinzens	C. Egli

Academic Guests
A. Hüseyin (01.09.2014 – 31.08.2015)

NCCR QSIT

Dr. I. Blatter	S. Künzel	Dr. J. Rössler

2.1 Quantum effects in a solid state environment

Semiconductors offer the unique ability to control the carrier density and therefore the position of the Fermi energy by tuning a gate voltage. In bilayer graphene not only the Fermi energy, but also the band structure as a whole can be tuned. In our group we have focused on the investigation of various quantum effect in order to better understand and control quantum systems in view of prospects for quantum information processing.

The coupled quantum well system InAs/GaSb embedded between AlSb barrier offers a peculiar band structure, where the conduction band of InAs can be below the valance band of GaSb. This fact has been know for decades and is now exploited in order to build tuning topological insulators from this material system. We have built gate tunable Hall bars and found a giant non-local response in the quantum Hall regime, which can be explained by the coexistence of and scattering between electron and hole-like edge states.

The integer and fractional quantum Hall effect is usually explained by an edge state picture. Using the tip of a scanning gate microscope we have examined the local position of and coupling between quantum Hall edge states in a point contact configuration. This experimental methods was also used to investigate quantum interference with a local probe.

The fractional quantum Hall effect has been examined using lateral constrictions and pronounced localization phenomena have been observed as a function of constriction width and magnetic field.

Quantum point contacts in p-type GaAs were investigated as a function of magnetic fields of various orientations. Peculiar crossings and anti-crossings of quantized conductance features were observed and explained in detail by a model considering spin-orbit effects for holes.

Bilayer graphene with vertical displacement fields as large as 1 V/nm displayed a Lifshitz transition, i.e. a tunable topology of the Fermi surface. Using Fabry-Perot resonances we could shown that anti-Klein-tunneling known from untapped bilayer graphene is suppressed for large displacement fields.

Localization in graphene naostructures is related to disorder. By fabricating and measuring ultra-short graphene constriction on clean and flat boron nitride substrates we have shown, that edge disorder plays a dominate role for the observed localization phenomena.

High-quality quantum dots fabricated in AlGaAs heterostructures were coupled ballistically. We demonstrated that equilibrium and non-equilibrium charge transfer can be analyzed with energy resolution.

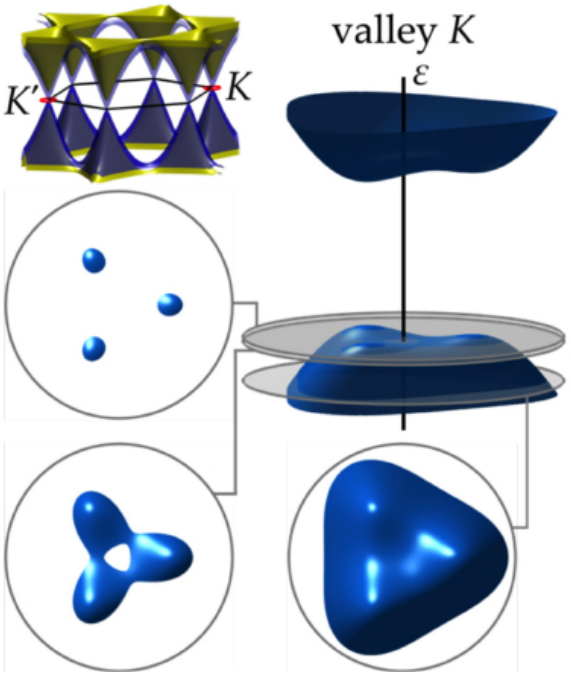

Figure 2.1: Bilayer graphene band structure. top left: The whole Brillouin zone up to 3 eV from the neutrality point, including low-energy bands (blue) and split bands (yellow). right: Valley K dispersion near the valence-band top in gapped bilayer graphene. In valleys K and K', the dispersion is inverted as a result of time-reversal symmetry. Insets show characteristic cross sections of constant energy surfaces.

Chapter 3

Dynamics of strongly correlated materials

(http://www.dscm.ethz.ch)

Head

Prof. Dr. Joël Mesot
Prof. Dr. Hans-Rudolf Ott

Academic Staff

Dr. Toni Shiroka
Marek Pikulski
Lukas Korosec (from 10.2014)
Nicolò Barbero (from 11.2014)

Master Students

Lukas Korosec (end 06.2014)
Federico Eggenschwiler (end 04.2014)

Administrative Staff

Gabriela Strahm
Claudia Vinzens

3.1 Pressure-tuning of $Cu(pz)_2(ClO_4)_2$ magnetic properties: An NMR study

N. Barbero, T. Shiroka, H.-R. Ott, and J. Mesot
in collaboration with C. P. Landee and S. Davis (Clark University, Worcester, MA, USA)

$Cu(pz)_2(ClO_4)_2$ (with *pz* denoting pyrazine $C_4H_4N_2$) is a two-dimensional spin-$^1/_2$ square-lattice antiferromagnet [1]. In comparison with the dominant intralayer interaction [2], the Cu-(pz) planes interact only weakly. Nevertheless, the orientation of the perchlorate counter-ions and the shearing distortions of the pyrazine rings play a key role in the magnetic properties of this two-dimensional magnet [3] by inducing a 3D-ordered spin structure at low temperature. Below the magnetic-ordering transition temperature a collinear spin arrangement is adopted, with the magnetic moments aligned along either the b or c crystallographic axis and subject to strong quantum fluctuations [4].

It is well established that the onset of such transitions at T_N can be influenced by varying external parameters such as magnetic field and pressure. The $[H, T]$ phase diagram has been established in previous works. In this project we attempt to map the $[p, T]$ phase diagram instead and the first results have recently been obtained.

The generation of external pressure in the range between 0 and 18 kbar is achieved by using a cell with a CuBe casing and MP35N alloy pistons. The pressure calibration is obtained from monitoring the ^{63}Cu NQR frequency of Cu_2O [5]. Preliminary ^{35}Cl NMR spin-lattice relaxation rate data $T_1^{-1}(T)$ demonstrate that T_N of $Cu(pz)_2(ClO_4)_2$ varies significantly with external pressure.

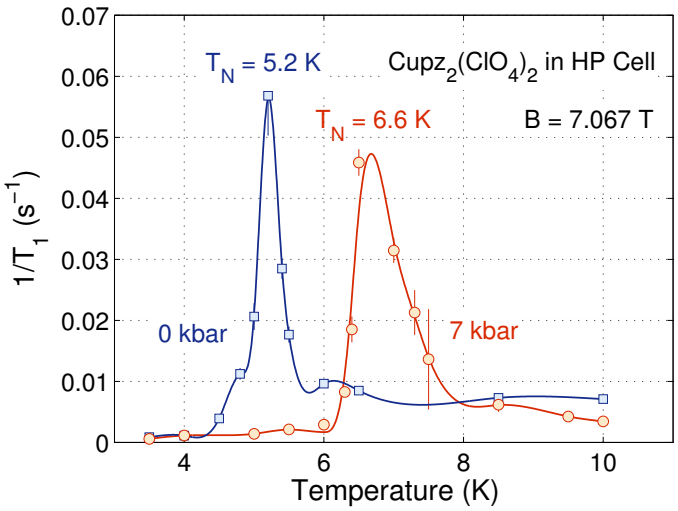

Figure 3.1: The inverse of the ^{35}Cl NMR spin-lattice relaxation time as a function of temperature at two different pressures (0 and 7 kbar) shows a substantial shift of the magnetic ordering temperature.

[1] J. Darriet *et. al.*, Inorg. Chem. **22**, 2679 (1979)
[2] F. Xiao *et al.*, Phys. Rev. B **79**, 134412 (2009)
[3] S. Vela *et al.*, Inorg. Chem. **52**, 12923 (2013)
[4] N. Tsyrulin *et al.*, Phys. Rev. B **81**, 134409 (2010)
[5] A.P. Reyes *et al.*, Rev. Sci. Instr. **63**, 3120 (1992)

3.2 Rare-earth nickelate perovskites $RNiO_3$

L. Korosec, M. Pikulski, T. Shiroka, H.-R. Ott, and J. Mesot
in collaboration with M. Medarde (PSI Villigen)

The rare-earth nickelate perovskites $RNiO_3$ are a family of correlated-electron materials which crystallize in the $GdFeO_3$-type orthorhombically-distorted perovskite structure.They are known to exhibit structural, electronic, and magnetic phase transitions as a function of the rare-earth ion radius (or perovskite tolerance factor) and temperature [1,2]. We are interested in the metal-insulator and magnetic-ordering transitions known to occur in $RNiO_3$ for R $\neq$ La at temperatures between 130–600 K and 130–225 K, respectively.

The metal-insulator transition is accompanied by a structural change from an orthorhombic to a monoclinic lattice. This distortion causes the appearance of two structurally inequivalent Ni sites at alternating positions in every direction. The inequivalent Ni sites are exposed to very different local electronic structures. Therefore, local probes such as NMR can give interesting new information on these materials.

Below the Néel temperature, antiferromagnetic order of the Ni magnetic moments occurs at a wavevector $k = (1/4, 1/4, 1/4)$ in the cubic perovskite unit cell, corresponding to an "up up down down" magnetic structure.

It has been shown that also $TlNiO_3$ exhibits very similar physical properties as the rare-earth nickelates. However, its magnetic structure in the antiferromagnetic phase has not yet been uniquely determined [3].

We study the $RNiO_3$ family by ^{17}O nuclear magnetic resonance (NMR) and $TlNiO_3$ by analogous experiments probing the ^{203}Tl and ^{205}Tl nuclei. Our goals are to understand the different local electronic structures at inequivalent Ni sites in the insulating phase, and to establish the magnetic structure of $TlNiO_3$ below T_N. The first NMR experiments on $TlNiO_3$ have been successfully performed as part of a Master thesis in our laboratory [4].

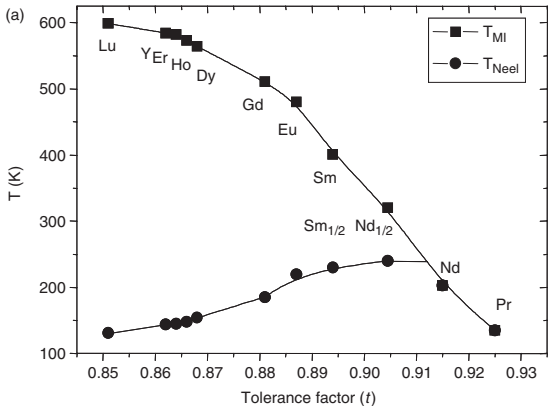

Figure 3.2: Phase diagram of the $RNiO_3$ family (adapted from [2]).

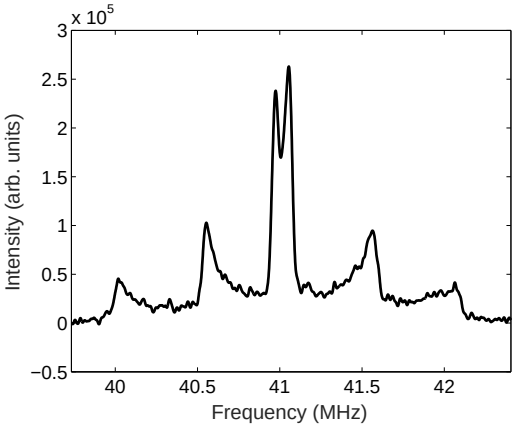

Figure 3.3: ^{17}O-NMR spectrum of $PrNi^{17}O_3$ as recorded at room temperature.

[1] M. L. Medarde, J. Phys.: Condens. Matter **9**, 1679 (1997)
[2] G. Catalan, Phase Transitions **81**, 729 (2008)
[3] S. J. Kim, Chem. Mater. **14**, 4926 (2002)
[4] L. Korosec, Master thesis, ETH Zurich (2014)

3.3 NMR investigation of the magnetism in $BiCu_2PO_6$ in high magnetic fields

M. Pikulski, T. Shiroka, H.-R. Ott, and J. Mesot

in collaboration with A. P. Reyes and P. L. Kuhn (NHMFL, Tallahassee, FL, USA)

The networks formed by the magnetic Cu^{2+} ions in the strongly-correlated material $BiCu_2PO_6$ are quasi-one-dimensional and it has been shown that they can be modeled as antiferromagnetic two-leg Heisenberg spin-1/2 ladders with frustrating next-nearest-neighbor couplings [1]. The elementary spin-excitations are triplet-like and gapped. When an external magnetic field is applied, the excitations are softened, giving rise to an unusual variety of magnetic phases (Fig. 3.4).

We focused on the case where the magnetic field is applied along the ladder legs. In this orientation, the first field-induced phase transition occurs at 20 T and nuclear magnetic resonance (NMR) is one of the few microscopic probes available at such high magnetic fields. In the past, NMR was successfully applied by our group to study the peculiar magnetic state adopted above the first critical field. The data were explained in terms of a lattice arrangement of field-induced solitons, i.e., quantum domain-walls resulting from the fractionalization of the triplet-like magnetic excitations [3]. The results were corroborated by a theoretical model, which also predicted an additional phase transition at an even higher magnetic field. Such a transition has indeed been observed by bulk experiments at ~ 34 T.

In order to investigate the magnetic order adopted above this second critical field, ^{31}P-NMR experiments were performed in the 45-T hybrid magnet at the DC-field facility of the National High Magnetic Field Laboratory (NHMFL) in Tallahassee, USA. Our data confirm the occurrence of the anticipated instability and the change in the magnetic structure of the compound is clearly reflected by the NMR-spectra. We are currently working to extend our existing model in order to explain the new results.

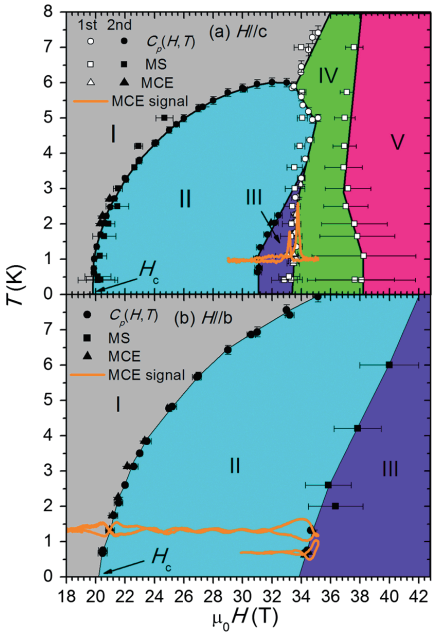

Figure 3.4: Phase diagram of $BiCu_2PO_6$ [2]. The magnetic-field orientation in our experiments was $H \parallel b$, corresponding to the lower panel of the figure.

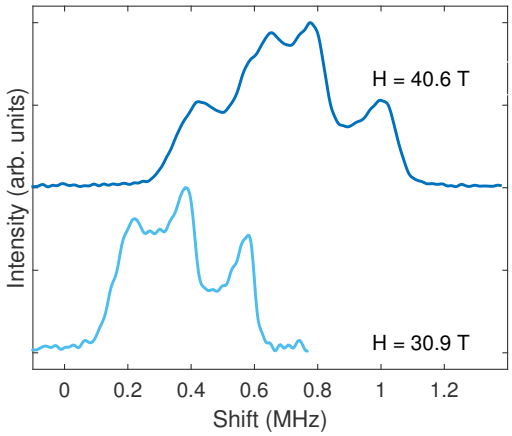

Figure 3.5: ^{31}P NMR spectra in $BiCu_2PO_6$ measured above and below the field-induced transition between the phases II and III.

[1] A. Tsirlin *et al.*, Phys. Rev. B, **82**, 144426 (2010)
[2] Y. Kohama *et al.*, Phys. Rev. Lett., **109**, 167204 (2012)
[3] F. Casola *et al.*, Phys. Rev. Lett., **110**, 187201 (2013)

3.4 Superconductivity in $SrPt_3P$: An NMR study and comparison with non-centrosymmetric $LaPt_3Si$ and $CePt_3Si$

T. Shiroka, H.-R. Ott, M. Pikulski, and J. Mesot
in collaboration with N. D. Zhigadlo and B. Batlogg (ETH Zurich)

The unusual properties of *non-centrosymmetric* superconductors, characterized by sizable antisymmetric spin-orbit couplings due to the lack of crystalline inversion symmetry, have attracted considerable interest [1]. However, the exact origin of their unconventional behaviour remains an open question. To identify the special features of this class of superconductors, we studied the properties of the *centrosymmetric* compound $SrPt_3P$ [2] and compared them with available results for $LaPt_3Si$ ($T_c = 0.6$ K) [3] and $CePt_3Si$ ($T_c = 0.75$ K) [4], which both adopt a crystal structure that only differs in the arrangement of the Pt octahedra from that of $SrPt_3P$.

Normal and superconducting properties of $SrPt_3P$ ($T_c = 8.5$ K) were investigated via ^{31}P NMR and magnetometry, which indicate a weakly correlated normal state and an s-wave type superconductivity [5]. A sharp drop of the (metallic) Knight shift below T_c, associated with a concomitant steep increase of the linewidth and a Hebel-Slichter type variation of the $1/(T_1T)$ ratio, are all consistent with an s-wave pairing in $SrPt_3P$.

While $SrPt_3P$ and $LaPt_3Si$ follow a perfect Korringa law down to T_c, the $1/(T_1T)$ ratio of $CePt_3Si$ increases upon cooling, indicating the development of $4f$-derived magnetic fluctuations. Electronically, both $SrPt_3Si$ and $LaPt_3Si$ are simple metals. The former exhibits conventional type-II superconductivity, while the nature of the superconducting state of the latter is not well established. The superconductivity of $CePt_3Si$ emerges from a heavy-electron state co-existing with antiferromagnetic order. The key differences between the considered centro- and non-centrosymmetric superconductors seem to be due to both the symmetry of the crystal lattice and to the cations of the chemical composition of the compounds.

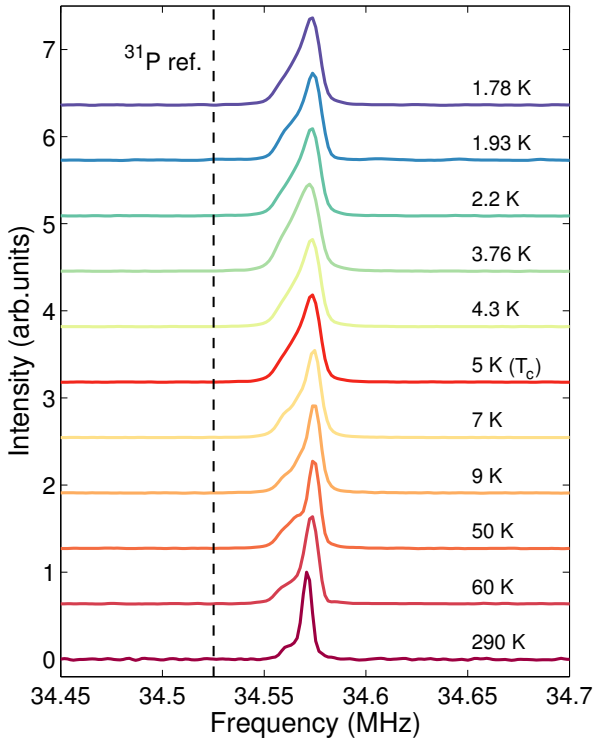

Figure 3.6: Representative ^{31}P NMR line shapes in $SrPt_3P$ at $\mu_0 H = 2.0$ T and temperatures in the range 1.75 to 290 K. The increasing line width and asymmetry below 5 K reflect the onset of the superconducting phase.

[1] E. Bauer and M. Sigrist, *Non-Centrosymmetric Superconductors*, LNP **847** (Springer, Berlin, 2012)
[2] T. Takayama *et al.*, Phys. Rev. Lett. **108**, 237001 (2012)
[3] M. Yogi *et al.*, Phys. Rev. Lett. **93**, 027003 (2004)
[4] M. Yogi *et al.*, J. Phys. Chem. Solids **67**, 522 (2006)
[5] T. Shiroka *et al.*, submitted to Phys. Rev. B

3.5 Magnetism vs. superconductivity in LaFeAsO with low H-doping level

T. Shiroka - in collaboration with

G. Lamura, F. Caglieris, M. R. Cimberle, and M. Putti (CNR-SPIN and Università di Genova, Italy)

P. Bonfà and R. De Renzi (Dipartimento di Fisica and Unità CNISM, Università di Parma, Italy)

S. Sanna (Dipartimento di Fisica and Unità CNISM, Università di Pavia, Italy)

S. Iimura and H. Hosono (Frontier Research Center, Tokyo Institute of Technology, Yokohama, Japan)

The evolution of the LaFeAsO ground state with negative charge doping has been the object of intense studies and, even to date, many interesting issues are still open. Unlike most Ln-1111 compounds, at low-charge doping the La system displays an abrupt first-order-like transition from a magnetic (M) to a superconducting (SC) phase [1]. This classification, originally based on nominal F-doping values, most probably reflects the initial difficulties in fine tuning the fluorine content in the narrow doping range $0.04 < x(\mathrm{F}) < 0.05$ where such a transition occurs. The lack of reliable compositional data has, therefore, put into question the anomalous behaviour of the La-system near the magnetic-to-superconducting crossover, with a second-order-like transition being the naturally expected (but never observed) type of transition.

To address the above issue we carried out an extensive study on two H-doped samples [2] with nominal hydrogen content $x(H) = 0.01$ and 0.05 by using dc resistivity, magnetometry and muon-spin spectroscopy [3]. Although counterintuitive, hydrogen seems to adopt a -1 charge state, realizing a similar (or better) electron doping in the LaO planes. The analysis of μSR data allowed us to establish a full equivalence between hydrogen and fluorine doping, with our results being in very good agreement with those of $x(F)$. Surprisingly, in the $x(H) = 0.05$ case, we found a short-range magnetically ordered phase, which extends over the whole sample volume and which coexists with bulk superconductivity. This unexpected result suggests a probable second-order-like M-SC phase transition. In addition, it hints that the presence of an M-SC crossover region could be a universal feature of the electron-doped Ln-1111 pnictides.

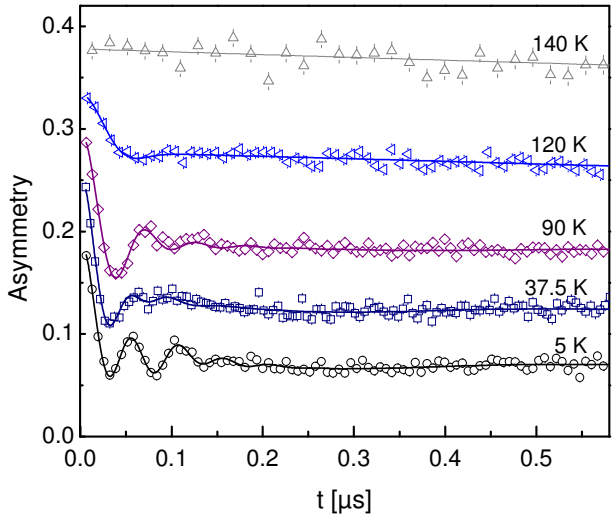

Figure 3.7: Zero-field μSR short-time spectra of $LaFeAsO_{1-x}H_x$ for $x = 0.01$ at selected temperatures. The highly damped oscillations observed at low temperatures are due to a superposition of different muon precession frequencies in the antiferromagnetic phase. The flat behaviour above 140 K indicates a transition to the paramagnetic phase.

[1] H. Luetkens et al., Nature Materials **8**, 305 (2009)
[2] S. Iimura et al., Nature Communications **3**, 943 (2012)
[3] G. Lamura, T. Shiroka, et al., J. Phys.: Cond. Matter **26**, 295701 (2014)

Chapter 4

Optical and Magneto-optical Spectroscopy

(http://www.spectro.ethz.ch)

Head
Prof. Dr. L. Degiorgi

Academic Staff
Dr. C. Mirri
A. Dusza (until April 2014)
M. Chinotti (since October 2014)

Administrative Staff
I. Mettler (until August 2014)
F. Steck (since August 2014)

4.1 Hysteretic behavior in the optical response of the underdoped Fe-arsenide - $Ba(Fe_{1-x}Co_x)_2As_2$ in the electronic nematic phase

C. Mirri, A. Duzsa, and L. Degiorgi

work in collaboration with I.R. Fisher and Geballe Laboratory for Advanced Materials and Department of Applied Physics, Stanford University, Stanford, California 94305-4045, U.S.A. and Stanford Institute for Materials and Energy Sciences, SLAC National Accelerator Laboratory, 2575 Sand Hill Road, Menlo Park, California 94025, U.S.A.

The tetragonal-to-orthorhombic structural phase transition at T_s, coincident or preceding the onset of an antiferromagnetic ground state at T_N, in the underdoped regime of many families of iron-pnictide and chalcogenide superconductors breaks the four-fold rotational symmetry of the tetragonal phase, implying the onset of a nematic phase. The relevance of nematicity, either electronic in nature or spin-induced, in shaping their phase diagram is certainly one of the most debated issue nowadays. Several experiments provide evidence for nematicity in iron-pnictides, as dc transport, thermopower, elastic shear-modulus also combined with nuclear magnetic resonance (NMR) results, neutron scattering, angle-resolved photoemission spectroscopy (ARPES), local probes such as scanning tunneling microscopy (STM) and magnetic torque, time-resolved spectroscopy, optical reflectivity and Raman spectroscopy.

Detailed quantitative measurements of the in-plane charge and spin anisotropy in the nematic phase have been mainly performed on the so-called 122 family of iron-pnictides, like $Ba(Fe_{1-x}Co_x)_2As_2$ on which we focus here our attention. Since the ferroelastic-like structural transition induces in these materials the formation of dense structural twins below T_s in order to minimize the elastic energy, applying large magnetic fields or uniaxial pressure turns out to be essential in order to detwin the specimens and thus to overrule the overcasting effect of randomly oriented domains when addressing the in-plane anisotropy of the orthorhombic phase over length scales greater than the average twin dimensions.

To enable our experiments, we have designed a novel pressure device, allowing us to perform optical reflectivity ($R(\omega)$) measurements as a function of temperature under a variable in-plane uniaxial stress, thus with adjustable population of the two twin orientations. The device consists of a sealed spring bellows, which can be expanded or retracted by varying the pressure of He-gas held inside, so that uniaxial stress on the lateral edge of the specimen can be tuned $in-situ$. Our as-grown single crystals were cut into rectangular pieces with the tetragonal a-axis oriented at 45^0 to the edges of the sample so that the direction of the applied stress lies parallel to the orthorhombic a and b axes. For compressive stress the shorter b-axis is preferentially aligned along the direction of the stress. The $R(\omega)$ spectra were collected with the electromagnetic radiation polarized perpendicular or parallel to the applied stress (i.e. along the majority a- or b-axis); in the following defined as $R_a(\omega)$ and $R_b(\omega)$, respectively. Here, we report results obtained from zero-pressure-cooled (ZPC) 'pressure-loop' experiments: we reach the selected temperature (T) without applying pressure (p) and at that fixed T we measure $R(\omega)$ at progressively increasing p from 0 up to a maximum pressure ranging between 0.8 and 1.2 bar, depending from the Co-doping. We subsequently collect $R(\omega)$ when stepwise releasing p back to 0 bar, thus completing the p-loop.

We focus our attention on the MIR spectral range, since clear signatures of the optical anisotropy have been previously recognized at those energies in experiments with samples constantly held under uniaxial stress. Fig. 4.1 displays a sampling of $R(\omega)$ data at 10 K and p = 0.8 bar in the MIR range as well as $R_{ratio}(p) = R_a/R_b$ at 10 K within the ZPC p-loop experiment for the x = 0% Co-doping compound. The results are very much representative for the underdoped regime.

It is well established that the real part $\sigma_1(\omega)$ of the optical conductivity displays a characteristic mid-infrared feature, peaked for twinned samples at frequencies (ω') between 900 cm^{-1} for x = 4.5% and 1500 cm^{-1} for x = 0% Co-doping (vertical dotted lines in upper right panel (f) of Fig. 4.2). Furthermore, this excitation turns out to be very much related to the onset of the SDW-like state in the orthorhombic phase and its polarization dependence was previously identified as the most evident signature of the pressure-induced optical anisotropy. We can thus identify ω' as a relevant energy scale where to read R_{ratio}. In order to comprehensively deploy our findings for the ZPC p-loop experiment, we show indeed in Fig. 4.2(a-e) the pressure dependence for x = 0% and 4.5% Co-doping of $\Delta R_{ratio} = R_{ratio}$-1, defining the deviation from the isotropic case (i.e., R_{ratio} = 1), at ω' and at temperatures above/below T_s. Fig. 4.2 thus allows a

comparison between two Co-dopings of the title compounds, spanning the underdoped regime of their phase diagram. The pressure dependence of ΔR_{ratio} for both compositions is rather similar at equivalent temperatures with respect to T_s, even though there is an overall depletion of ΔR_{ratio} upon doping.

We first point out some common features for all Co-dopings in $\Delta R_{ratio}(p)$ at $T << T_s$. When increasing the applied pressure up to 0.2 bar there is yet a moderate increase of ΔR_{ratio}, which is then progressively enhanced for pressures around and exceeding 0.4 bar. The saturation in ΔR_{ratio} for different Co-dopings is observed to set in for applied pressures above 0.6 bar. The saturation presumably reflects when the samples are fully detwinned. Simultaneously, there is an overall decrease of the achieved optical anisotropy at saturation for increasing Co-doping. By releasing pressure back to zero and consequently by removing $in-situ$ the stress, the anisotropy clearly persists and hence a remarkable imbalance of the two twin orientations remains frozen in place at $T << T_s$. ΔR_{ratio} at zero released pressure could be then considered as a direct measurement of the optical anisotropy in a single domain specimen even in the absence of any applied stress. At $T << T_s$, there is thus a clear half-hysteresis behavior of $\Delta R_{ratio}(p)$, which is squeezed upon Co-doping at equivalent T. Such a hysteretic behavior in detwinned iron-pnictides obviously bears a striking similarity with the situation in ferromagnets as far as the magnetization versus external magnetic field at $T << T_C$ (T_C being the Curie temperature) is concerned. In this context, we may coin the notions of 'initial anisotropy- or virgin-curve' and of 'remanent anisotropy' in order to define the evolution of ΔR_{ratio}, representing here the optical anisotropy, upon rising and releasing pressure, respectively.

By increasing T towards T_s, we observe, commonly to all Co-dopings, a narrowing of the hysteretic behavior, which fully collapses at $T \sim T_s$. Moreover, at zero released pressure ΔR_{ratio} is substantially reduced upon increasing T, since the thermally assisted domain-wall motion leads to retwinning of the sample in a stress free-environment. Above T_s there should not be any hysteresis since the material is tetragonal, as indeed observed experimentally. At $T \geq T_s$, the pressure dependence of ΔR_{ratio} may well be approximated with a linear behavior. These observations further reinforce the notion that there seems to be an equivalent impact of the pressure on ΔR_{ratio} in the title compounds as of the magnetic field with respect to the magnetization in a ferromagnet. In summary, we may state that the hysteretic behavior, observed in ΔR_{ratio} below T_s, arises due to the blocking of the twin boundary motion, which then appears to be thermally activated upon increasing T.

We shall now try to place our optical findings for all investigated Co-doped 122 iron-pnictides into a common context and perspective. Fig. 4.3(a) displays the temperature dependence of ΔR_{ratio} for x = 0%, 2.5% and 4.5% Co-doping at pressures where saturation occurs in the optical anisotropy (i.e., $p \geq 0.8$ bar at $T < T_s$, depending from the doping) as well as at released $p = 0$ bar (i.e., so-called remanent state), with the T scale normalized by T_s of each composition. There is a similar behavior for all compounds. First of all, the temperature dependence of ΔR_{ratio} at the remanent state undergoes a sudden drop close to and above T_s, which further points out the effect of the thermal activation of the twin boundary motion. Second, the inspection of the data reported in Fig. 4.2(a-e) and Fig. 4.3(a) emphasizes that the largest optical anisotropy at saturation and at $T < T_s$ is achieved for x = 0%. While several factors may influence the doping dependence, the largest anisotropy for x = 0% than for x = 2.5% or x = 4.5% Co-doping could derive from a stronger order parameter of the structural phase transition in the parent compound. Alternatively, we may state that the depleted optical anisotropy upon doping, at saturation and at each $T < T_s$, implies a decreasing lattice softness, going hand in hand with the Co-content dependence of the orthorhombicity $(a-b)/(a+b)$ (a and b are the lattice constants of the respective axes). This is explicitly shown in Fig. 4.3(b), which compares the Co-doping dependence (x) of ΔR_{ratio} at saturation for $T << T_s$ with respect to the measured orthorhombicity in $Ba(Fe_{1-x}Co_x)_2As_2$. Such a direct relationship between ΔR_{ratio} at saturation and $(a-b)/(a+b)$ contrasts with the non-monotonic anisotropy of the dc transport data upon doping. This might be the consequence of the multi-band nature of the title compounds. Since transport measurements are only sensitive to small energy scales close to the Fermi level, it is possible to get quite non-monotonic behavior of the transport anisotropy across the phase diagram depending on what the underlying bands are doing. Therefore, the comparison proposed in Fig. 4.3(b) may indicate that a direct mapping of the orthorhombicity and consequently of nematicity into the electronic structure can be identified most clearly at energy scales away from the Fermi level.

In conclusion, we demonstrate the capability of optics to get insights into the nematic-driven tetragonal-to-orthorhombic structural transition in the underdoped regime of the title compounds. The main findings evinced from our work are (i) the capability to release $in-situ$ p, as symmetry breaking field, and thus to observe the anisotropy of the electro-

dynamic response at $T << T_s$ for unstressed but fully detwinned crystals and (ii) the hysteretic nature of the optical anisotropy upon varying the stress due to the motion of the nematic domain walls. Our data give clear cut evidences for the impact of the ferro-elastic transition at energy scales deep into the electronic structure and for its fluctuations over a remarkable temperature interval above T_s. The discovered optical fingerprint of the nematic fluctuations originates from an intrinsic pressure-induced electronic anisotropy and bears testimony for the electronic nature of the structural phase transition. We have not observed any changes of the optical anisotropy in the superconducting state, which would suggest that superconductivity in the underdoped regime emerges within an electronic polarized state.

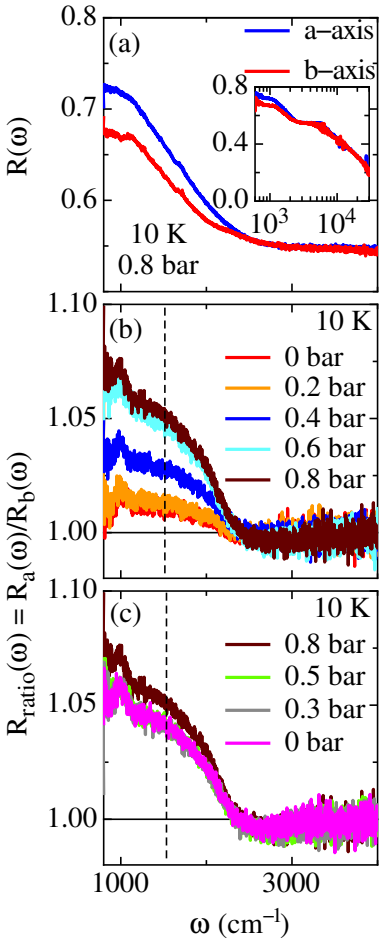

Figure 4.1: Representative data of the optical reflectivity of $BaFe_2As_2$ for the zero-pressure-cooled experiments: (a) Reflectivity ($R(\omega)$) measured at 10 K and p = 0.8 bar, displaying the optical anisotropy in the MIR spectral range. The inset shows $R(\omega)$ up to the visible and ultraviolet range with a logarithmic frequency scale. Above 3000 cm^{-1} the spectra for both polarization directions merge together. (b-c) p dependence of $R_{ratio}(\omega)$ (see text) at 10 K for increasing (b) and decreasing p (c). Values of $R_{ratio}(\omega)$ (see text) are determined at 1500 cm^{-1} (vertical dashed line). Applied stress is given in bar and corresponds to p of He gas inside the volume of the pressure device.

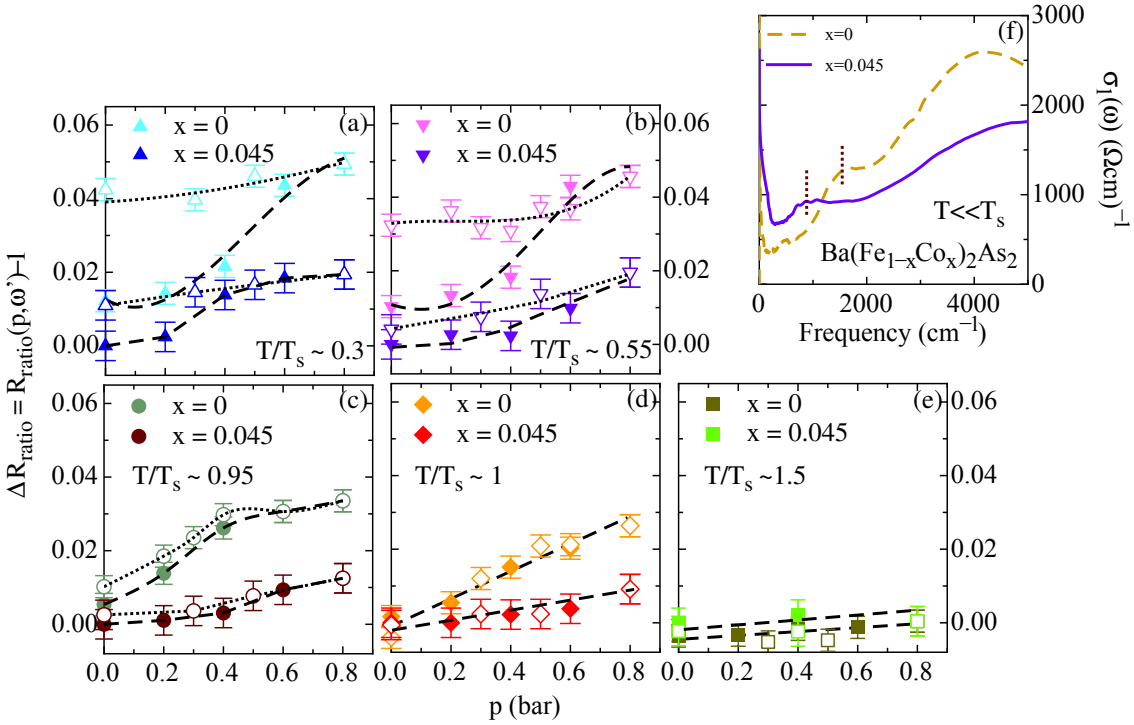

Figure 4.2: (a-e) Pressure dependence of $\Delta R_{ratio} = R_{ratio}(p,\omega')$-1 at selected temperatures above and below T_s achieved in the ZPC 'pressure-loop' experiment for x = 0% and 4.5% Co-doping (full and open symbols denote increasing and decreasing pressure, respectively). The dashed and dotted lines are guide to the eyes. The upper right panel (f) displays the real part $\sigma_1(\omega)$ of the optical conductivity for x = 0% and 4.5% Co-doping at $T < T_s$, emphasizing the mid-infrared peak overlapped to the low frequency tail of the stronger near-infrared absorption at about 4000 cm^{-1} on twinned specimens. The vertical dotted lines mark the position of the mid-infrared peak at ω' = 1500 and 900 cm^{-1} for x = 0% and 4.5% Co-doping, respectively, where R_{ratio} is read.

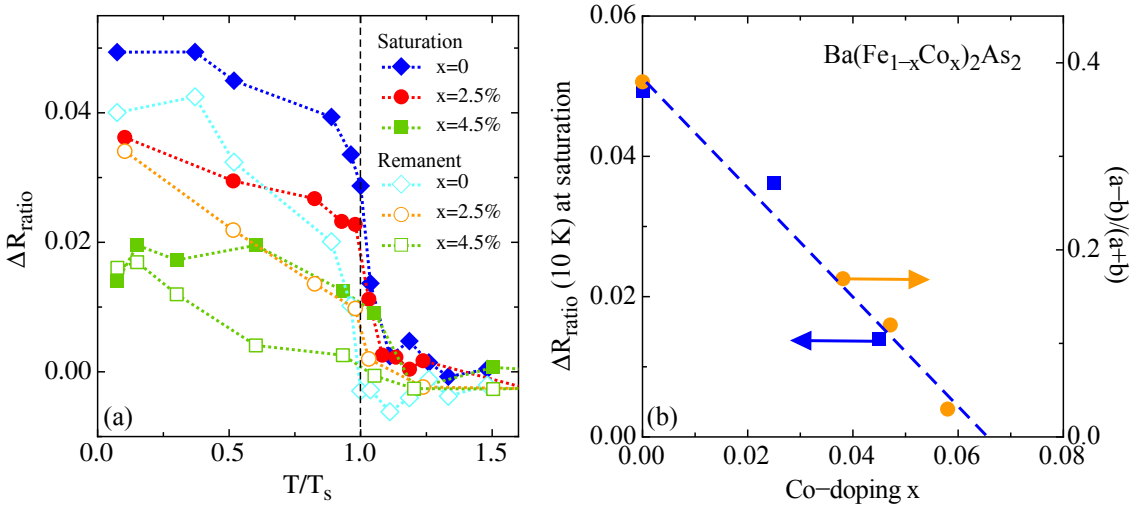

Figure 4.3: (a) Temperature dependence of $\Delta R_{ratio}(\omega')$ at saturation (i.e., at $p \geq 0.8$ bar, depending from Co-doping) as well as at its remanent state (i.e., at released p = 0 bar) for x = 0% ($T_s \sim 135$ K), 2.5% ($T_s \sim 98$ K) and 4.5% ($T_s \sim 67$ K) Co-doping. The T-axis is normalized by T_s and ω' is defined by the vertical dotted lines in Fig. 4.2(f). (b) Co-doping dependence (x) of ΔR_{ratio} at 10 K and at saturation (from panel (a)) and of the orthorhombicity $(a-b)/(a+b)$.

Chapter 5

Solid-State Dynamics and Education

(http://www.eduphys.ethz.ch/)

Head
Prof. Dr. Andreas Vaterlaus

Academic Staff
Dr. Yves Marc Acremann
Andreas Lichtenberger
Dr. Guillaume Schiltz
Dr. Andreas Fognini
Dr. Thomas Uli Michlmayr
Dr. Clemens Wagner
Rafael Gort
Gerard Salvatella Orgills

Master Students
Simon Däster

Technical Staff
Thomas Bähler

Administrative Staff
Andrea Weibel

Academic Guests
Prof. Dr. Joachim Stöhr, Stanford University

5.1 E-Learning and teaching support

30 lectures have been supplemented by the learning management system Moodle in 2014, reaching more than 5'000 students. Moodle was mainly used to support the course organization and to serve as a repository for course material. For some lectures, however, supplementary pedagogical scenarios, such as self-assessment tests, formative evaluations and collaborative tasks have been set up.

The project "video-solutions" started in 2013 could be extended to 6 lectures (MSc and BSc). The Department of Physics provided room and equipment for a recording studio (HPH F 18) where 97 new videos (length 15-25 min each) were produced in 2014. Each of these video clips covers a detailed solution to a physical problem. The videos are highly appreciated by the involved lecturers (Degiorgi, Kirch, Dissertori, Vaterlaus, Pescia) as well as by the students. In 2014 more than 15'000 views were attested (according to youtube).

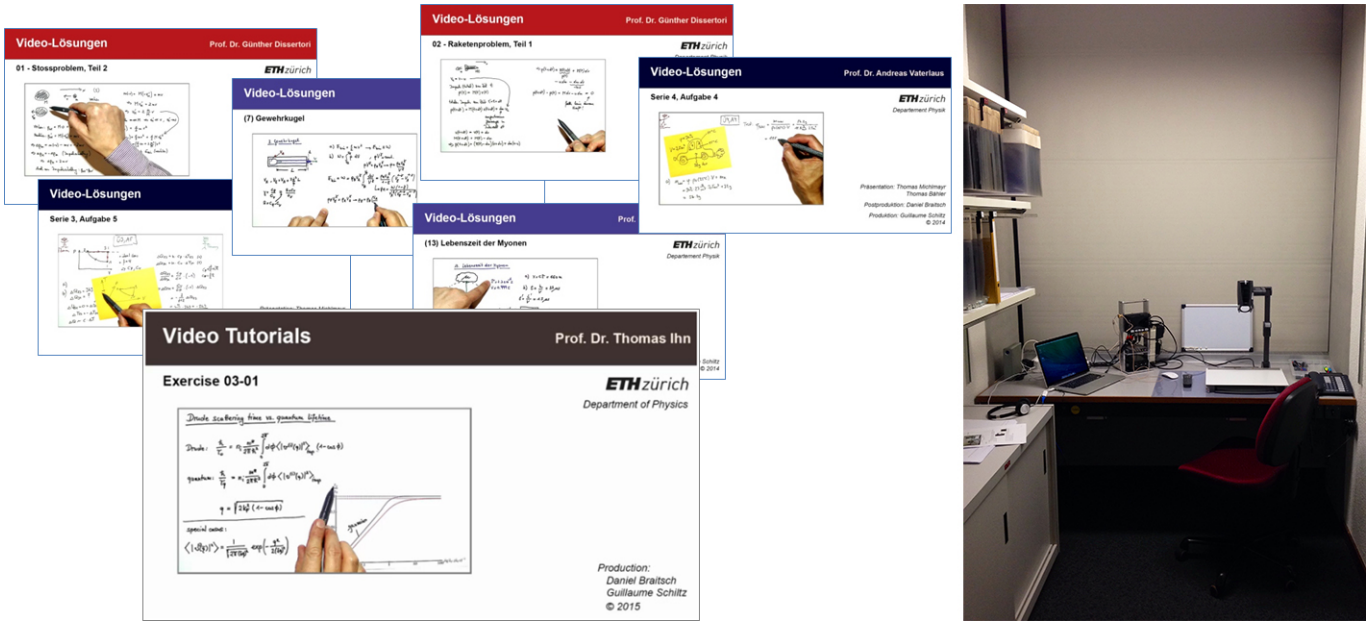

Figure 5.1: Video solutions (available from youtube, channel EduPhys) and the D-PHYS recording studio.

In responding to the repeal of "Testate" two compulsory midterm-tests (Günther Dissertori, Christian Degen) have been implemented. The Exercise-Market was adopted in further lectures where teaching assistants as well as lecturers were trained during a half-day workshop.

5.1.1 Promotion and Network

The teaching activities pursued at the department have been communicated to a greater public at two international conferences.

5.2 Ultrafast magnetism

For ultrafast demagnetization of a ferromagnet, spin angular momentum needs to be transported away from the spin system. Unlike other ultrafast processes in solids, the time scale of magneto-dynamics is believed to be dictated by the transfer of angular momentum. Therefore, the femtosecond magnetization dynamics is of fundamental interest. Laser-induced demagnetization is also of technological interest for magnetic recording devices: in order to optimize hard disks for fast writing times, long data retention times, and high storage densities, conventional writing needs to be combined with pulsed laser heating. The heat assisted magnetic recording (HAMR) technique therefore combines a magnetic field source with a pulsed laser diode to heat up the magnetic bit during writing.

5.2.1 Pump pulse length dependence of ultrafast demagnetization

The demagnetization process is expected to be caused by both, the excited electron gas as well as the lattice. If the ferromagnet is heated by a femtosecond laser pulse, the electron gas initially reaches a temperature, which exceeds the lattice temperature. This initial temperature rise in the electron gas is followed by thermalization with the lattice to a common temperature. In case of excitation by a picosecond laser pulse, the electron gas and the lattice stay close to thermal equilibrium during the whole demagnetization process.

We investigate if the demagnetization caused by a picosecond laser pulse can be described by the same mechanism as the demagnetization by a femtosecond pulse. This is achieved by studying the ultrafast demagnetization dynamics of a Ni film as a function of the pump pulse length. Our experiment demonstrates that the demagnetization by a picosecond laser pulse is described by the response to a femtosecond pulse convoluted with the pulse shape of the picosecond pulse, see Fig. 5.2. Therefore, the dynamics driven by the femtosecond pulse contains all information about the response to a picosecond pulse and is driven by the same physical processes. The demagnetization shows two components. One of them is independent of the pump pulse length and recovers on a time scale of heat diffusion. The second component is only present for pump pulses of less than 2 ps length. We interpret the decay of the fast component to be caused by the fast cooling of the electron gas. The fast demagnetization contribution can be achieved efficiently and quickly, yet, it is not a long lasting effect.

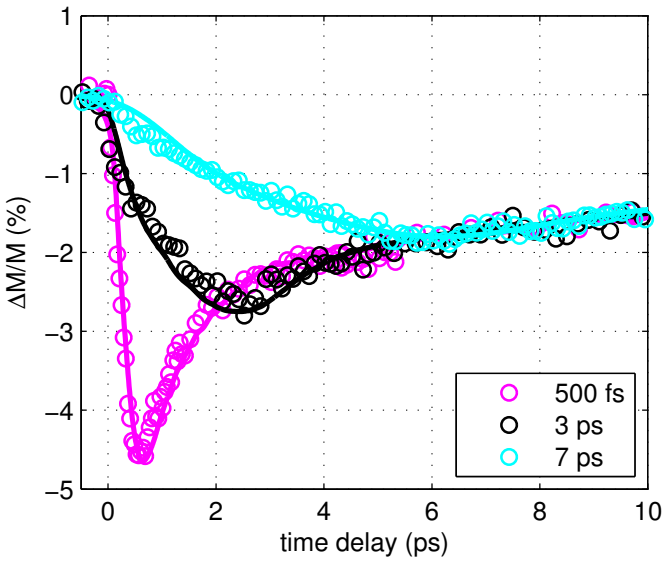

Figure 5.2: Measured demagnetization (circles) compared with the calculated demagnetization by convolution of the excitation pulse with the femtosecond magnetization response (lines).

5.2.2 Development of an imaging spin detector

We developed and tested a novel spin detector based on low energy scattering of spin polarized electrons on a Iridium crystal. The detector has been developed together with the group of Prof. Schönhense (University of Mainz, Germany). Electrons from the output of a hemispherical energy analyzer are elastically scattered on a an Iridium surface (Fig. 5.3). Due to the spin-orbit coupling within Ir, the reflectivity is spin dependent and therefore acts as a spin filter. As the scattering process is elastic, the imaging properties of the hemispherical analyzer can be preserved, allowing for parallel detection of electron energy and emission angle. Therefore, the efficiency of this detector is significantly better compared to a traditional Mott spin detector. This detector has been designed by our group, and has been manufactured by the physics machine shop. First tests have been performed.

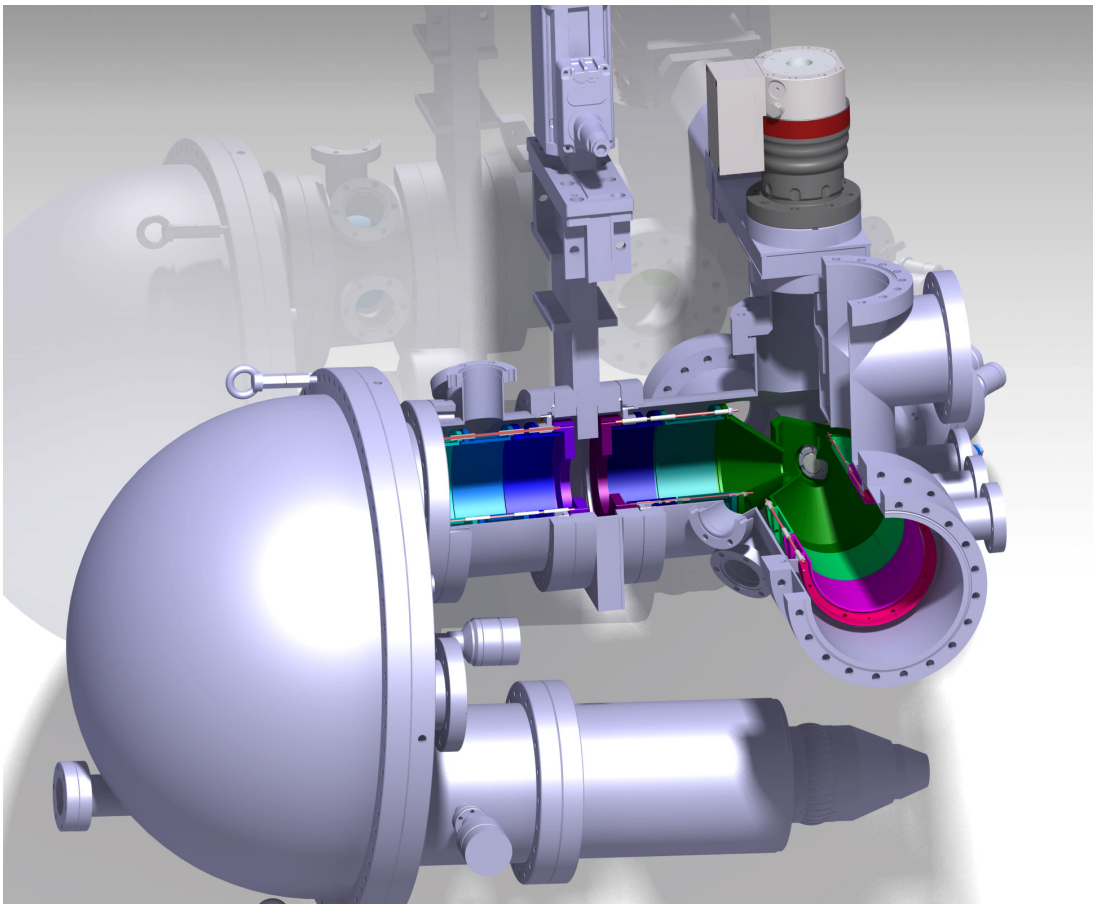

Figure 5.3: Drawing of the SPLEED spin analyzer attached to a hemispherical energy analyzer. The detector has been designed by our group and manufactured at the physics workshop at ETH.

5.2.3 Transport model of ultrafast demagnetization

We developed a model describing ultrafast demagnetization as a transport effect: The pump laser pulse causes a temperature gradient within the first surface layers of the sample. This gradient can be as large as 100 GK/m. The chemical potentials for minority- and majority electrons are altered by the temperature, leading to a gradient of the chemical potentials $\mu_\uparrow$, $\mu_\downarrow$ for the majority(↑)- and minority(↓) spin direction. It turns out, that $\mu_\uparrow$ is affected most, leading to a chemical potential gradient, which favors a spin current from the hot surface towards the substrate. Finite element calculations show, that the spin current pulse caused by this effect can be as short as 100 fs. The model is similar in spirit to the super-diffusion model from Battiato et al. (Phys. Rev. Lett. **105**, 027203 (2010)), yet it is based on a thermodynamic concept. It therefore contains the basic process in an analytically solvable form. The results will be compared to experimental data obtained through optical transport experiments.

5.3 Physics Education

5.3.1 SNF-Project: Fostering conceptual understanding of physics by formative assessment

Formative assessment is an assessment procedure without marks or grades. Rather the student can evaluate his or her understanding. For our project we have recruited 31 teachers from Swiss high schools form different parts of Switzerland ranging from St. Margarethen in the eastern part to Thun closed to the french speaking region of Switzerland. Since some of the teachers participate with several classes there are around 800 students involved. The teachers were divided in three groups, a control group, a frequent testing group and a formative assessment group. The frequent

testing group solves the same tests as the formative assessment group but without the formative assessment approach. In this way we can distinguish between the effect of frequent testing and of formative assessment. We have developed a concept test of kinematics, which we use as pre-, post- and follow up test. Furthermore we designed two clicker sessions with 15 multiple-choice problems each for the formative assessment approach. The diagnostic test then focuses on the detection of misconceptions. It is followed by a reflective lesson, where the students have the possibility to work on their deficits. We also provided teaching material for the reflective lesson. After a professional development course before summer holidays the different groups started to teach kinematics in the fall semester for 15 lessons including all physics tests (Fig. 5.4). In addition we administrated a cognitive performance test as well as motivation test to the students. However, we did not just evaluate the students but also the teachers. They were tested for their pedagogical content knowledge (PCK). Our major goal is to finish the data acquisition phase of the project in spring 2015 including the follow up test.

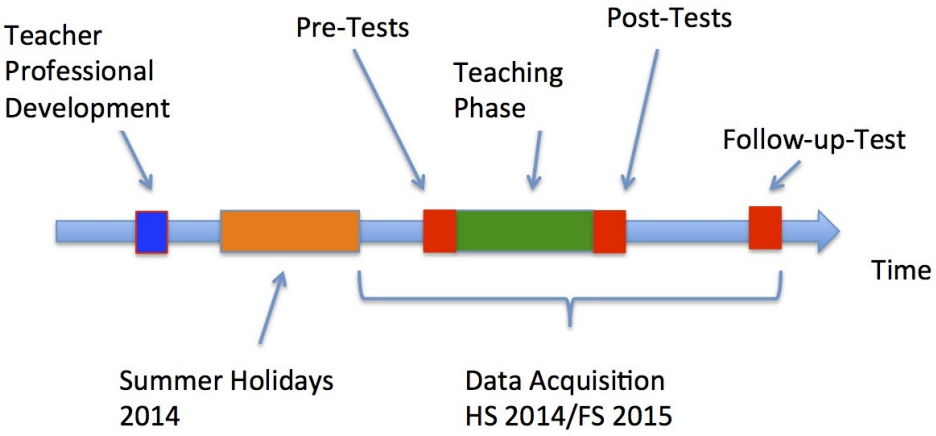

Figure 5.4: Time course of the data acquisition phase of the SNF-project. The PCK test was applied to the teachers during the professional development day. The motivation questionnaire was also administered as pre- and post test.

5.3.2 Correlation between mathematics and physics concepts in kinematics

We have developed a diagnostic test in kinematics to investigate the student concept knowledge at the high school level. The multiple-choice test items are based on seven basic kinematics concepts we have identified. We have performed an exploratory factor analysis on a data set collected from 56 students at two Swiss high schools. We have found that there are two basic mathematical concepts that are crucial for the understanding of kinematics: the concept of rate and the concept of vector (including direction and addition). The context and the content of the items seem to play only a minor role. If a student understands the concept of rate he is able to answer correctly to questions about velocity and acceleration in different contexts. We have further investigated the correlation between the mathematics and physics concepts by adding mathematics items to the test. A factor analysis has shown that the items that are associated to the mathematical concept of rate actually group with the items assigned to the kinematics concepts “velocity as rate” and “acceleration as rate”. Moreover the correlation of the total scores of the mathematics items about rate and the kinematics items about rate has a considerably high value of 0.63. This result has direct implications for the instruction. It suggests that in kinematics courses the focus should be first on the learning of the mathematical concepts. Transferring the mathematical concepts to physical contents and applying them in different contexts is suggested to be easier for students than learning physical concepts without a mathematical fundament.

5.3.3 Understanding Physics Concepts at Different Representation Levels — a Mutual Information Approach

We have analyzed student’s knowledge about physics concepts in kinematics at different representation levels. The concepts, we were looking at, were first, velocity as rate and second, velocity as one-dimensional vector. The problems

administrated to the students were multiple-choice questions using different representations. Questions at the first level are associated with figures like stroboscopic pictures. At the second level questions are furnished with diagrams and at the third representation level motions of object were represented by tables. Some of the questions about velocity as rate could be posed at all three representation levels. Correlation analysis is a linear method and doesn't take nonlinearities into account. Correlations can be zero although there is an obvious nonlinear relationship between data points. Thus we have used mutual information to analyze the data (Fig. 5.5), on the one hand to corroborate the linear correlations and to detect nonlinear relations. Our results reveal the same classification as the linear correlation analysis. Students solve the problems due to mathematical concepts like rate and 1d vector. Moreover we have found that the grouping due to representations is given by the solution strategy. Thus, stroboscopic representations of problems and representations as tables use the solution strategy "ratio of differences". It means that the student first has to find the Δx (or Δv) and divide it by Δt to solve the problem. In the case of diagrams the student has to determine first the tangent at one or several time points in order to answer the question. Including the concept velocity as 2d vector, we therefore expect at least five factors in a factor analysis of a large data set.

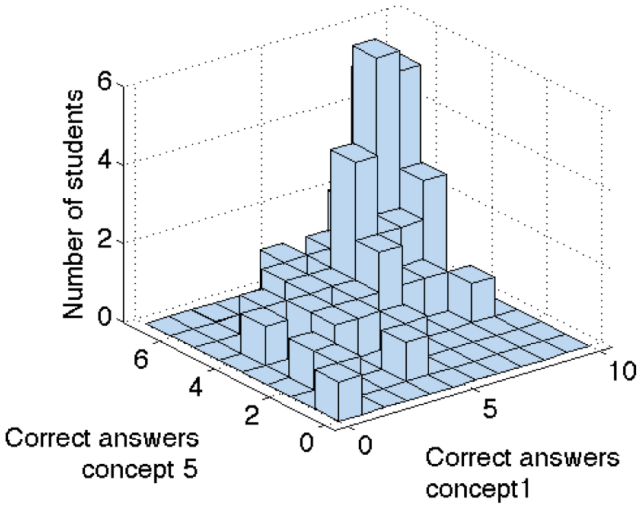

Figure 5.5: Preparation of data in order to calculate the mutual information between the knowledge of two concepts (concept 1: velocity as rate; concept 2: acceleration as rate). The data show the distribution of students with the number of correct answers to concept 1 questions versus the number of correct answers to concept 5 questions.

Chapter 6

Quantum Device Lab

(http://qudev.ethz.ch/)

Head
Prof. Dr. A. Wallraff

Academic Staff

Dr. A. Abdumalikov	Dr. M. Allan	S. Berger
M. Collodo	K. Cujia Pena	Dr. C. Eichler
J. Fankhauser	Dr. S. Filipp	D. Friese
S. Gasparinetti	A. Hambitzer	J. Heinsoo
L. Heinzle	L. Huthmacher	J. Koepsell
P. Kurpiers	F. Lüthi	P. Magnard
M. Melchner	S. Miesch	B. Mitchell
J. Mlynek	Dr. M. Mondal	Dr. A. Mustonen
M. Oppliger	M. Pechal	Dr. A. Potocnik
Dr. G. Puebla-Hellmann	A. Romila	A. Rubio Abadal
S. Ruffieux	Dr. A. Safavi-Naeini	Y. Salathe
M. Stammeier	A. Stockklauser	T. Thiele
T. Walter		

Technical Staff

S. Däster	J. Künzli	J. Lütolf

Administrative Staff

Dr. F. Bay	G. Strahm

Master Students

Cujia Pena Kristian (HS2014)	Heinsoo Johannes (HS2014)	Heinzle Lukas (FS2014)
Huthmacher Lukas (FS2014)	Lüthi Florian (FS2014)	Ruffieux Silvia (HS2014)

6.1 Microwave-Controlled Generation of Shaped Single Photons in Circuit Quantum Electrodynamics

M. Pechal, L. Huthmacher, C. Eichler, S. Zeytinoğlu, A. A. Abdumalikov, Jr., S. Berger, A. Wallraff, and S. Filipp

A coherent link between spatially separated nodes of a quantum network may be realized using itinerant photons as information carriers [1]. The necessary efficient absorption at the receiving node can be achieved by using a photon with a suitable temporal profile allowing time-reversal of the emission process [2].

Methods for generating shaped photons have recently been demonstrated in superconducting circuits [3]. In contrast with these schemes relying on fast flux biasing of the system, here we study a method which is fully microwave-controlled [4]. We make use of the transmon's second excited state and transfer its population into a resonator Fock state in a controlled way using a second-order transition driven by a classical coherent tone. The Fock state is subsequently emitted into the transmission line coupled to the resonator. We control the shape of this emitted photon by varying the rate of the second order transition in time. We also compensate the amplitude-dependent AC Stark shift induced by the strong drive with a suitable modulation of the drive phase. We demonstrate our scheme by preparing photon states with time-symmetric waveforms of controlled length. We also prepare photons with unusual multi-peaked shapes and show that the phases of the peaks can be adjusted individually. Such photon states are potentially useful for encoding higher-dimensional quantum states [5] into a travelling quantum information carrier.

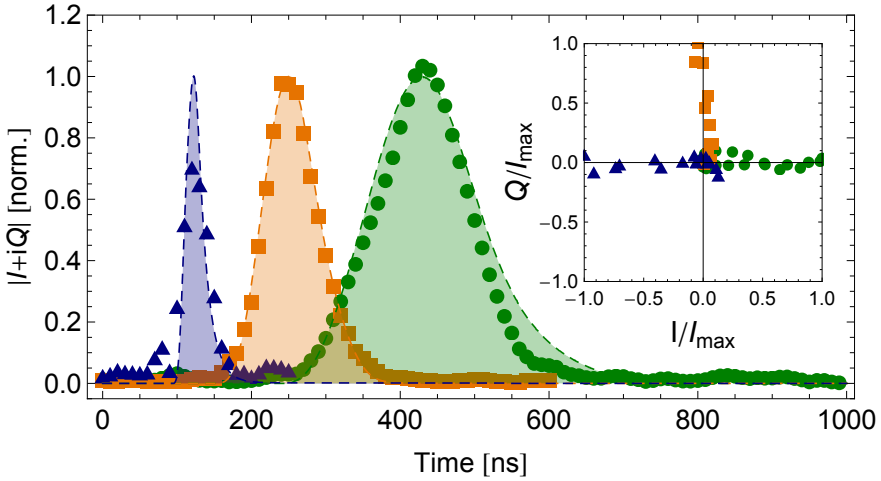

Figure 6.1: Symmetric photon waveforms of various lengths generated by the studied photon shaping process. The insets demonstrates stability of the photon phase.

[1] H. J. Kimble, Nature **453**, 1023 (2008)
[2] J. I. Cirac, P. Zoller, H. J. Kimble and H. Mabuchi, Phys. Rev. Lett. **78**, 3221 (1997)
[3] M. Pierre, I. Svensson, S. R. Sathyamoorthy, G. Johansson and P. Delsing, Appl. Phys. Lett. **104**, 232604 (2014)
[4] M. Pechal, L. Huthmacher, C. Eichler, S. Zeytinoğlu, A. A. Abdumalikov Jr., S. Berger, A. Wallraff and S. Filipp, Phys. Rev. X **4**, 041010 (2014)
[5] H. Bechmann-Pasquinucci and W. Tittel, Phys. Rev. A **61**, 062308 (2000)

6.2 Manipulating Rydberg Atoms Close to Surfaces at Cryogenic Temperatures

T. Thiele, S. Filipp, J. A. Agner, H. Schmutz, J. Deiglmayr, M. Stammeier, P. Allmendinger, F. Merkt, and A. Wallraff

Independent of the physical system, experiments that explore quantum mechanical effects at the single quantum limit need to fulfil a set of different criteria. Various systems such as neutral or charged atoms, superconducting circuits, nuclear spins, NV-centers or quantum dots, offer a diversity of physical properties to meet these requirements. For example, an important prerequisite for any quantum mechanical experiment is the fast and coherent manipulation of a set of quanta at time scales shorter than the coherence time of the system. However, the strength of one system generally comes with a weakness, e.g. long coherence time is accompanied by slow manipulation rates, limiting the variety of possible experiments. Other systems can have complementary properties, for example fast manipulation but only short short coherence time.

In our experiment we aim to combine the strengths of two physical systems; the long coherence times of highly excited, neutral (Rydberg) atoms and the fast manipulation times of superconducting circuits operating in the microwave regime. In detail, we couple helium Rydberg atoms with principal quantum numbers $n \geq 30$ to microwave photons in superconducting coplanar transmission line resonators at cryogenic temperatures. The main challenge in this experiment is to create conditions, under which the Rydberg atoms can be studied in a homogeneous static electric field close to the evanescent mode of the waveguide at the surface.

In 2014, we have achieved an important step towards this goal by observing coherent population transfer between the internal states of an ensemble of 1000 helium atoms in Rydberg states at a distance of 250 μm from a planar gold or superconducting surface at a temperature of 3 K [1]. With a repetition rate of 25 Hz, the atoms were excited to Rydberg states by a Nd:YAG pumped, frequency-doubled dye laser ($\lambda \approx 313$ nm) from a supersonic ($v = 1700$ m/s) beam of metastable $(1s)^1(2s)^1\ ^1S_0$ singlet atoms created in an electric discharge. The observed 34 s state population varies as a function of microwave amplitude (pulse length: 160 ns) and detuning Δ_0 from the field-free transition frequency at ≈ 27.966 GHz. The observed coherent population transfer is not symmetric with respect to the transition frequency at $\Delta_0 = 5$ MHz [Fig. 6.2(a)] which is explained by a model taking into account microwave and static electric field gradients over the atom cloud [Fig. 6.2(b)].

In 2015, we develop novel techniques to determine electric and microwave field distributions above patterned surfaces and set up a new helium source that reduces the temperature of the metastable beam using laser cooling. In a next step we plan to combine the two setups and observe the interaction between an ensemble of Rydberg atoms and a superconducting coplanar transmission line resonator.

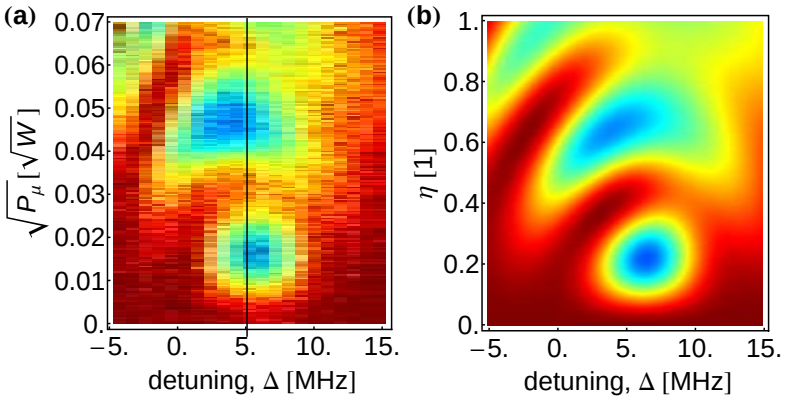

Figure 6.2: (a) Rabi oscillations for an ensemble of helium Rydberg atoms at a distance of 250 μm above a gold surface as a function of microwave amplitude $\propto \sqrt{P_\mu}$ and detuning Δ_0, see text. (b) Corresponding simulation with η beeing varied linearly between 0 and 1 as the experimentally set amplitude is varied. The color scale in both panels indicating the population ranges from 0.14 (blue) to 1 (dark red).

[1] T. Thiele, A. Filipp, J. A. Agner, H. Schmutz, J. Deiglmayr, M. Stammeier, P. Allmendinger, F. Merkt, and A. Wallraff, Phys. Rev. A **90**, 013414 (2014)

6.3 Evaluating Charge Noise Acting on Semiconductor Quantum Dots in the Circuit Quantum Electrodynamics Architecture

A. Stockklauser, J. Basset, D.-D. Jarausch, T. Frey, C. Reichl, W. Wegscheider, A. Wallraff, K. Ensslin, and T. Ihn

In recent years, hybrid circuit QED devices consisting of semiconductor double quantum dots coupled to microwave cavities have attracted a lot of attention. However, an important milestone that has not been reached with these systems is the strong coupling regime of cavity QED. Reaching this regime is challenging with quantum dots due to the lack of control over the decoherence mechanisms limiting charge relaxation and dephasing rates. We used a resonator-dot system to quantitatively extract charge fluctuations in the environment surrounding our single-electron GaAs double quantum dot, one source of decoherence in our experiment. We demonstrate a charge sensitivity of the microwave readout at the level of $8.5 \times 10^{-5}\ e/\sqrt{\mathrm{Hz}}$ and use this sensitivity to quantitatively probe the low-frequency charge noise of the heterostructure.

The presented analysis allows us to infer a lower bound for the dephasing rate originating from the low frequency charge noise in the vicinity of the double-dot. The inferred value is similar to that extracted from an analysis of frequency shifts and linewidth broadenings based on a master equation simulation. This emphasizes that charge noise is the main source of dephasing in our DQD-based charge qubit system.

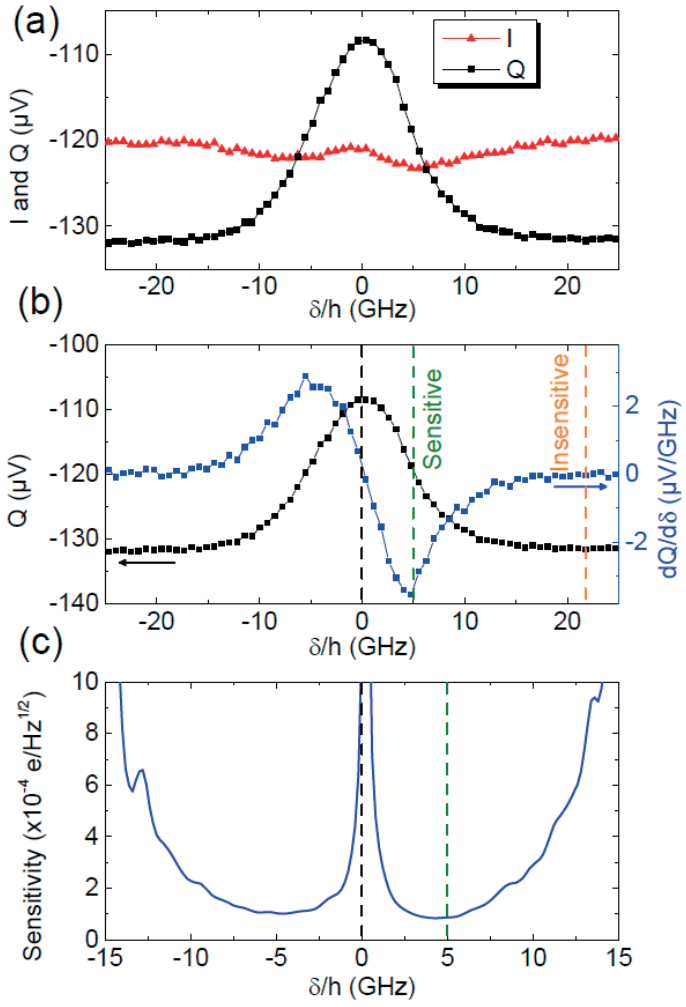

Figure 6.3: (a) Measured in-phase I and out-of-phase Q components of the signal transmitted through the resonator vs the detuning δ. (b) Measured quadrature signal Q and numerical derivative $\partial Q/\partial\delta$ of Q vs detuning δ. (d) Computed charge sensitivity along δ.

6.4 Observation of Dicke Superradiance for Two Artificial Atoms in a Cavity with High Decay Rate

A. A. Abdumalikov, J. A. Mlynek, C. Eichler, and A. Wallraff

The lifetime of any excited quantum state is limited and its decay to the ground state can only be described statistically according to the states “life expectancy”. This effect was first discussed by Einstein and is named spontaneous emission. However as soon as multiple excited emitters are brought into close vicinity their lifetime shows significant correlations as if they would come to an agreement about how and when to decay. Quantum scientists have now shown that the decay is also drastically altered if one excited emitter is brought into the vicinity of a second one even when it is in its ground state. This effect was predicted by Dicke in 1954 but remained unobserved until now.

In this work, we realized Dicke’s original two-emitter superradiance Gedankenexperiment. The small ensemble case of superradiance is brought to a new perspective by exploiting the ability to prepare any arbitrary separable initial state. We observe the collective decay dynamics and show how the dynamics is related to the built-up of correlations as the main mechanism of superradiance. Our study is completed by fully reconstructing the statistical properties of the collectively emitted field, something no physicist has yet been able to do. The experiment takes place in the bad cavity limit of circuit quantum electrodynamics. This regime is so far little explored in that field and points out a viable path for future experiments in the context of dissipative quantum systems which benefit strongly from a controlled decay into a single mode of the field.

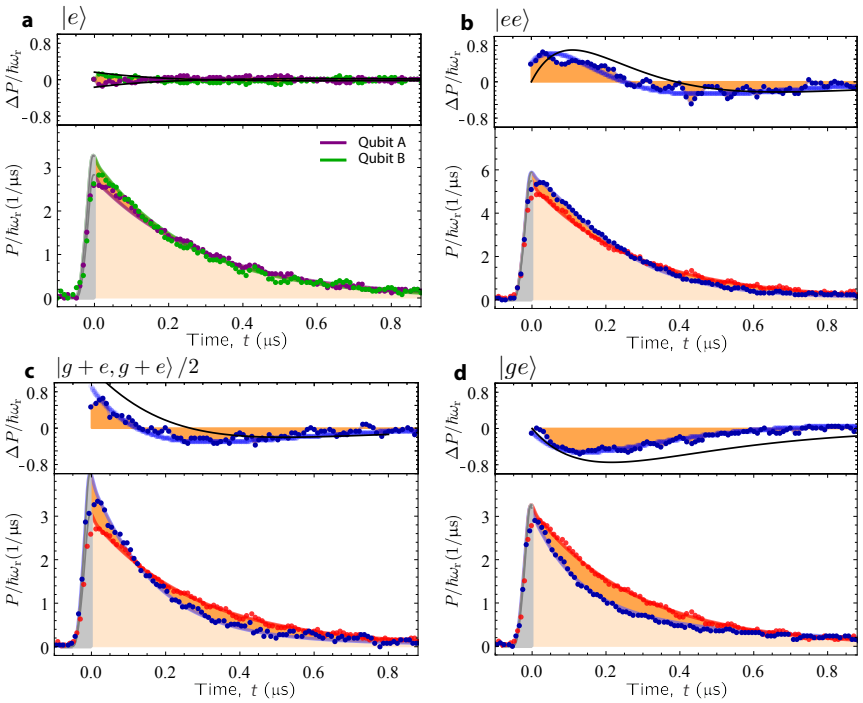

Figure 6.4: Time dependence of the emitted power P from different initial states (bottom) and the deviation ΔP (top) from the average single-qubit power (red points). Data (blue dots) are compared with a simple rate equation model (solid black lines) and full master equation simulations (solid blue lines). (a) Individual decay of qubits A (purple) or B (green) prepared in state $|e\rangle$. Collective decay for initial states (b) $|ee\rangle$, (c) $(|g\rangle + |e\rangle)(|g\rangle + |e\rangle)/2$, and (d) $|ge\rangle$. The orange area indicates the difference of the collective two-qubit decay with respect to the mean individual decay (dashed red line). For time $t < 0$ (greyed-out area), the emission dynamics is governed by the initial field build-up, which is not considered in the upper parts of each panel. All data were normalized by the the same constant, extracted by matching the emitted energy of the mean individual decay to what is expected from the master equation. The theoretical curves then are scaled by s to include variations in our detection efficiency, where in b, $s = 0.9$; in c, $s = 0.94$ and in d, $s = 1.07$. The reference curve of the mean individual decay was scaled accordingly.

6.5 Quantum-Limited Amplification and Entanglement in Coupled Nonlinear Resonators

C. Eichler, Y. Salathe, J. Mlynek, S. Schmidt, and A. Wallrafff

Quantum limited amplifiers have become an essential component in state-of-the-art cryogenic setups to enhance measurement efficiency towards its ultimate limit. We have recently developed a novel type of parametric amplifier, which we choose to refer to as a Josephson parametric dimer (JPD) [1]. In contrast to previous quantum limited amplifiers it can be operated both as a degenerate and as a nondegenerate amplifier. The large measured gain-bandwidth product of 250 MHz and the saturation at input photon numbers as high as 2000 per ms are both expected to be improvable even furrther. The gain medium of the JPD amplifier is described by the Bose Hubbard dimer Hamiltonian, in which the controlled interplay between effective photon-photon interactions and photon hopping leads to parametric coupling between two nondegenerate eigenmodes. The characteristic properties of the parametric gain are controlled by adjusting the frequency and the power of an externally applied pump field. The dynamic range of the amplifier is enhanced by using SQUID arrays rather than single SQUIDs in the resonant circuit [2]. The excellent performance of the amplifier becomes manifest in the large measured two-mode vacuum squeezing of more than 12 dB. In addition to its practical use as an amplifier our Bose-Hubbard-dimer system and its extension to larger arrays of cavities may prove interesting as an unconventional single photon source, for the study of Majorana modes in parametrically coupled cavities, and in general for experimental studies of nonequilibrium many-particle physics in photonic systems.

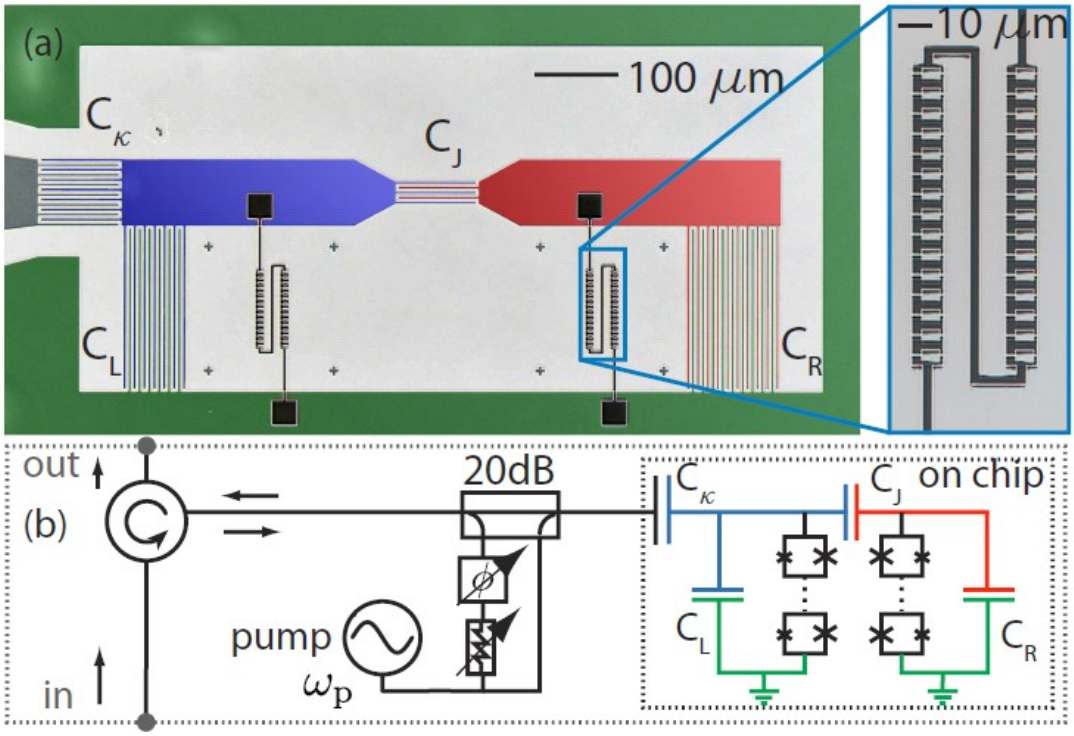

Figure 6.5: (a) False-color micrograph of the sample. The interdigitated finger structures form the capacitors of two coupled oscillators. An effective nonlinear inductance is realized as an array of SQUIDs in each resonator, also shown enlarged. (b) Simplified circuit diagram of the experimental setup. The circuit is driven with a pump field through a -20 dB directional coupler, of which the second port is used to interferometrically suppress the pump field reflected from the sample by more than -60 dB.

[1] C. Eichler, Y. Salathe, J. Mlynek, S. Schmidt, and A. Wallraff, Phys. Rev. Lett. **113**, 110502 (2014)
[2] C. Eichler, and A. Wallraff, EPJ Quantum Technology **1**, 2 (2014)

Chapter 7

Semiconductor Quantum Materials

(http://www.mbe.ethz.ch/)

Head
Prof. Dr. W. Wegscheider

Guest Professor
Prof. Dr. W. Dietsche

Academic Staff

M. Berl	Ch. Charpentier	Dr. S. Fält
Dr. T. Feil	Ch. Lehner	A. Maier
S. Peters	Dr. Ch. Reichl	S. Riedi
Dr. W. Stumpf	Dr. L. Tiemann	T. Tschirky
W. Wüster		

Master Students
M. Chanson (FS2014)
D. Wenzler (FS2014)
F. Schläpfer (FS2014)
R. Brossard (FS2014)
L. Alt (HS2014)

Technical Staff

J. Gmür	S. Heider	M. Sturzenegger

Secretaries

C. Egli	C. Vinzens

Since 2014 we have two GaAs/AlGaAs Molecular Beam Epitaxy (MBE) systems at our disposal, both capable of achieving low-temperature mobilities in excess of $2 \cdot 10^7$ cm^2/Vs. The highest mobility measured in our laboratory is close to $3 \cdot 10^7$ cm^2/Vs. The third MBE system equipped with a custom-designed Sb valved-cracker cell for the growth of Sb-based heterostructures was able to produce InAs/Al(Ga)Sb heterostructures with low-temperature mobilities of 560'000 cm^2/Vs as well as InAs/GaSb combined quantum well structures exhibiting clear signatures of a 2D topogical insulator, i.e. edge channel transport. Although this MBE system was not optimized for the fabrication of ultrapure two-dimensional electron gases (2DEGs), routinely achieved electron mobilities for GaAs/AlGaAs samples produced therein exceed the 10^7 cm^2/Vs mark.

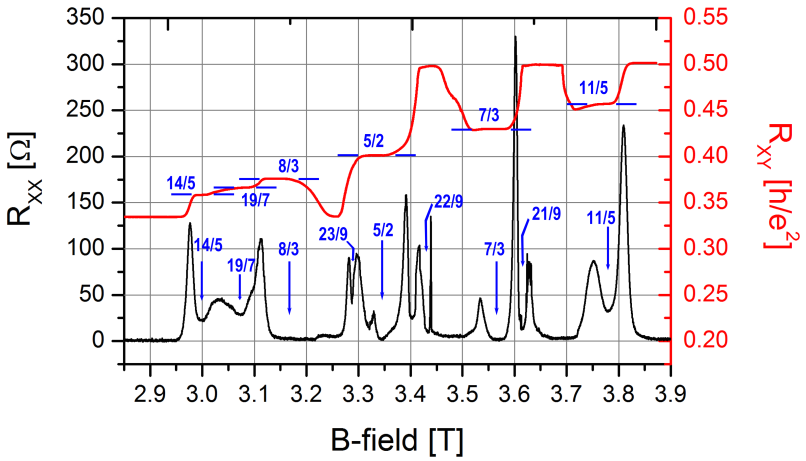

Figure 7.1: Longitudinal (black) and transverse resistance (red) for a high-mobility 2DEG sample, measured at 10 mK; marked in blue are the FQHE states that can be identified.

One highlight in 2014 was the optimization of 2DEG samples suitable for fractional quantum Hall effect (FQHE) investigations (see Fig. 7.1 for the current status). As the potential disorder created by remote ionized donors is currently considered to be the main factor prohibiting the development of these FQHE states and especially the $\nu = 5/2$ state, our strategy was to reduce this disorder. This led to an increase of the $\nu = 5/2$ state's activation energy by a factor of five, from 30 mK to 135 mK. This was achieved without illuminating or gate-tuning the 2DEG sample by optimizing the structural design combining an increased setback distance between 2DEG and doping layers as well as the implementation of a screening layer of immobile electrons close to the doping region [1] (The method of illumination yielded an activation energy of 214 mK, our current record value).

Since sample optimization has to be based on measurements taken at mK temperatures, which is rather time and work intensive, we also tried to establish a relation between 5/2 activation energies and other, faster obtainable characteristics of our 2DEG structures, thus, shortening the feedback loop for growth operations. We discovered a clear qualitative relation between 5/2 activation energy and certain features of the transversal resistance — the reentrant integer quantum Hall states, RIQHS — which can be obtained from a single magneto-transport measurement at very low temperatures (see Fig. 7.2).

Another important set of results was obtained on so-called Composite Quantum Wells (CQWs). These consist of neighbouring InAs and GaSb layers, which feature a type-II broken band gap lineup where for appropriate layer widths the lowest electron band of InAs lies below the uppermost hole band of GaSb. This leads to a hybridization of the electron and hole states and the opening of an energy gap at the band crossings due to spin-orbit coupling. This gives rise to the quantum spin Hall effect (QSHE), a topologically non-trivial state in which the bulk of the sample is insulating with helical, dissipationless conducting channels at the sample edge, which are protected against elastic backscattering in the presence of time-reversal symmetry. Applications in spintronics are of special interest due to the helicality of the edge channels. Topological quantum computing might be possible due to the theoretically predicted appearance of Majorana zero-modes with non-Abelian exchange statistics. These so-called 2D topological insulators were first observed in HgTe/CdTe quantum wells. The main advantages of InAs/GaSb CQWs are the technical feasibility due to the relatively well-known materials and the ability to tune the Fermi level into the topological state by

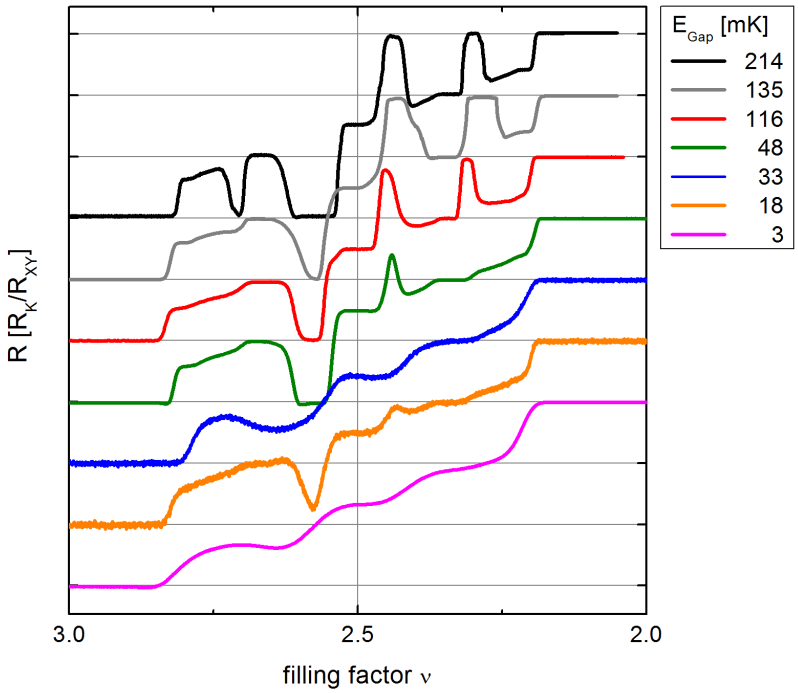

Figure 7.2: Transversal resistance traces in the magnetic field range corresponding to filling factors three to two. The correlation between activation energy and the appearance of up to four RIQHS could be used to develop a quality benchmark.

application of an electric field. This topological phase transition opens up a variety of possible experiments and can be applied for example in a topological transistor, where instead of changing between conducting and non-conducting states by carrier depletion the channels switch between normal conduction and helical, dissipationless conduction. The edge states of the described 2D topological insulators are very well suited to host Majorana zero modes. When brought close to a superconducting material the proximity effect can induce superconductivity and thus create a 1D topological superconductor in which the Majorana zero modes can be localized using a magnetic insulator. Due to their non-Abelian exchange statistics quantum computational operations can be performed by braiding the Majorana quasiparticles. These operations would be fault tolerant due to the topological protection of the edge states. Unlike in non-Abelian quantum Hall states, e.g. the 5/2 FQHE states described above, which require a strong external magnetic field, no external magnetic field is required. We have successfully grown CQW samples which show that the Fermi level can be tuned via gates from the electron regime to the hole regime with a gap in between, where the bulk becomes insulating as shown in Fig. 7.3. A major problem has been a residual conductance through the bulk of the sample, which masked edge channel transport. By introducing a moderate impurity concentration to localize the electrons without compromising the topologically protected edge channels, the bulk conductance could be considerably suppressed.

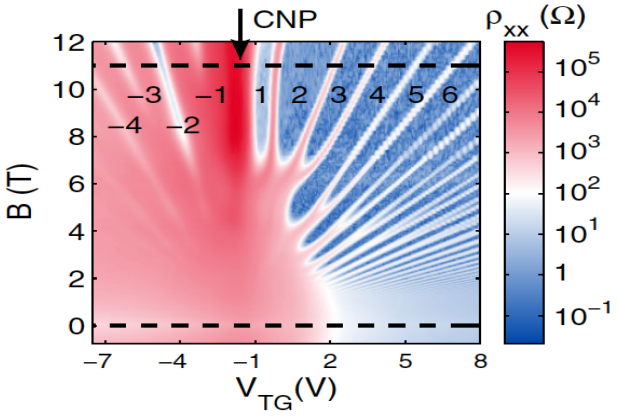

Figure 7.3: Longitudinal resistivity for different top-gate voltages and magnetic field strenghts measured on a InAs/GaSb CQW. The numbers indicate resistivity minima for electrons (positive) and holes (negative). CNP indicates the charge neutrality point where the Fermi level is inside the hybridization gap.

In collaboration with the group of Prof. K. Ensslin, nanostructured front gates were fabricated on these samples. Furthermore, we successfully produced working samples with MBE grown back gates to tune the Fermi level without distorting the band structure. Evidence for (helical) edge channels has been found by local and non-local transport measurements [2] as well as by superconducting quantum interference measurements performed in the group of Prof. L. Kouwenhoven, TU Delft [3], shown in Fig. 7.4. A wide conventional superconductor-normal-superconductor (SNS) junction yields the Fraunhofer pattern, as shown in Figs. 7.4a and e for electron and hole transport, respectively. The corresponding current density profile indicates that most of the current is carried by the bulk (see Figs. 7.4b and f). In the case of edge-mode superconductivity the junction effectively acts as a superconducting quantum interference device (SQUID) with a well-known ϕ_0-periodic interference pattern (Fig. 7.4c). In this regime, the supercurrent density is clearly edge-mode dominated (Fig. 7.4d).

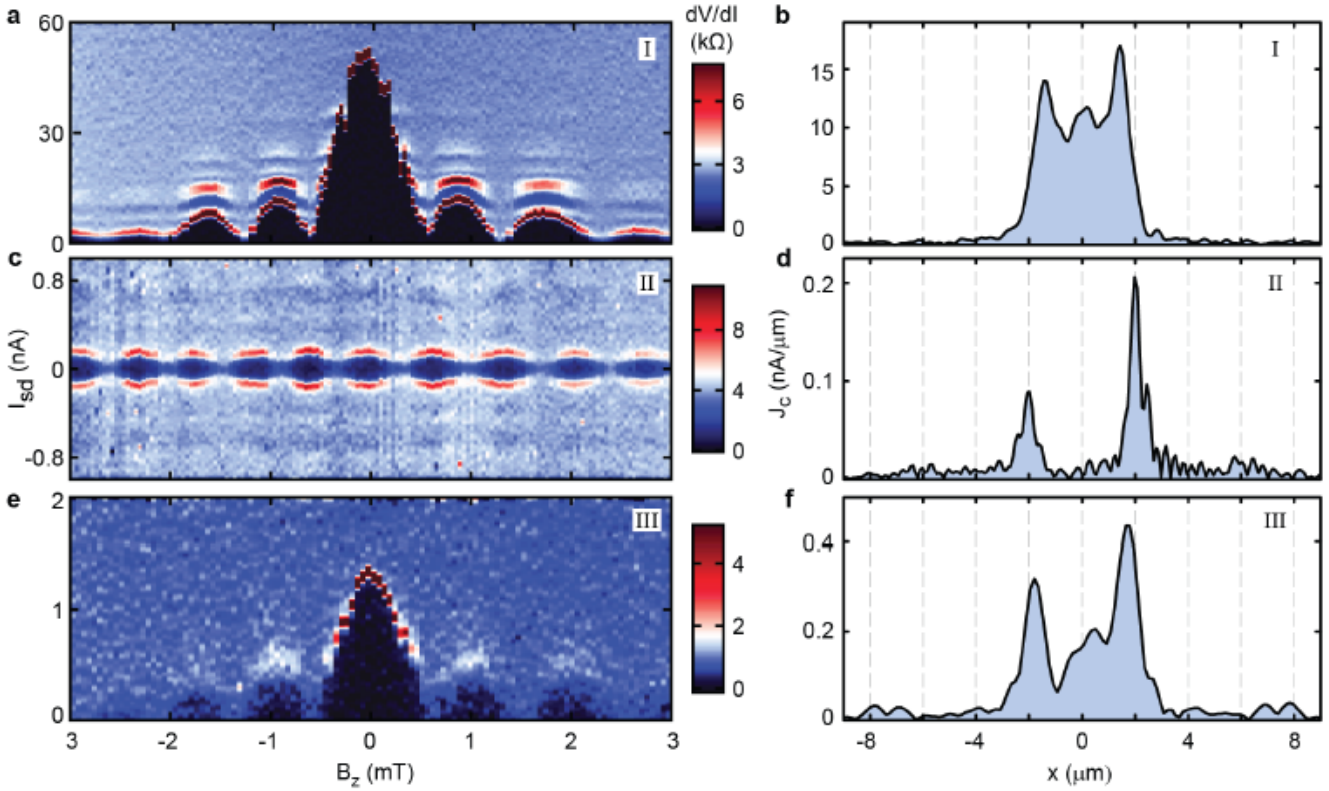

Figure 7.4: Superconducting quantum interference patterns and the corresponding current density profiles of a InAs/GaSb CQW. The Fermi level could be tuned from the normal conducting electron regime (a) to the hole regime (e) with the edge-transport dominated topological regime in-between.

[1] C. Reichl, J. Chen, S. Baer, C. Rössler, T. Ihn, K. Ensslin, W. Dietsche, W. Wegscheider, New J. Phys. **16**, 023014 (2014).
[2] F. Nichele, A. Nath Pal, P. Pietsch, T. Ihn, K. Ensslin, C. Charpentier, and W, Wegscheider, Phys. Rev. Lett. **112**, 036802 (2014).
[3] V. S. Pribiag, A. J. A. Beukman, F. Qu, M. C. Cassidy, C. Charpentier, W. Wegscheider and L. P. Kouwenhoven, Nature Nanotechnologie doi:10.1038/nnano.2015.86 (2015).

Chapter 8

Neutron scattering and magnetism

(http://www.neutron.ethz.ch/)

Head
Prof. Dr. A. Zheludev

Academic Staff

S. Chillal	Dr. S. Gvasaliya	M. Haelg
G. Perren	Dr. J. Moeller	A. Mannig
Dr. K. Povarov	D. Schmidiger	G. Simutis
M. Thede	E. Wulf	

Masters Students

A. Reichert	HS2014

Administrative Staff
B. Abt

In 2014, the main focus of our group's research was on critical phenomena in organic quantum magnets, largely using neutron scattering techniques.

One important set of results was obtained on the $S = 1$ quantum antiferromagnetic material DTN. It was previously hailed as the best prototype of so-called Bose-Einstein condensation of magnons. We performed a renewed investigation of the field-induced ordering transition in this spin system by means of neutron diffraction, AC magnetometry and relaxation calorimetry. We found that any interpretation of the data is strongly influenced by a finite distribution of transition fields in the samples. This inhomogeneity is due to residual stress and the extremely strong magneto-elastic coupling in this material. It is always present in as-grown crystals, but was disregarded in previous studies. Taking this effect into account, we found that the order parameter critical exponent β and the crossover exponent ϕ are inconsistent with the BEC universality class [1].

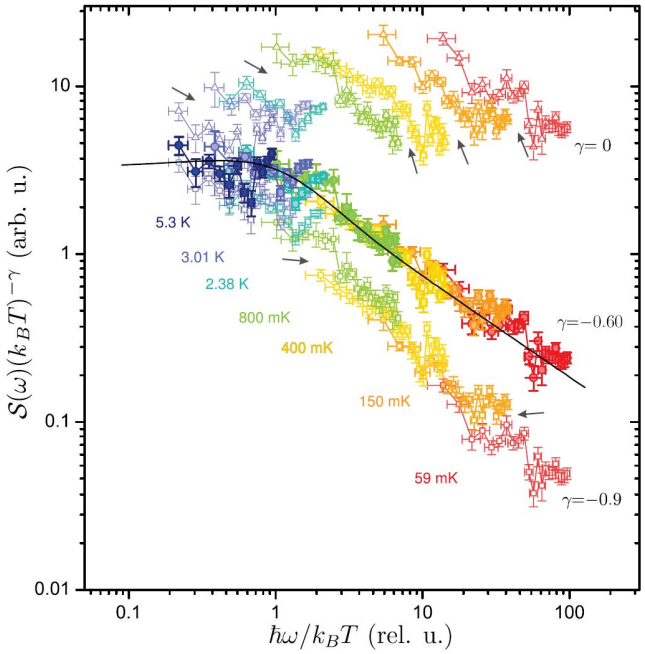

Figure 8.1: Local dynamic structure factor $S(\omega)$ measured in DIMPY at $H = 9$ T at several temperatures, plotted in the scaling representation with different scaling exponents γ Arrows mark the apparent violations of scaling for nonoptimal values of γ . The solid line is the exact TLL scaling function with the Luttinger parameter $K = 1.25$, corresponding to $\gamma = -0.6$.

Several new studies in our group were aimed at measuring universal scaling laws for spin correlation functions in one-dimensional systems. Particularly nice inelastic neutron data were obtained for the local dynamic structure factor in the quantum spin ladder $(C_7H_{10}N)_2CuBr_4$ (DIMPY) in its gapless quantum-critical phase [2]. We have show that the measured quantity has a scaling form consistent with expectations for a Tomonaga-Luttinger liquid with an *attractive* interactions between fermions. The measured Luttinger parameter K $\sim$ 1.25 and scaling function are in excellent agreement with density matrix renormalization group numerical calculations for the underlying spin Hamiltonian. The measured scaling of the local dynamic structure factor $S(\omega)$ is shown in Fig. 8.1. Another target compound was the anisotropic and bond-alternating spin-1 chain material [Ni(N,N'-bis(3-aminopropyl)propane-1,3-diamine(μ-NO_2)][ClO_4] (NTENP). The local dynamic structure factor was studied versus temperature using 3-axis and time-of-flight neutron spectroscopy at the field-induced quantum critical point. The results (Fig. 8.2) are in very good agreement with predictions for the quantum Ising model in a transverse field. Inelastic neutron scattering was also employed to study transverse spin correlations of a Heisenberg $S = 1/2$ chain compound 2(1,4-Dioxane)·2(H_2O)·$CuCl_2$ (CuDCl) in a magnetic field at half-saturation. We found a substantial increase of the Luttinger parameter to $K = 0.67$, compared to its zero-field value $K = 0.5$, and verified the theoretically predicted scaling relations for the transverse antiferromagnetic dynamic structure factor.

In addition to the study of *field*-induced criticality in quantum magnets, we investigated the *pressure*-induced quantum phase transitions that we previously discovered in the quantum spin liquid PHCC [3]. New neutron experiments

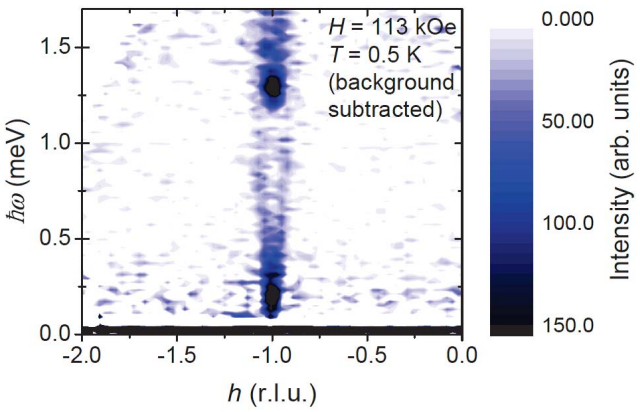

Figure 8.2: The low-energy inelastic neutron scattering spectra of NTENP at 0.5 K measured on LET spectrometer at the ISIS facility at $H = 113$ kOe.

performed at the SNS facility in Oak Ridge, TN, revealed a gapless excitation spectrum in both high-pressure phases, resolving a lingering controversy. An analysis of the data allowed us to attribute the phase transitions to a continuous variation in the strength of a single exchange constant, which has the strongest and most direct effect on the geometric frustration of exchange interactions in this compound. In addition to the transition in PHCC, we have discovered a new cascade of pressure-induced transitions in DTN, using muon spin rotation techniques. To better understand the physics underlying the phase transformations in both materials, we implemented a new capability of low-temperature Raman spectroscopy under high pressures. For this purpose we use diamond-anvil pressure cells, which enable us to track both structural (phonons) and magnetic excitations across all the relevant pressure-induced transitions.

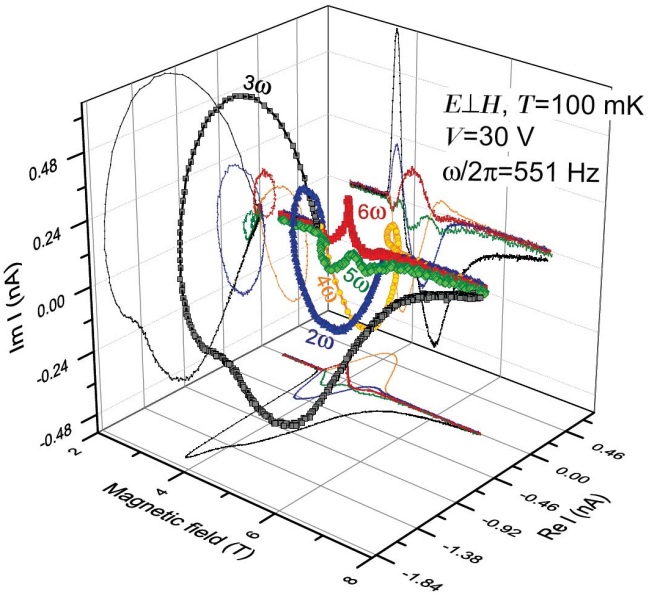

Figure 8.3: Current harmonics $I_n(H)$ for $n = 2 - -6$ measured in Sul-Cu_2Cl_4 at $T = 100\ mK$. Projections onto $Re - H$, $Im - H$ and $Re - Im$ planes are also shown. Drive voltage has amplitude $V = 30$ V and frequency $\omega/2\pi = 551$ Hz.

A totally new capability that we developed in the lab is measurements of dielectric properties at temperatures down to 50 mK. Using this setup, we study the behavior of the *dielectric* susceptibility and hypersusceptibilities at the field-induced *magnetic* quantum phase transition is the frustrated quantum spin ladder materials Sul-Cu_2Cl_4. Contrary to previous speculations, we have shown that electrical polarization is *not* critical at this quantum critical point. Instead, in the high-field state Sul-Cu_2Cl_4 is an *improper* quantum ferroelectric. Despite that, the dielectric response to even very small fields is huge and shows colossal non-linearities at the QCP. The magnetic-field dependence of several

dielectric hypersusceptibilities measured in Sul-Cu_2Cl_4 at $T = 100$ mK are shown in Fig. 8.3.

In addition to these studies of quantum criticality, we continued work on the effect of disorder on the ground states and excitations in quantum magnetic materials. A particular focus was on long-range magnetic ordering in weakly coupled quantum spin chains with exchange disorder. To this end, the random-bond antiferromagnet $BaCu_2(Si_{1-x}Ge_x)_2O_7$ was studied in muon spin rotation experiments as a function of disorder strength. Compared to the disorder-free parent materials, the saturation moment was found to be considerably reduced. More importantly, even in weakly disordered species, the magnetically ordered state was shown to be highly *inhomogeneous*. The results were interpreted in terms of the "infinite randomness" RG fixed point [4]. Another study focused on bulk and ESR measurements on the disordered strong-rung quantum spin ladders $Cu(Qnx)(Cl_{1-x}Br_x)_2$ [5].

As a separate project, we performed inelastic neutron scattering experiments and a series of bulk measurements to understand the behavior of weakly coupled quantum Heisenberg spin chains frustrated by Dzyaloshinskii-Moriya interactions. Our experiments enabled us to establish the hierarchy of relevant spin hamiltonian term for two such materials, namely $K_2CuSO_4Cl_2$ and $K_2CuSO_4Br_2$. The former compound is weakly frustrated and shows a rather conventional $H - T$ phase diagram. On the other hand, the Br-rich species has very strong DM frustration and, as a result, very unusual phase behavior [6].

[1] E. Wulf *et al.*, Phys. Rev. B **91**, 014406 (2015)
[2] K. Povarov *et al.*, Phys. Rev. B **91**, 020406(R) (2015)
[3] M. Thede *et al.*, Phys. Rev. Lett. **112**, 087204 (2014)
[4] M. Thede *et al.*, Phys. Rev. B **90**, 144407 (2014)
[5] K. Povarov *et al.*, JMMM **370**, 62 (2014)
[6] M. Helg *et al.*, Phys. Rev. B **90**, 174413 (2014)

Chapter 9

Spin Physics and Imaging

(www.spin.ethz.ch/)

Head
Prof. C. Degen

Academic Staff
Jens Boss
Urs Grob
Brad Moores
Ye Tao
Kevin Chang
Luca Lorenzelli
Tobias Rosskopf
Alexander Eichler
Michael Loretz
Hiroki Takahashi

Master Students
T. Holzherr (FS2014)

Technical Staff
C. Keck

Secretaries
J. Tamborini

In 2014, the spin physics group of Christian Degen has made further progress in the development and application of novel nanoscale magnetic microscopies. One highlight included the parallel imaging or multiple nuclear spin species in a nanowire test sample at $<$5 nm resolution and $<$1 nm positional accuracy. These measurements were enabled by a custom-built low-temperature scanning force microscope using nanomechanical sensors developed at the Binnig and Rohrer Nano Center. A second highlight was the application of a novel quantum sensor - the nitrogen-vacancy impurity in diamond - to the topological helimagnetic state of FeGe. Here we were able to show, for the first time, that the magnetic order undergoes both reversible and irreversible changes even far below the Neel temperature.

9.1 Highlights from the Diamond lab

Diamond has emerged as a unique material for a variety of applications, both because it is very robust and because it has defects with interesting properties. One of these defects, the nitrogen-vacancy center, has a single spin associated with it that shows quantum behavior up to room temperature. In the diamond lab we are exploiting the properties of single diamond spins for high resolution magnetic sensing applications.

9.1.1 Nanoscale nuclear magnetic resonance with a 1.9-nm-deep nitrogen-vacancy sensor

We have found a way to engineer extremely shallow NV centers, down to $\sim$2 nm, using a very slow oxygen etching technique. We have used a prepared sensor chip to detect nuclear magnetic resonance (NMR) signals from only $\sim$300 hydrogen nuclei located in a thin organic surface film, with a corresponding detection volume of about (1.8 nm)^3.

Loretz et al., Appl. Phys. Lett. 104, 033102 (2014).

9.1.2 Investigation of surface magnetic noise by shallow spins in diamond

We have analyzed the high-frequency spectrum of diamondâs magnetic surface states using shallow NV centers. These states are important as they cause decoherence of NV centers and limit the sensing capability. Our measurements indicate the presence of a least two types of magnetic states, one with fast (t_c $\sim$0.3 ns) and one with slow (t_c $\sim$1 us) fluctuations.

Rosskopf et al., Phys. Rev. Lett. 112, 147602 (2014).

9.1.3 Spurious harmonic response of multipulse quantum sensing sequences

We have discovered that a commonly used detection sequence, so called XY-decoupling, generates previously unrecognized harmonic signals. These spurious signals produce additional peaks in spectra, and interfere with nanoscale NMR detection.

Loretz et al., arXiv:1412.5768 (2014).

9.2 Highlights from the Magnetic resonance force microscopy lab

In the MRFM lab we investigate scanning force microscopy as a sensitive tool for measuring weak magnetic forces. Using micromechanical cantilevers, we measure nuclear magnetic resonance (NMR) signals from nanoscale sample volumes and study their spin physics. We exploit the scanning capability of MRFM to generate three-dimensional images of nanoscale objects, such as large biomolecules, with $<$10 nm spatial resolution. We are also interested in the physics of nanomechanical resonators, especially in what limits their sensitivity.

9.2.1 Single crystal diamond nanomechanical resonators with quality factors exceeding one million

Diamond has gained a reputation as a uniquely versatile material, yet one that is intricate to grow and process. Resonating nanostructures made of single-crystal diamond are expected to possess excellent mechanical properties, including high-quality factors and low dissipation. Here we demonstrate batch fabrication and mechanical measurements of single-crystal diamond cantilevers with thickness down to 85ânm, thickness uniformity better than 20ânm and lateral dimensions up to 240âμm. Quality factors exceeding one million are found at room temperature, surpassing those of state-of-the-art single-crystal silicon cantilevers of similar dimensions by roughly an order of magnitude. The corresponding thermal force noise for the best cantilevers is $5 \cdot 10^{-19}$ NâHz$^{-1/2}$ at millikelvin temperatures. Single-crystal diamond could thus directly improve existing force and mass sensors by a simple substitution of resonator material. Presented methods are easily adapted for fabrication of nanoelectromechanical systems, optomechanical resonators or nanophotonic devices that may lead to new applications in classical and quantum science.

Y. Tao et al., Nature Commun. 5, 3638 (2014).

9.2.2 Accelerated nanoscale MRI using phase multiplexing

We report a method for parallel detection of nanoscale nuclear magnetic resonance signals. Our technique relies on phase multiplexing, where the signals from different nuclear spin ensembles are encoded in the phase of an ultrasensitive magnetic detector. We demonstrate this technique by simultaneously acquiring statistically polarized spin signals from two different nuclear species (^{1}H, ^{19}F) and from up to six spatial locations in a nanowire test sample using a magnetic resonance force microscope. We obtain one-dimensional imaging resolution better than 5 nm, and subnanometer positional accuracy.

B. A. Moores et al., arXiv:1412.6914 (2014).

Chapter 10

Publications

P. Altmann, M. P. Walser, C. Reichl, W. Wegscheider, and G. Salis
Suppressed Decay of a Laterally Confined Persistent Spin Helix
Phys. Rev. B **90**, 201306 (2014)

S. Baer, C. Rössler, E. C. de Wiljes, P.-L. Ardelt, T. Ihn, K. Ensslin, C. Reichl, and W. Wegscheider
Interplay of fractional quantum Hall states and localization in quantum point contacts
Phys. Rev. B. **89**, 085424 (2014)

S. Baer, C. Rössler, T. Ihn, K. Ensslin, C. Reichl, and W. Wegscheider
Experimental Probe of Topological Orders and Edge Excitations in the Second Landau Level
Phys. Rev. B **90**, 075403 (2014)

C. Barraud, T. Choi, P. Butti, I. Shorubalko, T. Taniguchi, K. Watanabe, T. Ihn, and K. Ensslin
Field effect in the quantum Hall regime of a high mobility graphene wire
J. Appl. Phys. **116**, 073705 (2014)

J. Basset, A. Stockklauser, D.-D. Jarausch, T. Frey, C. Reichl, W. Wegscheider, A. Wallraff, K. Ensslin, and T. Ihn
Evaluating charge noise acting on semiconductor quantum dots in the circuit quantum electrodynamics architecture
Appl. Phys. Lett. **105**, 063105 (2014)

D. Bischoff, F. Libisch, J. Burgdörfer, T. Ihn, and K. Ensslin
Characterizing wave functions in graphene nanodevices: Electronic transport through ultrashort graphene constrictions on a boron nitride substrate
Phys. Rev. B **90**, 115405 (2014)

L. Bockhorn, I. V. Gornyi, D. Schuh, C. Reichl, W. Wegscheider, and R. J. Haug
Magnetoresistance Induced by Rare Strong Scatterers in a High-mobility Two-dimensional Electron Gas
Phys. Rev. B **90**, 165434 (2014)

F. R. Braakman, J. Danon, L. R. Schreiber, W. Wegscheider, and L. M. K. Vandersypen
Dynamics of Spin-flip Photon-assistend Tunneling
Phys. Rev. B **89**, 075417 (2014)

V. Chabanenko, E. Kuchuk, V. V. Yurchenko, P. Mikheenko, I. Abal'osheva, R. Cortés-Maldonado, F. Pérez-Rodriguez, J. Karpinski, N. D. Zhigadlo, S. Katrych, and R. Puzniak
Magnetic field penetration in MgB_2 single crystals: Pinning and Meissner holes
Low Temp. Phys. **40**, 621 (2014)

Y. S. Chen, S. Fält, W. Wegscheider, and G. Salis
Unidirectional Spin-orbit Interaction and Spin-helix State in a (110)-Orientied GaAs/(Al,Ga)As Quantum Well
Phys. Rev. B **90**, 121304(R) (2014)

S. Chillal, S. N. Gvasaliya, D. Schröter, M. Kraken, F. J. Litterst, T. A. Shaplygina, S. G. Lushnikov, and A. Zheludev
Magnetic short- and long-range order in $PbFe_{0.5}Ta_{0.5}O_3$
Phys. Rev. B **89**, 174418 (2014)

G. de Lange, D. Riste, M. J. Tiggelman, C. Eichler, L. Tornberg, G. Johansson, A. Wallraff, R. N. Schouten, and L. DiCarlo
Reversing Quantum Trajectories with Analog Feedback
Phys. Rev. Lett. **112**, 080501 (2014)

S. Dröscher, F. Molitor, T. Ihn, and K. Ensslin
Graphene constrictions
Book chapter in "Physics of Graphene", Springer (2014), Eds. H. Aoki, and M.S. Dresselhaus

I. L. Drichko, V. A. Malysh, I. Yu. Smirnov, L. E. Golub, S. A. Tarasenko, A. V. Suslov, O. A. Mironov, M. Kummer, and H. von Känel
In-plane magnetic field effect on hole cyclotron mass and gz-factor in high-mobility SiGe/Ge/SiGe structures
Phys. Rev. B **90**, 125436 (2014)

I. L. Drichko, V. A. Malysh, I. Yu. Smirnov, L. E. Golub, S. A. Tarasenko, A. V. Suslov, O. A. Mironov, M. Kummer, and H. von Känel
AC transport in p-Ge/GeSi quantum well in high magnetic fields
AIP Conf. Proc. **1610**, 53 (2014)

C. Eichler, and A. Wallraff
Controlling the dynamic range of a Josephson parametric amplifier
EPJ Quantum Technology **1**, 2 (2014)

C. Eichler, D. Bozyigit, C. Lang, L. Steffen, J. Fink, and A. Wallraff
Tomography schemes for characterizing itinerant microwave photon fields
Oxford Univ. Press, ISBN 978-0-19-968118-1 (2014)

C. Eichler, Y. Salathe, J. Mlynek, S. Schmidt, and A. Wallraff
Quantum-Limited Amplification and Entanglement in Coupled Nonlinear Resonators
Phys. Rev. Lett. **113**, 110502 (2014)

M. Eisterer, V. Mishev, M. Zehetmayer, N. D. Zhigadlo, S. Katrych, and J. Karpinski
Critical current anisotropy in Nd-1111 single crystals and the influence of neutron irradiation
Supercond. Sci. Technol. **27**, 044009 (2014)

C. V. Falub, T. Kreiliger, F. Isa, A. G. Taboada, M. Meduna, F. Pezzoli, R. Bergamaschini, A. Marzegalli, E. Müller, D. Chrastina, G. Isella, A. Neels, P. Niedermann, A. Dommann, L. Miglio, and H. von Känel
3D Heteroepitaxy of Mismatched Semiconductors on Silicon
Thin Solid Films **557**, 42 (2014)

C. G. Fatuzzo, Y. Sassa, M. Månsson, S. Pailhes, O. J. Lipscombe, S. M. Hayden, L. Patthey, M. Shi, M. Grioni, H. M. Ronnow, J. Mesot, O. Tjernberg, and J. Chang
Nodal Landau Fermi-liquid quasiparticles in overdoped $La_{1.77}Sr_{0.23}CuO_4$
Phys. Rev. B **89**, 205104 (2014)

A. Fognini
Ultrafast demagnetization. An electronic point of view
Dissertation ETH Zurich

A. Fognini, T. U. Michlmayr, G. Salvatella, C. Wetli, U. Ramsperger, T. Bähler, F. Sorgenfrei, M. Beye, A. Eschenlohr, N. Pontius, C. Stamm, F. Hieke, M. Dell'Angela, S. de Jong, R. Kukreja, N. Gerasimova, V. Rybnikov, A. Al-Shemmary, H. Redlin, J. Raabe, A. Föhlisch, H. A. Dürr, W. Wurth, D. Pescia, A. Vaterlaus, and Y. Acremann
Ultrafast reduction of the total magnetization in iron
Appl. Phys. Lett. **104**, 032402 (2014)

A. Fognini, G. Salvatella, T. U. Michlmayr, C. Wetli, U. Ramsperger, T. Bähler1, F. Sorgenfrei, M. Beye, A. Eschenlohr, N. Pontius, C. Stamm, F. Hieke, M. Dell'Angela, S. de Jong, R. Kukreja, N. Gerasimova, V. Rybnikov, H. Redlin, J. Raabe, A. Föhlisch, H. A. Dürr, W. Wurth, D. Pescia, A. Vaterlaus, and Y. Acremann
The role of space charge in spin-resolved photoemission experiments
New J. Phys. **16**, 043031 (2014)

F. Forster, G. Petersen, S. Manus, P. Hänggi, D. Schuh, W. Wegscheider, S. Kohler, and S. Ludwig
Characterization of Qubit Dephasing by Landau-Zener-Stückelberg-Majorana Interferometry
Phys. Rev. Lett. **112**, 116803 (2014)

C. Frigeri, S. Bietti, A. Scaccabarozzi, R. Bergamaschini, C. V. Falub, V. Grillo, M. Bollani, E. Bonera, P. Niedermann, H. von Känel, S. Sanguinetti, and L. Miglio
A structural characterization of GaAs MBE grown on Si pillars
Acta Physica Polonica A **125**, 986 (2014)

M. Frimmer, G. Puebla-Hellmann, A. Wallraff, and L. Novotny
The role of titanium in electromigrated tunnel junctions
App. Phys. Lett. **105**, 221118 (2014)

W. Fu, M. El Abbassi, T. Hasler, M. Jung, M. Steinacher, M. Calame, C. Schönenberger, G. Puebla-Hellmann, S. Hellmüller, T. Ihn, and A. Wallraff
Electrolyte gate dependent high-frequency measurement of graphene field-effect transistor for sensing applications
App. Phys. Lett. **104**, 013102 (2014)

C. Gadermaier, V. V. Kabanov, A. S. Alexandrov, L. Stojchevska, T. Mertelj, C. Manzoni, G. Cerullo, N. D. Zhigadlo, J. Karpinski, Y. Q. Cai, X. Yao, Y. Toda, M. Oda, S. Sugai, and D. Mihailovic
Strain-Induced Enhancement of the Electron Energy Relaxation in Strongly Correlated Superconductors
Phys. Rev. X **4**, 011056 (2014)

E. Gatti, F. Isa, D. Chrastina, E. Müller Gubler, F. Pezzoli, E. Grilli, and G. Isella
Ge/SiGe quantum wells on Si(111): Growth, structural, and optical properties
J. Appl. Phys. **116**, 043518 (2014)

V. N. Glazkov, G. Skoblin, D. Hüvonen, T. S. Yankova, and A. Zheludev
Formation of the ferromagnetically bound spin pairs in the bond-diluted spin-gap antiferromagnet PHCC
J. Phys.: Condens. Matter **26**, 486002 (2014)

S. Gustavsson, M. S. Rudner, L. S. Levitov, R. Leturcq, M. Studer, T. Ihn, and K. Ensslin
Ultra-narrow ionization resonances in a quantum dot under broadband excitation
Phys. Rev. B **89**, 115304 (2014)

S. N. Gvasaliya, R. A. Cowley, L. I. Ivleva, S. G. Lushnikov, B. Roessli, and A. Zheludev
Phase transition of the uniaxial disordered ferroelectric $Sr_{0.61}Ba_{0.39}Nb_2O_6$
J. Phys.: Condens. Matter **26**, 185901 (2014)

M. Hälg, W. E. A. Lorenz, K. Yu. Povarov, M. Månsson, Y. Skourski, and A. Zheludev
Quantum spin chains with frustration due to Dzyaloshinskii-Moriya interactions
Phys. Rev. B **90**, 174413 (2014)

A. Jacobsen, P. Simonet, K. Ensslin, and T. Ihn
Finite-bias spectroscopy of a three-terminal graphene quantum dot in the multilevel regime
Phys. Rev. B **89**, 165413 (2014)

F. Juranyi, M. Månsson, J. Gavilano, M. Mena, E. Pomjakushina, M. Medarde, J. Sugiyama, K. Kamazawa, B. Batlogg, H.-R. Ott, and T. Seydel
Dynamics across the structural transitions at elevated temperatures in $Na_{0.7}CoO_2$
EPJ Web of Conferences (2014)

S. Katrych, A. Pisoni, S. Bosma, S. Weyeneth, N. D. Zhigadlo, R. Gaal, J. Karpinski, and L. Forró
$L_4Fe_2As_2Te_{1-x}O_{4-y}F_y$ (L = Pr, Sm, Gd): a layered oxypnictide superconductor with T_c up to 45 K
Phys. Rev. B **89**, 024518 (2014)

R. Khasanov, A. Amato, P. K. Biswas, H. Luetkens, N. D. Zhigadlo, and B. Batlogg
$SrPt_3P$: A two-band single-gap superconductor
Phys. Rev. B **90**, 140507(R) (2014)

A. Kozikov, R. Steinacher, C. Rössler, T. Ihn, K. Ensslin, C. Reichl, and W. Wegscheider
Locally Induced Quantum Interference in Scanning Gate Experiments
New J. Phys. **16**, 053031 (2014)

T. Kreiliger, C. V. Falub, A. G. Taboada, F. Isa, S. Cecchi, R. Kaufmann, P. Niedermann, A. Pezous, S. Mouaziz, A. Dommann, G. Isella, and H. von Känel
Individual heterojunctions of 3D Germanium crystals on Silicon CMOS for monolithically integrated X-ray detector
Phys. Status Solidi A **211**, 131 (2014)

T. Kreiliger, C. V. Falub, F. Isa, G. Isella, D. Chrastina, R. Bergamaschini, A. Marzegalli, R. Kaufmann, P. Niedermann, A. Neels, E. Müller, M. Meduna, A. Dommann, L. Miglio, and H. von Känel
Epitaxial Ge-crystal arrays for X-ray detection
JINST **9**, C03019 (2014)

T. E. Kuzmicheva, S. A. Kuzmichev, and N. D. Zhigadlo
Doping Influence on $Sm_{1-x}Th_xOFeAs$ Superconducting Properties: Observation of the Effect of Intrinsic Multiple Andreev Reflections and Determination of the Superconducting Parameters
JETP Letters **99**, 136 (2014)

T. E. Kuzmicheva, S. A. Kuzmichev, M. G. Mikheev, Ya. G. Ponomarev, S. N. Tchesnokov, V. M. Pudalov, E. P. Khlybov, and N. D. Zhigadlo
Andreev spectroscopy of iron-based supercon-ductors: temperature dependence of the order parameters and scaling of $\Delta_{L,S}$ with T_c
Phys.-Usp. **57**, 819 (2014)

G. Lamura, T. Shiroka, P. Bonfà, S. Sanna, R. De Renzi, F. Caglieris, S. Iimura, H. Hosono, and M. Putti
Crossover between magnetism and superconductivity in LaFeAsO with low H-doping level
J. Phys.: Condens. Matter **26**, 295701 (2014)

U. Las Heras, A. Mezzacapo, L. Lamata, S. Filipp, A. Wallraff, and E. Solano
Digital Quantum Simulation of Spin Systems in Superconducting Circuits
Phys. Rev. Lett. **112**, 200501 (2014)

E. Liarokapis, M. Calamiotou, E. Siranidi, N. D. Zhigadlo, S. Katrych, and J. Karpinski
Pressure induced lattice anomalies in pnictides
J. Phys. Chem. Solids (2014)

A. Lichtenberger, C. Wagner, and A. Vaterlaus
Student concept knowledge in kinematics
Proceedings ESERA 2013, Strand 11, 1 (2014)

M. Loretz, J. M. Boss, T. Rosskopf, H. J. Mamin, D. Rugar, and C. L. Degen
Spurious harminic response of multipulse quantum sensing sequences
Cornell University Library arXiv:1412.5768

M. Loretz, S. Pezzagna, J. Meijer, and C. L. Degen
Nanoscale nuclear magnetic resonance with a 1.9-nm-deep nitrogen-vacancy sensor
Appl. Phys. Lett. **104**, 033102 (2014)

C. Maissen, G. Scalari, F. Valmorra, M. Beck, J. Faist, S. Cibella, R. Leoni, C. Reichl, C. Charpentier, and W. Wegscheider
Ultrastrong Coupling in the Near Field of Complementary Split-ring Resonators
Phys. Rev. B **90**, 205309 (2014)

T. Mathis, Y. Liu, L. Ai, Z. Ge, D. Lumpi, E. Horkel, B. Holzer, J. Froehlich, and B. Batlogg
Stable organic field-effect-transistors with high mobilities unaffected by supporting dielectric based on phenylene-bridged thienobenzothiophene
J. Appl. Phys. **115**, 043707 (2014)

M. Meduna, C. V. Falub, F. Isa, D. Chrastina, T. Kreiliger, G. Isella, A. G. Taboada, P. Niedermann, and H. von Känel
X-ray nano-diffraction on epitaxial crystals
Quantum Matter **3**, 290 (2014)

M. Meduna, C. V. Falub, F. Isa, D. Chrastina, T. Kreiliger, G. Isella, and H. von Känel
Reconstruction of crystal shapes by X-ray nanodiffraction from three-dimensional superlattices
J. Appl. Cryst. **47**, 2030 (2014)

A. Mezzacapo, L. Lamata, S. Filipp, and E. Solano
Many-Body Interactions with Tunable-Coupling Transmon Qubits
Phys. Rev. Lett. **113**, 050501 (2014)

C. Mirri, A. Dusza, X. Zhu, H. Lei, H. Ryu, L. Degiorgi, and C. Petrovic
Excitation spectrum in Ni- and Cu-doped $ZrTe_3$
Phys. Rev. B **89**, 035144 (2014)

C. Mirri, A. Dusza, S. Bastelberger, J.-H. Chu, H.-H. Kuo, I. R. Fisher, and L. Degiorgi
Hysteretic behavior in the optical response of the underdoped Fe-arsenide $Ba(Fe_{1-x}Co_x)_2As_2$ in the electronic nematic phase
Phys. Rev. B **89**, 060501(R) (2014)

C. Mirri, A. Dusza, S. Bastelberger, J.-H. Chu, H.-H. Kuo, I. R. Fisher, and L. Degiorgi
Nematic-driven anisotropic electronic properties of underdoped detwinned $Ba(Fe_{1-x}Co_x)_2As_2$ revealed by optical spectroscopy
Phys. Rev. B **90**, 155125 (2014)

J. A. Mlynek, A. A. Abdumalikov, C. Eichler, and A. Wallraff
Observation of Dicke superradiance for two artificial atoms in a cavity with high decay rate
Nature Communications **5**, 5186 (2014)

P. J. W. Moll, L. Balicas, X. Zhu, H.-H. Wen, N. D. Zhigadlo, J. Karpinski, and B. Batlogg
Critical current oscillations in the intrinsic hybrid vortex state of SmFeAs(O,F)
Phys. Rev. Lett. **113**, 186402 (2014)

P. J. W. Moll, X. Zhu, P. Cheng, H.-H. Wen, and B. Batlogg
Intrinsic Josephson junctions in the iron-based multi-band superconductor $(V_2Sr_4O_6)Fe_2As_2$
Nature Physics **10**, 644 (2014)

B. A. Moores, A. Eichler, Y. Tao, H. Takahashi, P. Navaretti, and C. L. Degen
Phase-multiplexed detection for accelerated nanoscale MRI
Cornell University Library arXiv:1412.6914

F. Nichele, S. Chesi, S. Hennel, A. Wittmann, C. Gerl, W. Wegscheider, D. Loss, T. Ihn, and K. Ensslin
Characterization of spin-orbit interactions of GaAs heavy holes using a quantum point contact
Phys. Rev. Lett. **113**, 046801 (2014)

P. Procházka, J. Mach, D. Bischoff, Z. Lišková, P. Dvořák, M. Vaňatka, P. Simonet, A. Varlet, D. Hemzal, M. Petrenec, L. Kalina, M. Bartošík, K. Ensslin, P. Varga, J. Čechal, and T. Šikola
Ultrasmooth metallic foils for growth of high quality graphene by chemical vapor deposition
Nanotechnology **25**, 185601 (2014)

F. Nichele, A. N. Pal, P. Pietsch, T. Ihn, K. Ensslin, C. Charpentier, and W. Wegscheider
Insulating State and Giant Nonlocal Response in an InAs/GaSb Quantum Well in the Quantum Hall Regime
Phys. Rev. Lett. **112**, 036802 (2014)

F. Nichele, A. N. Pal, R. Winkler, C. Gerl, W. Wegscheider, T. Ihn, and K. Ensslin
Spin-orbit Splitting and Effective Masses in p-type GaAs Two-dimensional Hole Gases
Phys. Rev. B **89**, 081306 (2014)

S. Ono, R. Häusermann, D. Chiba, K. Shimamura, T. Ono, and B. Batlogg
High performance organic field-effect transistors with ultra-thin HfO_2 gate insulator deposited directly onto the organic semiconductor
Appl. Phys. Lett. **104**, 013307 (2014)

H.-R. Ott
Extended Foreword, in *Strongly Correlated Systems, Experimental Techniques*
Springer Series in Solid State Sciences **180**, Eds. A. Avella and F. Mancini (Springer, Heidelberg) (2014)

N. Pascher, F. Timpu, C. Rössler, T. Ihn, K. Ensslin, C. Reichl, and W. Wegscheider
Resonant Electron Tunneling in a Tip-controlled Pontential Landscape
Phys. Rev. B **89**, 245408 (2014)

N. Pascher, C. Rössler, T. Ihn, K. Ensslin, C. Reichl, and W. Wegscheider
Imaging the Conductance of Integer and Fractional Quantum Hall Edge States
Phys. Rev. X **4**, 085406 (2014)

M. Pechal, L. Huthmacher, C. Eichler, S. Zeytinoğlu, A. A. Abdumalikov Jr., S. Berger, A. Wallraff, and S. Filipp
Microwave-Controlled Generation of Shaped Single Photons in Circuit Quantum Electrodynamics
Phys. Rev. X **4**, 041010 (2014)

F. Pezzoli, F. Isa, G. Isella, C. V. Falub, T. Kreiliger, M. Salvalaglio, R. Bergamaschini, E. Grilli, M. Guzzi, H. von Känel, and L. Miglio
Germanium crystals on silicon show their light
Phys. Rev. Applied **1**, 044005 (2014)

M. Pikulski, T. Shiroka, H.-R. Ott, and J. Mesot
A firmware-defined digital direct-sampling NMR spectrometer for condensed matter physics
Rev. Sci. Instrum. **85**, 093906 (2014)

K. Yu. Povarov, D. Schmidiger, N. Reynolds, A. Zheludev, and R. Bewley
Scaling of temporal correlations in an attractive Tomonaga-Luttinger spin liquid
Phys. Rev. B **91**, 020406(R) (2015)

K. Yu. Povarov, W. E. A. Lorenz, F. Xiao, C. P. Landee, Y. Krasnikova, and A. Zheludev
The tunable quantum spin ladder $Cu(Qnx)(Cl_{1-x}Br_x)_2$
JMMM 370, **62** (2014)

C. Rössler, S. Burkhard, T. Krähenmann, M. Roosli, P. Märki, J. Basset, T. Ihn, K. Ensslin, C. Reichl, and W. Wegscheider
Spectroscopy of Equilibrium and Nonequilibrium Charge Transfer in Semiconductor Quantum Structures
Phys. Rev. B **90**, 081302 (2014)

A. N. Ramanayaka, T. Ye, H.-C. Liu, W. Wegscheider, and R. G. Mani
Interaction of Microwave Radiation with the High Mobility Two-dimensional Electron System in GaAs/AlGaAs Heterostructures
Phys. B. **453**, 43 (2014)

C. Reichl, J. Chen, S. Baer, C. Rössler, T. Ihn, K. Ensslin, W. Dietsche, and W. Wegscheider
Increasing the $\nu = 5/2$ Gap Energy; an Analysis of MBE Growth Parameters
New J. Phys. **16**, 023014 (2014)

T. Rosskopf, A. Dussaux, K. Ohashi, M. Loretz, R. Schrihagl, H. Watanabe, S. Shikata, K. M. Itoh, and C. L. Degen
Investigation of surface magnetic noise by shallow spins in diamond
Phys. Rev. Lett. **112**, 147602 (2014)

G. Salis, M. P. Walser, P. Altmann, C. Reichl, and W. Wegscheider
Dynamics of Localized Spin Excitation Close to the Spin-helix Regime
Phys. Rev. B **89**, 045304 (2014)

A. Scaccabarozzi, S. Bietti, A. Fedorov, H. von Känel, L. Miglio, and S. Sanguinetti
Photoluminescence study of the strain relaxation of GaAs crystals grown on deeply patterned Si substrates
J. Cryst. Growth **401**, 559 (2014)

P. Scarlino, E. Kawakami, P. Stano, M. Shafiei, C. Reichl, W. Wegscheider, and L. M. K. Vandersypen
Spin-Relaxation Anisotropy in GaAs Quantum Dot
Phys. Rev. Lett. **113**, 256802 (2014)

C. Schönhuber, M. P. Walser, G. Salis, C. Reichl, W. Wegscheider, T. Korn, and C. Schüller
Inelastic Light-scattering from Spin-density Excitations in the Regime of the Persistent Spin Helix in a GaAs-AlGaAs Quantum Well
Phys. Rev. B **89**, 085406 (2014)

G. Schiltz, and A. Vaterlaus
Mobile Lab Classes. Scanning Tunneling Microscopy for secondary school students (ages 16-18)
ICPE-EPEC 2013 Conference Proceedings, 1034 (2014)

R. Schirhagl, K. Chang, M. Loretz, and C. L. Degen
Nitrogen-Vacancy Centers in Diamond: Nanoscale Sensors for Physics and Biology
Annu. Rev. Phys. Chem. **65**, 83 (2014)

E. Schubert, J. Heyder, F. Bauer, B. Waschneck, W. Stumpf, W. Wegscheider, J. von Delft, S. Ludwig, and A. Högele
Toward Combined Transport and Optical Studies of the 0.7-anomaly in a Quantum Point Contact
Phys. Status Solidi B **251**, 1931(2014)

K. Shibata, N. Pascher, P. J. J. Luukko, E. Räsänen, S. Schnez, T. Ihn, K. Ensslin, and K. Hirakawa
Electron magneto-tunneling through single self-assembled InAs quantum dashes
Appl. Phys. Express **7**, 045001 (2014)

S. Smolka, W. Wüster, F. Haupt, S. Fält, W. Wegscheider, A. Imamoglu
Cavity Quantum Electrodynamics with Many-body States of a Two-dimensional Electron Gas
Science **346**, 332 (2014)

A. G. Taboada, T. Kreiliger, C. V. Falub, F. Isa, M. Salvalaglio, L. Wewior, D. Fuster, M. Richter, E. Uccelli, P. Niedermann, A. Neels, F. Mancarella, B. Alén, L. Miglio, A. Dommann, G. Isella, and H. von Känel
Strain relaxation of GaAs/Ge crystals grown on micro patterned Si substrates by MOVPE
Appl. Phys. Lett. **104**, 022112 (2014)

Y. Tao, J. M. Boss, B. A. Moores, and C. L. Degen
Single crystal diamond nanomechanical resonators with quality factors exceeding one million
Nature Communications **5**, 3638 (2014)

M. Thede, T. Haku, T. Masuda, C. Baines, E. Pomjakushina, G. Dhalenne, A. Revcolevschi, E. Morenzoni, and A. Zheludev
Inhomogeneous ordering in weakly coupled Heisenberg S = 1/2 chains with random bonds
Phys. Rev. B **90**, 144407 (2014)

M. Thede, A. Mannig, M. Månsson, D. Hüvonen, R. Khasanov, E. Morenzoni, and A. Zheludev
Pressure-induced quantum critical and multicritical points in a frustrated spin liquid
Phys. Rev. Lett. **112**, 087204 (2014)

T. Thiele, S. Filipp, J. A. Agner, H. Schmutz, J. Deiglmayr, M. Stammeier, P. Allmendinger, F. Merkt, and A. Wallraff
Manipulating Rydberg atoms close to surfaces at cryogenic temperatures
Phys. Rev. A **90**, 013414 (2014)

R. Völkl, M. Schwemmer, M. Griesbeck, S. A. Tarasenko, D. Schuh, W. Wegscheider, C. Schüller, and T. Korn
Spin Polarization, Dephasing, and Photoinduced Spin Diffusion in (110-)grown Two-dimensional Electron Systems
Phys. Rev. B **89**, 075424 (2014)

A. Varlet, D. Bischoff, P. Simonet, K. Watanabe, T. Taniguchi, T. Ihn, K. Ensslin, M. Mucha-Kruczynski, and V. I. Falk
Anomalous sequence of quantum Hall liquids revealing tunable Lifshitz transition in bilayer graphene
Phys. Rev. Lett. **113**, 116602 (2014)

A. Varlet, M.-H. Liu, V. Krueckl, D. Bischoff, P. Simonet, K. Watanabe, T. Taniguchi, K. Richter, K. Ensslin, and T. Ihn
Fabry-Perot interference in gapped bilayer graphene with broken anti-Klein tunneling
Phys. Rev. Lett. **113**, 116601 (2014)

H. von Känel, F. Isa, C. V. Falub, E. J. Barthazy, E. Müller, D. Chrastina, G. Isella, T. Kreiliger, A. G. Taboada, M. Meduna, R. Kaufmann, A. Neels, A. Dommann, P. Niedermann, F. Mancarella, M. Mauceri, M. Puglisi, D. Crippa, F. La Via, R. Anzalone, N. Piluso, R. Bergamaschini, A. Marzegalli, and L. Miglio
Three-dimensional Epitaxial Si1-xGex, Ge and SiC Crystals on Deeply Patterned Si Substrates
ECS Transactions **64**, 631 (2014)

C. Wagner, and A. Vaterlaus
Non-slipping domains of a pulled spool
Eur. J. Phys. **35**, 0650023 (2014)

C. Wagner, and A. Vaterlaus
Agent Based Simulation of Group Work Performance
ICPE-EPEC 2013 Proceedings, 929 (2014)

J. S. White, C. J. Bowell, A. S. Cameron, R. W. Heslop, J. Mesot, J. L. Gavilano, S. Strässle, L. Mächler, R. Khasanov, C. D. Dewhurst, J. Karpinski, and E. M. Forgan
Magnetic field dependence of the basal-plane superconducting anisotropy in $YBa_2Cu_4O_8$ from small-angle neutron scattering measurements of the vortex lattice
Phys. Rev. B **89**, 024501 (2014)

E. Wulf, D. Hüvonen, R. Schönemann, H. Kühne, T. Herrmannsdörfer, I. Glavatskyy, S. Gerischer, K. Kiefer, S. Gvasaliya, andÂ A. Zheludev
Critical exponents and intrinsic broadening of the field-induced transition in $NiCl_2{\cdot}4SC(NH_2)_2$
Phys. Rev. B **91**, 014406 (2015)

N. Xu, P. K. Biswas, J. H. Dil, R. S. Dhaka, G. Landolt, S. Muff, C. E. Matt, X. Shi, N. C. Plumb, M. Radovic, E. Pomjakushina, K. Conder, A. Amato, S. V. Borisenko, R. Yu, H.-M. Weng, Z. Fang, X. Dai, J. Mesot, H. Ding, and M. Shi
Direct observation of the spin texture in SmB_6 as evidence of the topological Kondo insulator
Nature Communications **5**, 4566 (2014)

N. Xu, C. E. Matt, E. Pomjakushina, X. Shi, R. S. Dhaka, N. C. Plumb, M. Radovic, P. K. Biswas, D. Evtushinsky, V. Zabolotnyy, J. H. Dil, K. Conder, J. Mesot, H. Ding, and M. Shi
Exotic Kondo crossover in a wide temperature region in the topological Kondo insulator SmB_6 revealed by high-resolution ARPES
Phys. Rev. B **90**, 085148 (2014)

T. Ye, H.-C. Liu, W. Wegscheider, and R. G. Mani
Combined Study of Microwave-Power/Linear-Polarization Dependence of the Microwave-Radiation-Induced Magnetoresistance Oscillations in GaAs/AlGaAs Devices
Phys. Rev. B **89**, 155307 (2014)

T. Ye, W. Wegscheider, and R. G. Mani
Evolution of the Linear-polarization-angle-dependence of the Radiation-induced Magnetoresistance-oscillations with Microwave Power
App. Phys. Lett. **105**, 191609 (2014)

M. E. Zayed, C. Rüegg, T. Strässle, U. Stuhr, B. Roessli, M. Ay, J. Mesot, P. Link, E. Pomjakushina, M. Stingaciu, K. Conder, and H. M. Ronnow
Correlated decay of triplet excitations in the Shastry-Sutherland compound $SrCu_2(BO_3)_2$
Phys. Rev. Lett. **113**, 067201 (2014)

N. D. Zhigadlo
Spontaneous growth of diamond from MnNi solvent-catalyst using opposed anvil-type high-pressure apparatus
J. Cryst. Growth **395**, 1 (2014)

N. D. Zhigadlo
Crystal growth of hexagonal boron nitride (hBN) from Mg-B-N solvent system under high pressure
J. Cryst. Growth **402**, 308 (2014)

T. Zimmerling, and B. Batlogg
Improving charge injection in high-mobility rubrene crystals: From contact-limited to channel-dominated transistors
J. Appl. Phys. **115**, 164511 (2014)

Chapter 11

Presentations

11.1 Talks

(⋆ **invited)**

Baer, S.
Quantum dots in the Quantum Hall regime
NCCR QSIT evaluation, ETH Zürich, Switzerland, 08.12.2011

⋆ Batlogg, B.
Slow Abrikosov to fast moving Josephson vortex transition in REFeAs(O,F)
Electronic Materials and Applications Conference EMA2014, Orlando, FL, USA, 23.01.2014

⋆ Batlogg, B.
Charge transport and trapping in organic molecular semiconductors
The 8th International Symposium on Organic Molecular Electronics, Tokyo, Japan, 15.05.2014

⋆ Batlogg, B.
Charge transport and trapping in organic molecular semiconductors
NAIST Nara Institute of Science and Technology, Kansai Science City, Nara, Japan, 16.05.2014

⋆ Batlogg, B.
Electronic properties of layered superconductors: where details matter
Third International Conference on Advanced Materials Modelling ICAMM-2014, Nantes, France, 08.07.2014

⋆ Batlogg, B.
Wieviel Technik brauchen wir?
IngCH Technikwoche Kantonsschule Enge, Zurich, Switzerland, 29.09.2014

⋆ Batlogg, B.
Exploring charge transport in high quality single crystal OFET devices
Workshop on Exotic Electronic Transport, Chiba, Japan, 16.10.14

⋆ Batlogg, B.
In search of the mobility edge in organic molecular semiconductors
International Workshop on Field-Effect Transistors and Functional Interfaces FET2014, Kashiwa, Japan, 17.10.2014

⋆ Batlogg, B.
Trap states and mobility edge in organic molecular crystals
Workshop on Exotic Electronic Transport, Chiba, Japan, 22.10.14

Berger, S.
Exploring the Effect of Noise on the Berry Phase using circuit QED
APS March Meeting, Denver, CO, USA, 03.03.2014

⋆ Berger, S.
What noise does to the Berry phase, in terms of circuit QED
Advanced many-body physics and statistical methods in mesoscopic systems II, Brasov, Romania, 05.09.2014

Berl, M.
Independently Contacted High Mobility AlGaAs/GaAs-Quantum Wires
QSIT Junior Meeting, Passugg, Switzerland, 11.06.2014

⋆ Bischoff, D.
Characterizing electron wave-functions in ultrashort graphene nanoribbons on a hexagonal boron nitride substrate
Graphene Week 2014, Gothenburg, Sweden, 23.06.2014

Blülle, B.
Bulk and interface charge transport in organic molecular crystals
Workshop on Exotic Electronic Transport, Chiba, Japan, 16.10.2014

Blülle, B.
Similarities between bulk and interface charge transport in rubrene single crystals
International Workshop on Field-Effect Transistors and Functional Interfaces FET2014, Kashiwa, Japan, 17.10.2014

Boss, J.
Toward hyperpolarization of nuclear spins on diamond surfaces
COST Annual Meeting on “Spin Hyperpolarisation in NMR and MRI”, Zurich, Switzerland, 27.06.2014

Braem, B. A.
Helium Heater: Warm up the helium recovery line
Qstarter award lunch, Zurich, Switzerland, 24.09.2014

Chang, T.
Nanoscale Magnetic Imaging by Scanning Diamond Magnetometry
55th Experimental Nuclear Magnetic Resonance Conference, Boston, MA, USA, 03.03.2014

Charpentier, C.
MBE Growth of High-quality Sb-based Semiconductor Heterostructures
NCCR QSIT General Meeting, Arosa, Switzerland, 07.02.2014

Chillal, S.
Magnetic short and long range order in a disordered perovskite
APS March Meeting, Denver, CO, USA, 03.03.2014

Chinotti, M.
muSR studies of the pressure dependent superconducting properties of Ca3Ir4Sn13 compound
Master thesis, ETH Zurich, PSI Villigen, Switzerland, 15.09.2014

Degen, C.
Diamond-based quantum sensing
QSIT Winter School, Arosa, Switzerland, 03.02.2014

Degen, C.
Diamond-based quantum sensing
Hasselt Diamond Workshop, Hasselt, Belgium, 19.02.2014

Degen, C.
Adventures in ultrasensitive force detection
Swiss Nanoconvention, Brugg, Switzerland, 21.05.2014

Degen, C.
Nitrogen vacancy centers in diamond: Nanoscale sensors for physics and biology
CCMX Technology Aperitif on "New Perspectives on Magnetic Sensors", ETH Zurich, Switzerland, 05.06.2014

Degen, C.
Nitrogen vacancy centers in diamond: Nanoscale sensors for physics and biology
From Solid State to Biophysics VII, Cavtat/Dubrovnik, Croatia, 07.06.2014

Degen, C.
Magnetic-resonance force microscopy
CIMST Summer School, ETH Zurich, Switzerland, 03.09.2014

Degen, C.
Recent progress in nanoscale NMR
53th Annual Meeting of the Nuclear Magnetic Resonance Society of Japan, Osaka, Japan, 04.11.2014

⋆ Degiorgi, L.
Charge Dynamics in Broken Symmetry Correlated States
Guest Lecture of the Doctoral School 'Solid4Fun', Technical University Vienna, Austria, 04.04.2014

⋆ Degiorgi, L.
Chasing the nematic phase in detwinned $Ba(Co_xFe_{1-x})_2As_2$ with optical investigations
Spring Meeting of the Materials Research Society, San Francisco, CA, USA, 21.04.2014

⋆ Degiorgi, L.
Chasing the nematic phase in detwinned $Ba(Co_xFe_{1-x})_2As_2$ with optical investigations
International Conference on Superconductivity and Magnetism (ICSM2014), Antalya, Turkey, 27.04.2014

⋆ Degiorgi, L.
Hysteretic behavior in the optical response of the underdoped Fe-arsenide $Ba(Co_xFe_{1-x})_2As_2$ in the electronic nematic phase
International Conference on Low Energy Electrodynamics in Solids (LEES), Amboise Loire Valley, France, 29.06.2014

* Degiorgi, L.
Hysteretic behavior in the optical response of the underdoped Fe-arsenide $Ba(Co_xFe_{1-x})_2As_2$ in the electronic nematic phase
International Workshop Superstripes 2014, Erice, Italy, 25.07.2014

* Degiorgi, L.
Hysteretic behavior in the optical response of the underdoped Fe-arsenide $Ba(Co_xFe_{1-x})_2As_2$ in the electronic nematic phase
International Workshop on Electronic Crystals, ECRYS 2014, Cargese, France, 11.08.2014

* Degiorgi, L.
Nematic-driven anisotropic electronic properties of underdoped detwinned $Ba(Co_xFe_{1-x})_2As_2$ revealed by optical spectroscopy
International Workshop on Magnetism, Bad Metals and Superconductivity: Iron Pnictides and Beyond, University of California, Santa Barbara, CA, USA, 01.09.2014

Dussaux, A.
Scanning diamond magnetometry with single nitrogen-vacancy centers
De Beers Diamond Conference, Warwick, United Kingdom, 07.07.2014

Eichler, A.
The role of broken potential symmetry for nanomechanical resonators
APS March Meeting, Denver, CO, USA, 03.03.2014

Eichler, A.
An new phase multiplexing technique to speed up magnetic resonance force microscopy
Swiss Physical Society Meeting 2014, 01.07.2014

Eichler, A.
Towards subnanometer magnetic resonance imaging through phase multiplexing
Seminar at ICFO, Barcelona, Spain, 17.10.2014

* Eichler, C.
Amplification of Microwave Signals at the Quantum Limit
Meeting of the CCQED fellows, Venet, Austria, 24.03.2014

* Eichler, C.
Quantum limited amplification and entanglement of microwave fields with coupled nonlinear cavities
QSIT lunch seminar, ETH Zurich, Zurich, Switzerland, 03.04.2014

* Eichler, C.
Exploring Quantum Microwave Radiation Using Linear Detectors
Workshop on Quantum Radar, Naval Research Laboratories, Washington D.C., USA, 18.08.2014

* Eichler, C.
Quantum Simulations with Microwave Radiation
67th Fujihara seminar, Tomakomai, Hokkaido, Japan, 24.09.2014

⋆ Eichler, C.
Simulating an interacting quantum gas with superconducting circuits
EPIQ Seminar for quantum information science, University of Sherbrooke, Canada, 03.11.2014

⋆ Ensslin, K.
Electron transport through quantum dots
18th International Winterschool on New Developments in Solid State Physics, Mauterndorf, Austria, 23.02.2014

⋆ Ensslin, K.
Graphene quantum dots: localized states, edges and bilayer system
APS March Meeting, Denver, CO, USA, 03.03.2014

⋆ Ensslin, K.
Graphene quantum dots: localized states, edges and bilayer system
International Winterschool on Electronic Properties of Novel Materials: Molecular Nanostructures, Kirchberg, Austria, 08.03.2014

⋆ Ensslin, K.
Change of Fermi level topology in bilayer graphene
Graphene flagship, meeting of modul on Fundamental Science, Lancaster, United Kingdom, 07.04.2014

⋆ Ensslin, K.
Graphene quantum structures
International Symposium on Carbon Electronics (ISCE), Seoul National University, Korea, 08.05.2014

⋆ Ensslin, K.
Insulating state and giant non-local response in an InAs/GaSb quantum well in the quantum Hall regime
9th Research Workshop NANOPETER: Fundamentals of Electronic Nanosystems, St. Petersburg, Russia, 21.06.2014

⋆ Ensslin, K.
Spin-orbit effects in p-type QPCs
Second School and Conference on Spin-based Quantum Information Processing, Konstanz, Germany, 18.08.2014

⋆ Ensslin, K.
Imaging integer and fractional quantum Hall edge states
XXXVIII International Conference of Theoretical Physics, Correlations and Coherence at different scales, Ustron, Poland, 05.09.2014

⋆ Ensslin, K.
Imaging of integer and fractional quantum Hall edge states
Workshop on Nanoscience and Low Dimensional Quantum Matter, Dublin, Ireland, 10.11.2014

⋆ Ensslin, K.
Imaging integer and fractional quantum Hall edge states
1st International Symposium on Interactive Material Science Cadet Program, Osaka, Japan, 17.11.2014

⋆ Ensslin, K.
Graphene quantum devices
MRS Meeting, Boston, MA, USA, 30.11.2014

* Ensslin, K.
Waren Sie schon einmal gleichzeitig an zwei verschiedenen Orten? Quantenphysik und Informationsverarbeitung
ETH Unterwegs, Gymnasium Münchenstein, Switzerland, 19.03.2014

* Ensslin, K.
Local investigation of ballistic transport in semiconductor nanostructures
Seminar at ESPCI, Laboratoire Physique et Etude des Matériaux, Paris, France, 20.03.2014

* Ensslin, K.
Waren Sie schon einmal gleichzeitig an zwei verschiedenen Orten? Quantenphysik und Informationsverarbeitung
ETH Unterwegs, Kantonale Mittelschule Uri, Altdorf, Switzerland, 28.03.2014

* Ensslin, K.
Waren Sie schon einmal gleichzeitig an zwei verschiedenen Orten? Quantenphysik und Informationsverarbeitung
ETH Unterwegs, Kantonsschule Baldegg, Switzerland, 03.04.2014

* Ensslin, K.
Waren Sie schon einmal gleichzeitig an zwei verschiedenen Orten? Quantenphysik und Informationsverarbeitung
Rotary Club Küsnacht, Switzerland, 03.04.2014

* Ensslin, K.
Lifschitz transition in bilayer graphene
Seminar at Fudan University, Shanghai, China, 05.05.2014

* Ensslin, K.
Lifschitz transition in bilayer graphene
Seminar at Hefei University, Hefei, China, 06.05.2014

* Ensslin, K.
Neuartige Quantensysteme mit Graphen?
Volkshochschule Zurich, Switzerland, 18.09.2014

* Ensslin, K.
Semiconductor nanostructures: where does the current flow?
Physics colloquium, Univ. Augsburg, Germany, 20.10.2014

* Ensslin, K.
Waren Sie schon einmal gleichzeitig an zwei verschiedenen Orten? Quantenphysik und Informationsverarbeitung
ETH Unterwegs, Kantonsschule Chur, Switzerland, 21.10.2014

* Ensslin, K.
Waren Sie schon einmal gleichzeitig an zwei verschiedenen Orten? Quantenphysik und Informationsverarbeitung
ETH Unterwegs, Kantonsschule Wil, Switzerland, 28.10.2014

* Ensslin, K.
Waren Sie schon einmal gleichzeitig an zwei verschiedenen Orten? Quantenphysik und Informationsverarbeitung
TECDAY der Schweizerischen Akademie der Wissenschaften, Kantonsschule Limmattal, Switzerland, 04.11.2014

⋆ Ensslin, K.
Non-local transport in InAs-GaSb quantum wells
NTT Research, Atsugi, Japan, 20.11.2014

⋆ Ensslin, K.
Quantum mechanics and information processing
Interdisziplinäres Forschungskolloquium des Collegium Helveticum, ETH Zurich, Switzerland, 12.12.2014

⋆ Filipp, S.
Testing Quantum Mechanics with Superconducting Artificial Atoms
Workshop on 'Quantum Mechanics Tests in Particle, Atomic, Nuclear and Complex Systems: 50 Years after Bell's Renowned Theorem', Trento, Italy, 24.02.2014

⋆ Filipp, S.
Exploring geometric phases and gates with superconducting quantum circuits
21st biennial Australian Institute of Physics Congress âThe Art of Physicsâ, Australian National University, Canberra, Australia, 07.12.2014

Hofmann, A.
Thermodynamics of coupled quantum dot systems in AlGaAs/GaAs
10th Capri Spring School 2014, Capri, Italy, 28.04.2014

⋆ Ihn T.
Bilayer Graphene: Phase-coherent transport and broken symmetry states
25. Edgar Lüscher Seminar 2014, Klosters, Switzerland, 1.2.2014

⋆ Ihn, T.
Semiconductor (Nano)Structures
3rd NCCR QSIT Winter School, Arosa, Switzerland, 03.02.2014

⋆ Ihn, T.
Low-temperature scanning probe investigations of nanostructures at high- and low magnetic fields
DPG Spring Meeting, Dresden, 30.03.2014

Ihn, T.
Local Imaging of Graphene and Quantum Hall Systems
Q-NET meeting, San Sebastian, Spain, 20.2.2014

⋆ Ihn, T.
Imaging electron transport in semiconductor nanostructures on the scale of the electron wavelength
CeNS workshop, Venice, Italy, 22.09.2014

Isa, F.
Photoluminescence of dislocation-free Ge quantum well micro-crystals on patterned Si substrates
10th Intl. Workshop on Epitaxial Semiconductors on Patterned Substrates and Novel Index Surfaces ESPS-NIS 2014, Traunkirchen, Austria, 20.07.2014

Isa, F.
Epitaxial growth and structural characterization of 3D Ge quantum well crystals on patterned Si substrates
Fall-EMRS 2014, Warsaw, Poland, 15.09.2014

Kreiliger, T.
InGaAs quantum well emission from epitaxial crystals on patterned Si substrates
E-MRS fall meeting 2014, Warsaw, Poland, 16.09.2014

Kreiliger, T.
3C-SiC Epitaxy on Deeply Patterned Si Substrates
23rd European Workshop on Heterostructure Technology (Hetech2014), Marburg, Germany, 13.10.2014

Lichtenberger, A.
Correlation Between Mathematics and Physics Concepts in Kinematics
GIREP-MPTL 2014, Palermo, Italy, 07.07.2014

Loretz, M.
Diamond-based nano scale nuclear magnetic resonance
QDiamond14, Lamington NP/Brisbane, Australia, 18.08.2014

Möller, J.
Evolution of magnetic interactions in a pressure-induced Jahn-Teller driven magnetic dimensionality switch
International Conference on Muon Spin Rotation, Relaxation, and Resonance, Grindelwald, Switzerland, 01.06.2014

Möller, J.
Playing quantum Hyde-and-seek with the muon
13th International Conference on Muon Spin Rotation, Relaxation, and Resonance, Grindelwald, Switzerland, 01.06.2014

Maier, A.
Probing the intrinsic Spin-Hall Effect in high-mobility AlGaAs/GaAs 2DHSs
32nd International Conference on the Physics of Semiconductors (ICPS 2014), Austin, TX, USA, 12.08.2014

Mathis, T.
Controlled charge transfer doping of organic crystals to observe impurity band transport
Workshop on Exotic Electronic Transport, Chiba, Japan, 16.10.2014

Mirri, C.
Anisotropic optical response of detwinned $BaFe_2As_2$ in the electronic nematic phase
CMD 25-JMC 14: Condensed Matter in Paris, Paris, France, 28.08.2014

Mirri, C.
Optical anisotropy in the electronic nematic phase of underdoped detwinned $Ba(Co_xFe_{1-x})_2As_2$
SuperFOx 2014, Rome, Italy, 25.09.2014

Mlynek, J. A.
Observation of superradiance in a small ensemble of artificial atoms
APS March Meeting, Denver, CO, USA, 03.03.2014

* Moll, P.
Microstructuring correlated electron systems: From vortices to heavy fermions
MPI CPfS Physics Seminar, Dresden, Germany, 10.02.2014

Moll, P.
Intrinsic Josephson Junctions in the iron-based multi-band superconductor $(V_2Sr_4O_6)Fe_2As_2$
APS March Meeting, Denver, CO, USA, 03.03.2014

* Moll, P.
Microstructuring correlated electron systems: From vortices to heavy fermions
EPFL Seminar, Lausanne, Switzerland, 26.03.2014

* Moll, P.
SPG Award Talk
SPG Jahrestagung, Fribourg, Switzerland, 01.07.2014

* Moll, P.
Oscillatory vortex phenomena: Fingerprints of the order parameter in iron-arsenide superconductors
MPI Seminar Talk, MPI CPfS, Dresden, Germany, 21.09.2014

* Moll, P.
The heavy-fermion compound $CeRhIn_5$: d-wave superconductivity and density waves
Physics Colloquium, Cavendish Laboratory, Cambridge, UK, 15.10.2014

* Moll, P.
Intrinsic Josephson Junctions in the iron-based multi-band superconductor $(V_2Sr_4O_6)Fe_2As_2$
THz-PLASMA 2014, Kyoto University, Kyoto, Japan, 30.11.2014

* Mondal, M.
Digital Quantum Simulation of Heisenberg Spin-Spin Interactions with Superconducting Qubits
ScaleQIT workshop, Saarbrücken, Germany, 10.02.2014

Mondal, M.
Digital Quantum Simulation of Heisenberg Spin-Spin Interactions with Superconducting circuits
Condensed Matter in Paris 2014, Paris, France, 26.08.2014

Moores, B.
Implementation of NMR pulse sequences for Magnetic Resonance Force Microscopy
APS March Meeting, Denver, CO, USA, 04.03.2014

Moores, B.
Chemically selective spin signal multiplexing with Magnetic Resonance Force Microscopy
The 10th EUROMAR, Zurich, Switzerland, 29.06.2014

Morf, T.
Effects of uniaxial strain in single crystal Rubrene FETs
Workshop on Exotic Electronic Transport, Chiba, Japan, 16.10.2014

Pechal, M.
Microwave-controlled generation of shaped photons in circuit QED
APS March Meeting, Denver, CO, USA, 03.03.2014

⋆ Rössler, C.
Non-Equilibrium Single Electron Transfer
18th International Winterschool on New Developments in Solid State Physics, Mauterndorf, Austria, 23.02.2014

Rössler, C.
Sub-Thermal Non-Equilibrium Electron Transfer
8th International Conference on Quantum Dots, Pisa, Italy, 11.05.2014

Rössler, C.
Sub-Thermal Non-Equilibrium Electron Transfer
32nd International Conference on the Physics of Semiconductors (ICPS 2014), Austin, USA, 10.08.2014

Riedi, S.
Optimizing Cleaved Edge Overgrowth for Quantum Wire Fabrication
32nd International Conference on the Physics of Semiconductors (ICPS 2014), Austin, TX, USA, 10.08.14

Salathe, Y.
Digital Quantum Simulation of Heisenberg Spin-Spin Interactions with Superconducting Qubits
APS March Meeting, Denver, CO, USA, 03.03.2014

⋆ Schiltz, G.
Flipped Classroom
Hochschuldidaktik-Weiterbildung: didactica, Zurich, Switzerland, 09.05.2014

⋆ Schiltz, G.
Flipped Classroom
Hochschuldidaktik-Weiterbildung: didactica, Zurich, Switzerland, 05.11.2014

⋆ Schiltz, G.
Hat die klassische Vorlesung ausgedient? Neue Wege der Physikausbildung am Departement
Departementstag Physik, Zurich, Switzerland, 10.06.2014

⋆ Schiltz, G.
Flipped Classroom
Studiengang: Exzellenz in der Lehre, Hochschule Luzern, 27.06.2014

Schiltz, G.
Physics tutorial videos: producing educational videos in a self-service setting
E-Learn 2014 AACE, New Orleans, LA, USA, 29.10.2014

Shiroka, T.
Nature of pairing in the optimally-doped BiS_2-based superconductors
Intl. Conference on Superconductivity and Magnetism, Antalya, Turkey, 29.04.2014

Shiroka, T.
Low-temperature magnetic phases in $Ba_2CuGe_2O_7$
Intl. Conference on Muon Spin Rotation (μSR 2014), Grindelwald, Switzerland, 05.06.2014

* Shiroka, T.
One-dimensional spin systems: A laboratory for complex quantum matter
CNISM and Dipartimento di Fisica M. Melloni, Università di Parma, Parma, Italy, 05.05.2014

* Shiroka, T.
1D spin systems at high magnetic fields: from toy models to research tools
Workshop on Unconventional High-T_c Superconductors, IFW Dresden, Germany, 17.07.2014

Simonet, P.
Graphene - GaAs hybrid nanostructures
Q-NET network meeting, San Sebastian, Spain, 21.02.2014

Simonet, P.
Electronic transport in graphene nanoribbons, relevance of etching process and substrate
Q-NET Workshop, Pisa, Italy, 09.12.2014

Simutis, G.
Spin Pseudogap in Ni-Doped $SrCuO_2$
APS March Meeting, Denver, CO, USA, 03.03.2014

Stammeier, M.
Modefunction and DC electric field measurements inside a rectangular 3D cavity
CCQED, Aarhus, Denmark, 29.10.2014

Steinacher, R.
Guiding of branched electron flow and interference effects in a cavity with variable size using a scanning gate
32nd International Conference on the Physics of Semiconductors (ICPS 2014), Austin, USA, 03.08.2014

Takahashi, H.
Dynamic nuclear polarisation enhanced solid-state NMR spectroscopy and magnetic resonance force microscopy for structural biology
RSC NMR Discussion Group: Spring Meeting 2014 (NMR in Structural Biology), Cambridge, United Kingdom, 10.04.2014

Takahashi, H.
On-cell DNP-NMR: towards structural studies of bacterial cell walls
The 10th EUROMAR, Zurich, Switzerland, 29.07.2014

Takahashi, H.
Dynamic nuclear polarisation enhanced solid-state NMR spectroscopy and magnetic resonance force microscopy for structural biology
53rd Annual Meeting of the Nuclear Magnetic Resonance Society of Japan, Osaka, Japan, 04.11.2014

Tao, Y.
Single-Crystal Diamond Nanolithography
MaP Graduate Symposium, ETH Zurich, Switzerland, 05.06.2014

Thiele, T.
Manipulating Rydberg atoms close to surfaces at cryogenic temperatures
QSIT General Meeting, Arosa, Switzerland, 06.02.2014

Thiele, T.
Coherent manipulation of Rydberg states above surfaces at cryogenic temperatures
APS March Meeting, Denver, CO, USA, 03.03.2014

Thiele, T.
Microwave transitions between Rydberg states above (patterned) surfaces at cryogenic temperatures
CCQED, Aarhus, Denmark, 29.10.2014

* Vaterlaus, A.
Die Lehre im Fokus
ETH Departement Physik, Departementstag, Zurich, Switzerland, 10.06.2014

* Vaterlaus, A.
Über das Suchen und etwas Anderes finden
Forum des Departements Chemie der ETH, Collegium Helveticum, Zurich, Switzerland, 31.10.2014

* von Känel, H.
Hot topics in silicon hetero-epitaxy
Summer School Epioptics-13 and Silicene-1, Erice, Italy, 26.07.2014

von Känel, H.
Three-dimensional Epitaxial $Si_{1-x}Ge_x$, Ge and SiC Crystals on Deeply Patterned Si Substrates
2014 ECS and SMEQ Joint International Meeting, Cancun, Mexico, 05.10.2014

von Känel, H.
Defect Reduction in Epitaxial 3C-SiC on Si(001) and Si(111) by Deep Substrate Patterning
European Conference on Silicon Carbide and Related Materials, Grenoble, France, 21.09.2014

* Wachter, P.
Chemical and physical properties of some stoichiometric Rare Earth Nitride single crystals
19. Int. Conference on Solid Compounds of Transition Elements, Genova, Italy, 21.06.2014

* Wallraff, A.
Deterministic quantum teleportation with feed-forward in a solid state system
Topological quantum technology, Hongo campus of The University of Tokyo, Tokyo, Japan, 27.01.2014

* Wallraff, A.
Teleporting Quantum Information with Superconducting Circuits
18th International Winterschool on New Developments in Solid State Physics, Mauterndorf, Austria, 23.02.2014

* Wallraff, A.
Deterministic Quantum Teleportation with Feed-Forward in a Solid State System
APS March Meeting, Denver, CO, USA, 03.03.2014

* Wallraff, A.
Photon-Mediated Interactions between Distant Artificial Atoms in Waveguide QED
invited by Prof. D. Schuster, James Franck Institute, University of Chicago, Chicago, IL, USA, 22.04.2014

* Wallraff, A.
Quantum Microwave Photonics
MPL Distinguished Lecturer Series, Max Planck Institute of Light, Erlangen, Germany, 08.05.2014

* Wallraff, A.
Hong-Ou Mandel interference and single photon generation in Circuit QED
American Physical Society's Division of Atomic, Molecular and Optical Physics (DAMOP) Annual Meeting 2014, Madison, WI, USA, 02.06.2014

* Wallraff, A.
Quantum Optics with Propagating Microwave Photons
Special Quantum Information Seminar invited by Prof. N. Katz, The Hebrew University of Jerusalem, Jerusalem, Israel, 10.06.2014

* Wallraff, A.
Quantum Optics with Microwave Photons
9th Advanced Research Workshop NanoPeter 2014, Fundamentals of Electronic Nanosystems, Saint Petersburg, Russia, 21.06.2014

* Wallraff, A.
Detecting Quantum Properties of Microwave Radiation
Quantum Technologies for Metrology and Sensing Workshop, Lancaster University, Lancaster, United Kingdom, 30.06.2014

* Wallraff, A.
Exploring the Quantum Properties of Propagating Microwave Fields
invited by Prof. Aash Clerk, Special CPM Seminar, Department of Physcis, McGill, Montreal, Canada, 18.07.2014

* Wallraff, A.
Towards Hybrid Cavity Quantum Electrodynamics with Atoms and Circuits
Ultracold Rydberg Physics, Initial Training Network COHERENCE, Casas del Chapiz, Granada, Spain, 10.09.2014

* Wallraff, A.
Photon-Mediated Interactions between Artificial Atoms in One Dimension: Quantum Optics with Superconducting Circuits
invited by Profs. Hossein Sadeghpour and John Doyle, Institute for Theoretical Atomic, Molecular, and Optical Physics and Harvard Quantum Optics Center Cambridge, MA, USA, 24.09.2014

* Wallraff, A.
Semiconductor Quantum Dots, Rydberg Atoms and Superconducting Qubits: Exploring Hybrid Quantum Systems using Circuit Quantum Electrodynamics
invited by Alexandre Cooper, Interdisciplinary Quantum Information Science and Engineering (iQuISE) program, MIT, Cambridge, MA, USA, 25.09.2014

* Wallraff, A.
Exploring Quantum Science and Technology with Superconducting Circuits
invited by Andreas Fuhrer, IBM Research - Zurich, Zurich, Switzerland, 01.10.2014

* Wallraff, A.
Simulating an Interacting Quantum Gas with Superconducting Circuits
invited by Leo DiCarlo, TU Delft, Delft, The Netherlands, 17.10.2014

* Wallraff, A.
Simulating an Interacting Quantum Gas with Superconducting Circuits
ARC Centre of Excellence for Engineered Quantum Systems (EQuS) Workshop, Coogee, Sydney, Australia, 04.12.2014

* Wallraff, A.
Simulating an Interacting Quantum Gas using Matrix Product States generated with Superconducting Circuits
Cavity QED from Angstrom to Millimeter Scale, Association for the Cultivation of Science (IACS), Jadavpur, Kolkata - 700032, India, 08.12.2014

* Wallraff, A.
Exploring Quantum Optics with Superconducting Circuits
invited by R Vijayaraghavan, Tata Institute of Fundamental Research, Mumbai, India, 17.12.2014

* Wegscheider, W.
Growth and Transport Studies of the Tunable 2D Topological Insulator System in InAs/GaSb
18th International Winterschool, Mauterndorf Castle, Austria, 23.02.2014

* Wegscheider, W.
The Tunable 2D Topological Insulator System InAs/GaSb
Annual Meeting of the Swiss Physical Society 2014, University Fribourg, Switzerland, 30.06.2014

Willa, K.
Measuring the Seebeck coefficient in organic semiconductors
Workshop on Exotic Electronic Transport, Chiba, Japan, 16.10.2014

* Wüster, W.
Cavity Quantum Electrodynamics with many-body states of a two-dimensional electron gas
Institute for Theoretical Physics, University of Cologne, Germany, 05.12.2014

Wüster, W.
Cavity Quantum Electrodynamics in the Quantum Hall Regime
3rd NCCR QSIT General Meeting, Arosa, Switzerland, 05.02.2014

Wüster, W.
Cavity Quantum Electrodynamics as a Sensitive Probe of Many-Body Physics in Two Dimensional Electron Gases
32nd International Conference on the Physics of Semiconductors (ICPS 2014), Austin, TX, USA, 10.8.2014

* Zheludev, A.
The Heisenberg spin ladder: finished
Conference on Field Theory Methods in Low-Dimensional Strongly Correlated Quantum Systems, Trieste, Italy, 25.08.2014

* Zheludev, A.
The futile search for the magnetic BG/BEC QCP
Workshop “Quantum Spin Dynamics”, Dresden, Germany, 01.09.2014

* Zheludev, A.
The futile search for the magnetic BG/BEC QCP
Workshop “Quantum Disordered Systems: whatâs next?”, Toulouse, France, 24.06.2014

* Zheludev, A.
An attractive Tomonaga-Luttinger spin liquid
International Conference on Strongly Correlated Electron Systems (SCES) 2014, Grenoble, France, 07.07.2014

Zheludev, A.
The perfect spin ladder
29th workshop on Novel Materials and Superconductors, Obertraun, Austria, 08.02.2014

Zhigadlo, N.
LnFeAsO single crystals: growth, substitutions, structural and superconducting properties
4th International Conference on Superconductivity and Magnetism (ICSM 2014), Antalya, Turkey, 27.04.2014

* Zhigadlo, N.
Overview of contemporary superconductors grown under high pressure
The International Conference SUPERSTRIPES 2014, Erice, Italy, 19.07.2014

* Zhigadlo, N.
Synthesis of new materials under high pressure and prospect of their application
School-seminar “Applied and Fundamental Aspects of Theoretical Physics” devoted to the 75th anniversary of the department of theoretical physics and astronomy of the Belarusian State University, Minsk, Belarus, 10.10.2014

* Zhigadlo, N.
Opportunities and challenges in high-pressure synthesis of complex oxides and intermetallic superconductors
Interdisciplinary Seminar of the International Laboratory of High Magnetic Fields and Low Temperatures PAS, Wroclaw, Poland, 23.10.2014

Zimmerling, T.
Pure Gold makes for Poor Contacts
Workshop on Exotic Electronic Transport, Chiba, Japan, 16.10.2014

11.2 Posters

Abdumalikov, A.
Imaging of Eigenmodes in a Chain of Microwave Oscillators
BRNC Ralph Eichler Symposium, IBM Zurich, Zurich, Switzerland, 08.12.2014

Arrieta, J. P.
Magnetocapacitance measurements of undoped AlGaAs/GaAs heterostructures
18th International Winterschool on New Developments in Solid State Physics, Mauterndorf, Austria, 23.02.2014

Baer, S.
Experimental probe of topological orders and edge excitations in the second Landau level
International workshop on Emergent Phenomena of Quantum Hall Systems-5 (EPQHS-5), Weizmann Institute of Science, Rehovot, Israel, 06.07.2014

Baer, S.
Quantum dots in the Quantum Hall regime
NCCR QSIT evaluation, ETH Zurich, 08.12.2011

Barbero, N.
Degradation of charge collection efficiency of n-type Fz silicon diode under MeV proton irradiation
Intl. Conference on Nuclear Microprobe Technology and Applications, Padova, Italy, 07.07.2014

Berger, S.
Exploring the Effect of Noise on Geometric Phases
QSIT Meeting 2014, Arosa, Switzerland, 05.02.2014

Blülle, B.
Similarities between bulk and interface charge transport in rubrene single crystals
International Workshop on Field-Effect Transistors and Functional Interfaces FET2014, Kashiwa, Japan, 17.10.2014

Braem, B. A.
Local Investigation and Manipulation of Quantum States
NCCR QSIT evaluation, ETH Zurich, 06.11.2014

Hälg, M.
New Heisenberg $S = 1/2$ Chain with DM Interactions
International Conference on Strongly Correlated Electron Systems (SCES) 2014, Grenoble, France, 07.07.2014

Hälg, M.
New Heisenberg $S = 1/2$ Chain with DM Interactions
International Conference on Low Temperature Physics (LT) 2014, Buenos Aires, Argentina, 07.08.2014

Hennel, S.
Sustained temporal resistance oscillations in constrained geometries at the $\nu = 2/3$ spin phase transition
International workshop on Emergent Phenomena of Quantum Hall Systems-5 (EPQHS5), Weizmann Institute of Science, Rehovot, Israel, 06.07.2014

Hofmann, A.
Investigating transport in GaAs/AlGaAs and InAs/GaSb based 2D systems
4th NCCR QSIT General Meeting, Arosa, Switzerland, 03.01.2014

Hofmann, A.
Thermodynamics of few electron quantum dots
18th International Winterschool on New Developments in Solid State Physics, Mauterndorf, Austria, 23.02.2014

Hofmann, A.
Measurements of the equilibrium free energy change in a quantum dot driven out of thermodynamic equilibrium
Spin-based quantum information processing, Konstanz, Germany, 18.08.2014

Isa, F.
Epitaxial growth and characterization of 3D GaN micro-crystals on (001) patterned Si substrate by plasma-assisted MBE
Fall-EMRS 2014, Warsaw, Poland, 15.09.2014

Jung, A.
Quantum Well Emission from InGaAs/GaAs grown on Patterned Silicon Substrates
17th Int. Conference on Metalorganic Vapor Phase Epitaxy (ICMOVPE) at Ecole Polytechnique Fédérale de Lausanne EPFL, Lausanne, Switzerland, 13.07.2014

Kozikov, A. A.
Electrostatics of a cavity and locally induced Aharonov-Bohm interference in scanning gate experiments
18th International Winterschool on New Developments in Solid State Physics, Mauterndorf, Austria 23.02.2014

Kozikov, A. A.
Local investigation of interference and quantum coherence in ballistic nanostructures using a scanning gate
CIMTEC 2014, Montecatini Terme, Italy, 15.06.2014

Kozikov, A. A.
Inducing & Controlling Aharonov-Bohm Oscillations with a Scanning Gate
32nd International Conference on the Physics of Semiconductors (ICPS 2014), Austin, TX, USA, 10.08.2014

Kurpiers, P.
Deterministic quantum teleportation with feed-forward in a solid state system
QSIT Meeting 2014, Arosa, Switzerland, 05.02.2014

Lorenz, W.
Dzyaloshinskii-Moriya induced inter-chain frustration in a new spin-chain compound
APS March Meeting, Denver, CO, USA, 03.03.2014

Maier, A.
Probing the intrinsic Spin-Hall Effect in high-mobility AlGaAs/GaAs 2DHSs
32nd International Conference on the Physics of Semiconductors (ICPS 2014), Austin, TX, USA, 10.08.2014

Mathis, T.
Controlled charge transfer doping of organic crystals to observe impurity band transport
International Workshop on Field-Effect Transistors and Functional Interfaces FET2014, Kashiwa, Japan, 17.10.2014

Morf, T.
Effects of uniaxial strain in single crystal Rubrene FETs
International Workshop on Field-Effect Transistors and Functional Interfaces FET2014, Kashiwa, Japan, 17.10.2014

Mueller, S.
Transport Measurements in Mesoscopic Devices of the 2D Topological Insulator Candidate InAs/GaSb
32nd International Conference on the Physics of Semiconductors (ICPS 2014), Austin, TX, USA, 10.08.2014

Nichele, F.
Transport Experiments in InAs/GaSb in the Quantum Hall Regime
21st International Conference on High Magnetic Fields in Semiconductor Physics, Panama City Beach, FL, USA, 03.08.2014

Pal, A. N.
Quantum Hall effect and insulating state near the charge neutrality point in an InAs/GaSb quantum well
APS March meeting, Denver, CO, USA, 03.03.2014

Pal, A. N.
Insulating State & Strong Non-Local Response Near the Charge Neutrality Point in an InAs/GaSb Composite Quantum Well
32nd International Conference on the Physics of Semiconductors (ICPS 2014), Austin, TX, USA, 10.08.2014

Pascher, N.
Resonant electron tunneling in a tip-controlled potential landscape
18th International Winterschool on New Developments in Solid State Physics, Mauterndorf, Austria, 23.02.2014

Pascher, N.
Imaging the Conductance of Integer & Fractional Quantum Hall Edge States
32nd International Conference on the Physics of Semiconductors (ICPS 2014), Austin, TX, USA, 10.08.2014

Pikulski, M.
An FPGA-based direct-digital NMR spectrometer: How software replaces the soldering iron
Annual Meeting of the Swiss Physical Society, Fribourg, Switzerland, 30.06.2014

Potocnik, A.
Lumped Element Resonators for Quantum Information Processing
BRNC Ralph Eichler Symposium, IBM Zurich, Zurich, Switzerland, 08.12.2014

Povarov, K.
Cu(Qnx)($Cl_{(1-x)}Br_x$)$_2$ as a tunable quantum spin ladder
Moscow International Symposium on Magnetism 2014 (MISM 2014), Moscow, Russia, 29.06.2014

Povarov, K.
Cu(Qnx)($Cl_{(1-x)}Br_x$)$_2$ as a tunable quantum spin ladder
International Conference on Strongly Correlated Electron Systems (SCES 2014), Grenoble, France, 07.07.2014

Povarov, K.
Uniform Dzyaloshinskii-Morya interaction in a novel spin-chain material $K_2CuSO_4Br_2$
27th International Conference on Low Temperature Physics, Buenos Aires, Argentina, 06.08.2014

Schiltz, G.
Exercise class market: Applying differentiated instruction to physics tutorials
International Conference on Physics Education ICPE 2014, Cordoba, Argentina, 21.08.2014

Shiroka, T.
Superconductivity in eutectically-grown mixed ruthenates: A μSR study
Intl. Conference on Muon Spin Rotation (μSR 2014), Grindelwald, Switzerland, 02.06.2014

Shiroka, T.
From order to randomness: a one-dimensional journey to disorder
Annual Meeting of the Swiss Physical Society, Fribourg, Switzerland, 30.06.2014

Simonet, P.
Improving confinement in graphene nanostructures
4th NCCR QSIT General Meeting, Arosa, Switzerland, 05.02.2014

Simonet, P.
Towards graphene-GaAs hybrid nanostructures
Graphene week 2014, Gothenburg, Sweden, 23.06.2014

Simonet, P.
Charge Detection in a Hybrid Graphene-GaAs Nanostructure
32nd International Conference on the Physics of Semiconductors (ICPS 2014), Austin, TX, USA, 10.08.2014

Simutis, G.
Defect-induced spin pseudogap in antiferromagnetic $S = 1/2$ Heisenberg chain
International Conference on Strongly Correlated Electron Systems (SCES), Grenoble, France, 07.07.2015

Stammeier, M.
Using Rydberg Atoms to measure the mode function and the DC electric field inside a rectangular 3D cavity
CCQED, Aarhus, Denmark, 29.10.2014

Steinacher, R.
Inducing and controlling quantum phenomena using a scanning gate
NCCR QSIT General Meeting, Arosa, Switzerland, 05.02.2014

Stockklauser, A.
Circuit QED with Semiconductor Single-Electron Charge Qubits
Winterschool Mauterndorf 2014, Mauterndorf, Austria, 24.02.2014

Stockklauser, A.
Circuit QED with Semiconductor Single-Electron Charge Qubits
Conference on spin-based quantum infromation processing, Konstanz, Germany, 22.08.2014

Thede, M.
Pressure-induced quantum critical and multicritical points in a frustrated spin liquid
13th International Conference on Muon Spin Rotation, Relaxation and Resonance (μSR2014), Grindelwald, Switzerland, 01.06.2014

Tschirky, T.
MBE Growth Optimization of Antimony Based Semiconductors
Deutscher MBE Workshop 2014, Darmstadt, Germany, 15.09.2014

Varlet, A.
Tunable Fermi surface topology in gapped bilayer graphene
32nd International Conference on the Physics of Semiconductors (ICPS 2014), Austin, TX, USA, 10.08.2014

Willa, K.
Measuring the Seebeck coefficient in organic semiconductors
International Workshop on Field-Effect Transistors and Functional Interfaces FET2014, Kashiwa, Japan, 17.10.2014

Wulf, E.
Quantum phase transition in DTN by neutron diffraction
27th International Conference on Low Temperature Physics, Buenos Aires, Argentina, 06.08.2014

Zheludev, A.
Pressure-induced quantum phase transitions in PHCC
27th International Conference on Low Temperature Physics, Buenos Aires, Argentina, 06.08.2014

Zimmerling, T.
Pure Gold makes for poor Contacts
International Workshop on Field-Effect Transistors and Functional Interfaces FET2014, Kashiwa, Japan, 17.10.2014